Hybrid Frequency Phase Modulation: Performance Analysis and Applications

by

Ibrahim Ghareeb, B.Sc., M.Sc

A thesis submitted to the

School of Graduate Studies and Research

in partial fulfilment of the requirements for the degree of

Doctor of Philosophy

Ottawa-Carleton Institute for Electrical Engineering

Department of Electrical Engineering

Faculty of Engineering

University of Ottawa

April 1994

ISBN 0-612-04909-4

Abstract

This thesis studies the performance of joint frequency-phase modulation (JFPM) communication systems, it considers its spread spectrum as well as narrow band applications.

JFPM signal has been mathematically modeled. Its power spectral density and bandwidth efficiency have been analyzed. A bit error rate performance of JFPM signals in AWGN as well as in Rayleigh fading channels is obtained. Assuming statistical independence of the diversity channels, we have analyzed the diversity combining reception of JFPM over Rayleigh fading channels. These analytical results show that, JFPM signals are characterized by relative simplicity in obtaining large set of waveforms, and thus by varying its parameters it can be suitable for either bandwidth-limited or power-limited applications. Compared to M-ary FSK signals that use the same number of tones, the needed minimum frequency separation between two adjacent tones for JFPM signals to satisfy the orthogonality condition is reduced.

A spread spectrum system referred to as frequency hopped/joint frequency-phase modulation (FH/JFPM) has also been presented. The system model is described for both slow frequency hopping (SFH/JFPM) and fast frequency hopping (FFH/JFPM). Bit error rate performance for SFH/JFPM in the presence of broadband and partial-band noise jamming is analyzed, and the worst case jamming performance of this system is evaluated. It is shown that SFH/JFPM is less sensitive to broadband and partial-band noise jamming than the conventional frequency hopped systems. The design and analysis of the FFH/JFPM system over Rayleigh fading channels is presented. An expression for the probability of a bit error is obtained. Results have shown that the FFH/JFPM outperforms the conventional frequency hopped systems.

A detailed analysis for the probability density function of the received signal phase in the presence of multitone jamming is provided. The probability density function is derived for any arbitrary transmitted signal phase. Based on this analysis, the probability of error for the FH/M-ary DPSK system in the presence of multitone jamming is obtained. The performance of coherent frequency hopped M-ary PSK system in multitone jamming environments has also been presented. Bit error rate performance of this system is analyzed. A simple expression for the probability of a bit error is obtained. The performance of this system in worst case jamming is also given.

I hereby declare that I am the sole author of this thesis. I authorize The University of Ottawa to lend this thesis to other institutions or individuals for the purpose of scholarly research.

Ibrahim Ghareeb

I further authorize The University of Ottawa to reproduce this thesis by photocopying or by other means, in total or in part, at the request of other institutions or individuals for the purpose of scholarly research.

Ibrahim Ghareeb

To my family

Acknowledgments

To all those who contributed so much towards the completion of this study I would like to express my sincere gratitude and appreciation.

Dr. A. Yongaçoḡlu, my thesis supervisor, for his continuous encouragement, constructive comments, invaluable suggestions and steady guidance throughout the research. Many thanks to him for being as a good friend over the whole period of my graduate study.

My examiner's committee, Drs. Mohsen Kavehrad, Peter Galko, David Falconer and Paul Wittke for there constructive comments and helpful suggestions which led to significant improvements to my thesis.

Dr. T. Aboulnasr for her help throughout my stay at the University of Ottawa.

CIDA and Jordan University of Since and Technology for there scholarship that cover a big period of my study.

My epitome thanks go to my wife Iman and our son and daughter Mousa and Razan, who made this whole effort much more enjoyable than it would have otherwise been.

Special thanks to my parents whose love, for their patience, sacrifice, and support during all those years of my studies.

Contents

List of Figures

List of Tables

Acronyms

AWGN	Additive white Gaussian Noise
BER	Bit error rate
BFSK	Binary frequency shift keying
BPSK	Binary phase shift keying
BDPSK	Binary differential phase shift keying
CDMA	Code division multiple access
CFSK	Continuous frequency shift keying
DPSK	Differential phase shift keying
DS	Direct Sequence
FH	Frequency hop
FFH	Fast frequency hopping
FSK	Frequency shift keying
JFPM	Joint frequency-phase modulation
MSK	Minimum shift keying
PN	Pseudo noise
PSK	Phase shift keying
QPSK	Quaternary phase shift keying
SFH	Slow frequency hoping
SS	Spread spectrum

Nomenclature

$2f_d$	frequency separation between two adjacent signals
α_k	path gain of the k-th path in fading channels
β_{bin}	bandwidth of a bin
β_{ch}	bandwidth of a frequency slot
β_{ss}	total spread spectrum bandwidth
C	complexity
Δf	minimum frequency separation
$\Delta(\rho_b)_{DPSK}$	The asymptotic gain performance of FH/M-ary JFPM for worst case partial-band noise jamming over the conventional FH/M-ary DPSK
$\Delta(\rho_b)_{FSK}$	The asymptotic performance of FH/M-ary JFPM for worst case partial-band noise jamming over the conventional FH/M-ary FSK
E_b	energy per bit
E_s	energy per symbol
η^2	the ratio of the received jamming power for each tone to the signal power
γ	the fraction of the spread spectrum bandwidth that is jammed
γ_{wc}	worst case value of γ
I_F	improvement factor for the FSK part
I_P	improvement factor for the DPSK part
J	average jamming power
k_F	number of bits per symbol used to determine the signal frequency
k_P	number of bits per symbol used to determine the signal phase
k_s	number of the bits per symbol
L	number of diversity branches
M	number of modulating signals
M_F	number of frequencies used to shift the frequency of the carrier
M_P	number of phases used to shift the phase of the carrier
μ_{B_i}	power contained in bandwidth
μ_{B_o}	fractional out of band power
N_0	noise power spectral density
N	number of frequency bins in the available channel bandwidth
N_j	one-sided power spectral density of the jamming signal

n_j	the power spectral density of the jamming signal in the jammed fraction γ
p	the probability that the jammer will hit a frequency bin
P_{b1}	probability of a bit error due to an error in the frequency
P_{b2}	probability of a bit error due to an error in the phase given that the noncoherent decision on the frequency was correct
$P_b(M)$	probability of a bit error of a signal with M waveforms
P_c	average probability of a correct reception of a symbol
$P_{e,j}$	the probability of symbol error for symbol intervals which are jammed
$P_{e,FSK}$	the probability of an erroneous noncoherent decision on the frequency
$P_e(M)$	probability of a symbol error of a signal with M waveforms
$P_{e,PSK\|FSK}$	the probability of an incorrect decision on the phase given that the noncoherent decision on the frequency was correct
PG	processing gain
PG_{DPSK}	processing gain of the DPSK-part
PG_F	processing gain of the conventional FH/M_F-ary FSK system
PG_{FSK}	processing gain of the FSK-part
PG_P	processing gain of the conventional FH/M_P-ary DPSK system
ϕ_k	phase shift of the k-th path in fading channels
q_t	number of jamming tones
r	complex-valued correlation coefficient
R_b	information bit rate (in bit per second)
$\frac{R_b}{W}$	bandwidth efficiency (in bit/s/Hz)
R_h	hop-rate
ρ, $\frac{E_s}{N_0}$	signal energy per symbol to noise density ratio
ρ_{b0}	the value of the signal energy per bit to jamming noise density ratio (E_b/n_j) that maximizes the the probability of a bit error
ρ_b, $\frac{E_b}{N_0}$	signal energy per bit to noise density ratio
$\bar{\rho}_c$	average signal-to-noise ratio per diversity channel
$\bar{\rho}$	average signal-to-noise ratio per symbol
$\bar{\rho}_b$	average signal-to-noise ratio per bit
$\bar{\rho}_h$	average signal-to-noise ratio per hop
R_s	symbol rate (in symbols per second)
S	average signal power
τ_k	propagation delay of the k-th path in fading channels
T_b	bit duration time
T_h	hop-duration
T_s	symbol duration time
W	required channel bandwidth
xF/yP	the JFPM format results from the combination of x-frequencies and y-phases

Chapter 1

Introduction

1.1 Motivation

There is no single class of modulation techniques that is suitable for all applications, since communication channels and performances requirements vary widely. The conventional classification of various modulation schemes is based on their power and bandwidth utilization efficiencies [1]-[4]. However, there are other aspects of modulation signals and channels that might be taken into account in classification of modulation schemes, such as the modulated signals' properties including their spectral characteristics, amplitude variations and correlation properties. In this respect a constant envelope property of a modulated signal is desirable, so that it can be transmitted over nonlinear and/or fading channels, and nonlinear amplifiers can be used [5]. A measure of the spectral characteristics of a modulation scheme can be drawn from the attenuation of the power spectrum at a specified separation from the center frequency. It is very important to keep the sidelobes of the spectrum as small as possible to avoid degradation due to adjacent-channel interference. In general for frequencies far from the center frequency, the rate at which the spectrum falls-off is equally important. Continuous phase modulation is often preferred for compact spectrum in some applications, as several papers in [6] indicate. For a given modulation technique with a given number of points in the constellation, the bandwidth efficiency improvement can usually be achieved by filtering/pulse shaping. This improvement is usually at the expense of some power efficiency loss and increased complexity.

When M-ary orthogonal signals are used, the bandwidth increases proportionally to the number of transmitted tones M. Thus, in a system using M-ary orthogonal signals the bandwidth is traded off for a reduction in the required E_b/N_0 to achieve a given bit error rate. On the other hand, for efficient usage of bandwidth, more signal points for a given dimensionality are desired. This results in the reduction of the minimum Euclidean distance between the signals in the same constellation, which degrades the error rate performance. M-ary PSK and the combined digital modulation techniques, such as combined amplitude-phase modulation and quadrature amplitude modulation, are bandwidth efficient digital modulation techniques, where the bandwidth efficiency increases in proportion to the number of levels M. For $M > 4$, the cost of achieving the same bit error rate is an increase in the required E_b/N_0.

So far, we have only considered the main criteria guiding the choice of modulation techniques. Other aspects that must be taken into account are the type of demodulation to be employed, the sensitivity to various impairments, interference, jamming etc.

The demodulation process is the complementary operation of modulation and is performed in the receiver. Demodulation can be either coherent or noncoherent. In coherent detection, the receiver needs a carrier reference whose phase is approximately close to the phase of the incoming signal. This means that coherent detection requires the extracting and maintaining the phase of the incoming carrier. Noncoherent detection does not require the absolute phase information and essentially performs a nonlinear operation.

Spread spectrum techniques are generally used in antijam applications where a low level of interference within the desired signal bandwidth can be achieved. The use to frequency hopping or direct sequence spread spectrum techniques depends on a number of factors, particularly the type of jamming.

1.2 Why Joint Frequency-Phase Modulation?

As can be seen from brief descriptions in the previous section, there are several modulation schemes which are in use or will be coming into use in the near future. There is of course, no single class of modulation technique that is suitable for all applications. Hence, it is very desirable to employ a modulation scheme that is hybrid in its properties, and which includes the most desirable properties of the conventional modulation schemes. Joint Frequency-Phase Modulation (JFPM) is one such hybrid modulation scheme derived from multi-frequency and multi-phase signals. JFPM is a constant envelope digital modulation technique, where both the frequency and the phase of the signal are simultaneously keyed. Such signals are characterized by relative simplicity in obtaining large set of waveforms. This modulation technique includes cases which permit it to be classified as an bandwidth efficient modulation or power efficient modulation technique. Because JFPM signals have a constant envelope property, this modulation technique can be used in nonlinear and/or fading channels, where nonlinear amplifiers can be used. The minimum frequency separation needed between two adjacent tones for JFPM signals to satisfy the orthogonality condition is reduced compared to M-ary FSK signals that use the same number of tones. In JFPM signals, the number of signal points in a given dimension are varied.

Thus, it is possible, by combining this fact and proper coding techniques for JFPM signals, to achieve an improvement in bit error rate performance without expanding the bandwidth.

The concept of JFPM was first proposed by Reed and Scholtz as "N-orthogonal phase modulated codes". In that initial work [7], the matched filter receiver criteria for coherent detection in a Gaussian channel were developed and integral expressions for the probability of error were derived. Simple upper and lower bounds on these probabilities were derived by Viterbi and Stiffler [8]. Several suboptimum receiver structures for "N-orthogonal phase modulated codes" were demonstrated by Lindsey and Simon [9]. Recently a coded modulation format based on expanding the signal size by utilizing both frequency and phase was suggested by [10]-[15] to achieve further coding gain for the same number of trellis states. Fleisher and Qu studied the effect of MSK type pulse shaping in JFPM signals [16]. The performance of a nonconstant envelope JFPM format derived from binary frequency shift keying in the Gaussian and Rayleigh fading channel is given in [17], which also provides the spectral characteristics of this kind of JFPM format.

Generally speaking, all of the previous work has been devoted to study of the performance of coherent JFPM systems; no general work has been done on noncoherent or differential detection JFPM systems. This thesis presents a performance analysis in Gaussian and Rayleigh fading channels for JFPM system, employing noncoherent demodulation for the frequency part of the JFPM signals and differential phase-shift-keyed modulation and differentially coherent demodulation for the phase part of the JFPM signals. A differential modulation system has most of the performance advantage of a coherent system at high signal-to-noise ratios. Also, it has no phase ambiguity problem and needs no sophisticated phase tracking system.

1.3 The Role of JFPM in Spread Spectrum

The ultimate objective of any communication system, for both military and civilian users, is to transmit the information to the receiver as reliably as possible. Unfortunately, mobile channels are always susceptible to hostile or unintentional interference and environmental effects. Both Direct Sequence (DS) and Frequency Hopping (FH) spread spectrum systems are widely used in mobile communication systems to combat severe fading and to improve antijam capabilities.

Frequency hopped systems usually employ either noncoherently detected M-ary FSK (FH/M-ary FSK) or differentially detected M-ary PSK (FH/M-ary DPSK). Several mobile communication systems are based on FH/M-ary FSK system, because of the high processing gain and the ability of a wide-band signal to resist the effects of multipath fading [18]-[19]. Much of the previously published research has been devoted to study the performance of slow FH/M-ary DPSK systems [20]-[26]. This interest is based on the fact that a SFH/DPSK system can support a much higher data rate than Fast Frequency Hopping (FFH) while having the same hop rate. FFH/DPSK has been proposed as a possible way of providing mobile radio service to a large number of users [27]-[30], where linear and nonlinear receivers are considered. The performance of a FFH/DPSK system in jamming environment is given in [31]-[33].

In radio transmission, the desired signal is often disturbed by jamming signals and interference from other users which affect the band occupied by the desired signal. This interference leads to a degradation in the bit error rate of the desired user. To overcome this degradation, the processing gain of the spread spectrum system must be increased. FFH with diversity combining is used in spread spectrum systems to limit the effect of jamming interference. As the number of diversity branches is increased, the error rate decreases. By keeping the hopping rate fixed, the price paid for this improvement is a reduction in data rate available for each user.

Improvements in the performance of the FH system can be achieved by employing modulation techniques more powerful than basic FSK or basic DPSK. For this purpose, we have investigated the impact of using hybrid modulation techniques. In this thesis the design and analysis of a slow as well as fast frequency hopped JFPM system is given in jamming environments and over fading channels.

In the general literature, from analytical point of view, the performance of coherent FH/PSK and FH/DPSK systems in the presence of multitone jamming presented a difficulty in the past. Since differentially coherent detection of M-ary DPSK signals employs two symbols in a symbol decision interval, each of the data symbols may or may not have been subjected to the jamming interference in a multitone jamming strategy situation. Thus, the detection of M-ary DPSK signals takes place in four possible circumstance. In the general literature, the authors in [20, 21] and [23, 24] considered the performance of the FH/DPSK system in a multitone jamming environment. Their analysis is applicable to the case where either a whole hop is jammed or not (both adjacent symbols are always assumed to be jammed by continuous tone jamming). By deriving the expression for the probability density function of the received signal phase in the presence of multitone jamming, this thesis provides a theoretical basis for the analysis of coherent frequency hopped M-ary PSK and frequency hopped M-ary DPSK systems in multitone jamming environments. Based on this analysis, work on JFPM with multitone jamming can be done, but this will not be attempted in this thesis.

1.4 Outline of the Thesis

The outline of this thesis is as follows (see Fig. 1.1). In Chapter 2 a mathematical description of JFPM signals is given. The power spectral density is analyzed, and the bandwidth efficiency is derived based on the minimum frequency separation bandwidth (maximum frequency deviation), null-to-null bandwidth and fractional power containment bandwidth. The bandwidth efficiency is calculated for different combinations of JFPM signals and compared with various other modulation schemes.

Chapter 3 is devoted to study of the demodulation and error rate performance of JFPM signals over AWGN channels. Background information for coherent detection of JFPM signals is provided. A receiver structure employing noncoherent detection for the frequency part of JFPM signals and differentially coherent detection for the phase part of the JFPM signals is introduced and the probability of a bit error is obtained. The performance given in this chapter is presented in terms of bandwidth efficiency and bit error rate.

Chapter 4 presents the performance of JFPM over Rayleigh fading channels. The channel model under consideration is described. Bit error rate performances of coherent and differentially coherent detection are analyzed. The performance with diversity combining in multipath fading channel is evaluated.

In Chapter 5 a description of the proposed frequency hopped/joint frequency-phase modulation is given. The performance analysis of SFH/JFPM system is obtained in the presence of broadband and partial-band noise jamming, and the optimal jamming strategy is evaluated and compared with the conventional frequency hopped systems. A receiver structure for FFH/JFPM signals is introduced and its performance in Rayleigh fading channels is analyzed.

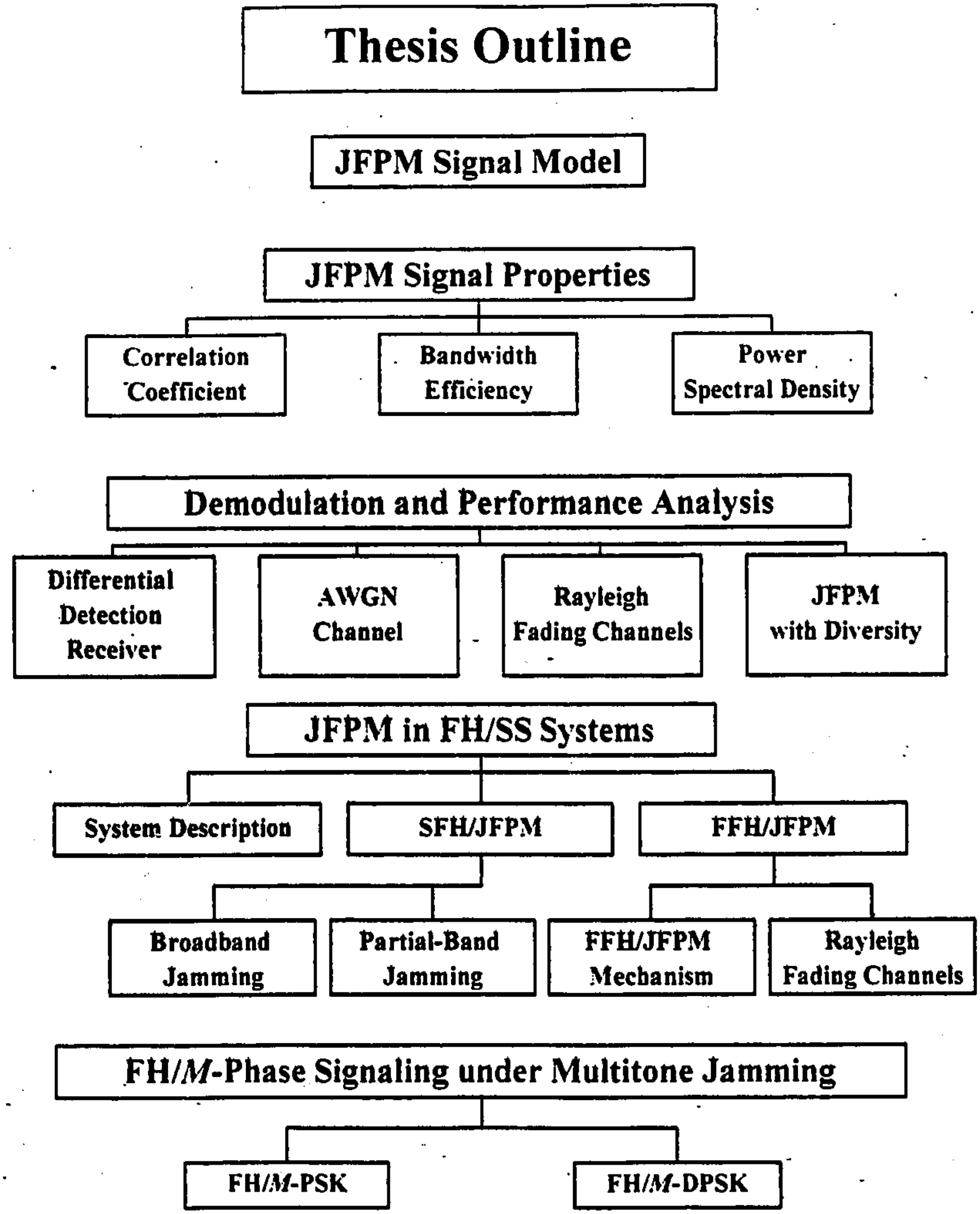

Figure 1.1 : Outline of the thesis

In Chapter 6 the performance of frequency hopped/multi-phase signals in the presence of multitone jamming is studied. The probability of a bit error and the worst case jamming strategy of coherent frequency hopped M-ary PSK system are obtained. Also, an analysis of the probability of error for the FH/M-ary DPSK system in the presence of multitone jamming is obtained.

Chapter 7 summarizes the conclusions reached in this thesis and discusses some of the potential future research topics.

Appendix A presents the derivation of inverse transformation of u (the received signal phase the presence of multitone jamming).

Appendix B presents the derivation on the bounds of u.

1.5 Contributions of the Thesis

In this thesis, many new areas have been explored and results obtained [34]-[42]. In terms of joint frequency-phase modulation, a mathematical model for JFPM signals is given and the correlation coefficient is obtained. The power spectral density and the spectral efficiency of joint frequency-phase modulation is analyzed. The power spectral density of JFPM does not contain a discrete component and in some cases the same bandwidth efficiency can be obtained by using a different JFPM format. This gives an additional degree of freedom to the system designer.

The probability of error for JFPM signals over AWGN channels is analyzed and an expression for the probability of a bit error is obtained. Results show that this modulation technique includes many formats which may be classified as bandwidth efficient modulation or power efficient modulation technique.

The probability of error performance of JFPM signals in slowly fading frequency-nonselective Rayleigh channels is analyzed. Error rate performance using diversity techniques is evaluated. Results show that JFPM performs better than conventional noncoherent M-ary FSK or M-ary DPSK of comparable spectral efficiency.

A frequency hopped spread spectrum system (FH/JFPM) is introduced. A description of both slow and fast FH/JFPM systems is given. The performance of SFH/JFPM systems in broadband and partial-band noise jamming are analyzed and the optimal jamming strategy is evaluated. The performance of an FFH/JFPM in Rayleigh fading channels is analyzed and an expression for the probability of a bit error is obtained. As was previously shown, for a given channel bandwidth and at a fixed data rate, the processing gain of the two parts of FH/JFPM system is improved and for a given data rate and hop rate the diversity level of this system could be increased. Results also show that FH/JFPM outperforms the conventional frequency hopped systems.

The performance of frequency hopped/multi-phase signals in the presence of multitone jamming is presented, and a theoretical basis in the performance of coherent frequency hopped M-ary PSK system in multitone jamming environments is provided. The probability of a bit error and the worst case jamming strategy of this system are analyzed. Also, analysis of the probability of error for the FH/M-ary DPSK system in the presence of multitone jamming is obtained. Related results are obtained for the probability density functions of the received signal phase in the presence of multitone jamming. Equations were derived describing the probability density function of the received signal phase for any arbitrary transmitted phase.

Chapter 2

Description of a JFPM System, Signal Properties and Power Spectral Density

2.1 Introduction

As the previous chapter has indicated, in radio communication links, the bandwidth and/or power are limited. This forces one to search for a good modulation scheme that compromises between the bandwidth and the power available for transmission. The power and bandwidth efficiency of a modulation scheme depend on the signal constellation of the transmitted waveforms. This chapter is devoted to study of the properties of Joint Frequency-Phase Modulation (JFPM) signals. Such signals are characterized by relative simplicity in obtaining a large set of waveforms and the ability to be either bandwidth or power efficient. In this chapter, a mathematical model for JFPM signals is presented and a framework is provided for analyzing power spectral density and bandwidth efficiency.

The chapter is organized as follows. Section 2.2 presents the mathematical representation and the correlation coefficient of the transmitted JFPM signals. In Section 2.3 the power spectral density of JFPM signals is analyzed. The bandwidth efficiency is derived and the fractional out-of-band power is obtained in Section 2.4. The numerical results and comparisons are given in Section 2.5. Finally Section 2.6 presents the conclusions of this chapter.

2.2 JFPM Signal Properties

2.2.1 Transmitted Signal Model

A block diagram depicting the modulation process of JFPM signals is shown in Fig. 2.1. In this figure, every k_s-bits of the source stream is divided into two streams. The first stream (denoted as k_F) is used to shift the frequency of the carrier by using a frequency synthesizer or M_F-ary FSK modulator. At the same time, the other stream of data bits (denoted as k_P) is differentially encoded and is used to shift the phase of the carrier generated by the frequency synthesizer. In each symbol interval the

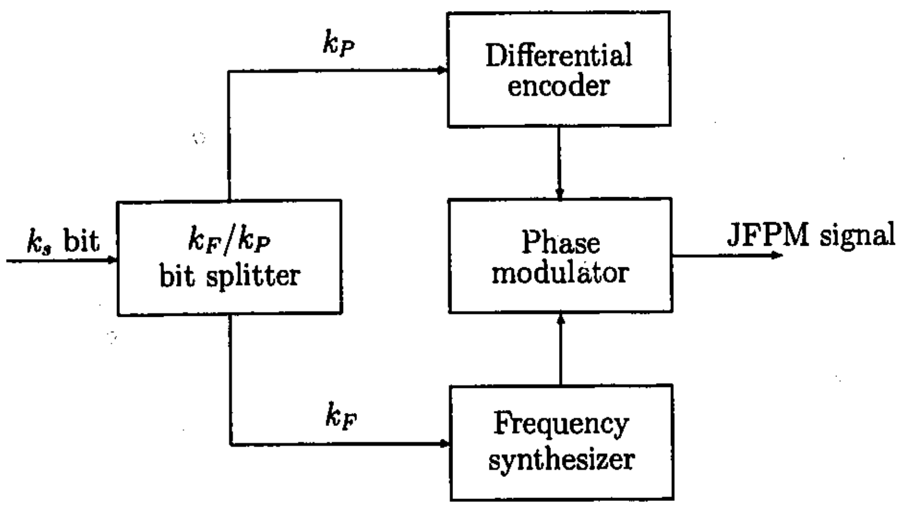

Figure 2.1 : Block diagram of a JFPM modulator.

tone at the output of frequency synthesizer are all assumed to start with the same initial phase. This assumption is made to relax the requirements on the receiver with noncoherent detection. This model represents the situation in which the tones are generated by oscillator whose frequencies are such that their phase changes over an interval of T_s is a multiple of 2π, allowing each to have the same initial phase in each symbol time interval. In practice this can be achieved with the digital generation of the signal waveforms [69].

Adopting the notation of [45], the frequency-phase modulated signal corresponding to a sequence of K messages can be represented as

$$v(t) = \Re\left\{\sum_{k=0}^{K-1} s(t-kT_s;\zeta_k,\lambda_k)e^{j2\pi f_c t}\right\} \qquad 0 \le t \le KT_s \tag{2.1}$$

where $\Re\{\ \}$ denotes the real part of the argument. The signal $s(t-kT_s;\zeta_k,\lambda_k)$ represents the k-th transmitted symbol associated with the random variables ζ_k, λ_k, and is given by

$$s(t-kT_s;\zeta_k,\lambda_k) = \zeta_k u(t-kT_s;\lambda_k) \tag{2.2}$$

where the random variable ζ_k is given by

$$\zeta_k = e^{j\theta_k} \tag{2.3}$$

and θ_k takes values in the set

$$\left\{\frac{2\pi}{M_P}(i-1)\right\} \qquad \text{for} \quad i = 1,2,...,M_P. \tag{2.4}$$

The random process $u(t-kT_s;\lambda_k)$ represents the equivalent low pass waveform of the transmitted signal, which can be written in the form of

$$u(t-kT_s;\lambda_k) = g(t-kT_s)e^{j2\pi f_d\lambda_k(t-kT_s)+j\varphi} \tag{2.5}$$

where $2f_d$ is the separation between adjacent frequencies, φ is the initial phase introduced by the frequency synthesizer and the random variable λ_k takes values in the set

$$\{2i-1-M_F\} \qquad \text{for} \quad i=1,2,...,M_F. \tag{2.6}$$

The discrete random sequences $\{\zeta_k\}$ and $\{\lambda_k\}$ are independent and stationary, and are referred to as source symbol sequences.

In the simplest form of JFPM, the complex envelope $g(t)$ in (2.5) has a constant amplitude $\sqrt{2S}$ and symbol duration T_s. Thus, the waveforms generated by the JFPM modulator can be expressed as

$$\begin{aligned} s_{mn}(t) &= \Re\left\{\beta_{0mn}(t)e^{j2\pi f_c t}\right\} \qquad 0 \le t \le T_s \qquad (2.7)\\ &= \sqrt{2S}\cos(2\pi f_m t + \theta_n + \varphi) \quad m=1,2,...,M_F \text{ and } n=1,2,...,M_P \end{aligned}$$

where the modulation process $\beta_{kmn}(t)$ denotes the mn-th signal transmitted during the k-th symbol interval and it is given by

$$\beta_{kmn}(t) = \sqrt{2S}e^{j(2\pi f_d \lambda_m (t-kT_s)+\theta_n+\varphi)}. \tag{2.8}$$

In (2.7), f_m is one of the modulated frequencies and takes its value from the set

$$f_m = f_c + (2m-1-M_F)\,f_d \qquad m=1,2,...,M_F. \tag{2.9}$$

The signal set represented in (2.7) can be divided into M_F sets of M_P signals each. It is assumed that the signals in different sets are uncorrelated and orthogonal, and the $M_F \times M_P$ signals have equal energy and equal time duration.

The source emits a random symbol from a set of M symbols every T_s seconds, where

$$M = 2^{k_F+k_P}, \qquad k_F = \log_2 M_F, \qquad k_P = \log_2 M_P, \qquad k_s = k_F + k_P. \tag{2.10}$$

The relationship between the symbol duration T_s and the bit duration T_b is given by $T_s = (k_F + k_P)T_b$.

2.2.2 Correlation Coefficient

The complex-valued correlation coefficient of the JFPM signals can be defined as

$$r = \frac{1}{2E_s}\int_{kT_s}^{(k+1)T_s} \beta_{kmn}(t)\beta_{kil}^{*}(t)dt \tag{2.11}$$

where the signal energy $E_s = ST_s$ and the asterisk denotes the complex conjugate. Without loss of generality, if $k = 0$, the complex-valued correlation coefficient in (2.11) can be written as

$$\begin{aligned} r &= \frac{1}{2E_s}\int_{0}^{T_s} \beta_{0mn}(t)\beta_{0il}^{*}(t)dt \\ &= \frac{1}{T_s}\int_{0}^{T_s} e^{j2\pi f_d\lambda_m t+j\theta_n+j\varphi}e^{-j2\pi f_d\lambda_i t-j\theta_l-j\varphi}dt. \end{aligned} \tag{2.12}$$

By setting $\lambda_k = 2k-1-M_F$ and substituting for λ_m and λ_i, the integral in (2.12) gives (for $m \neq i$)

$$r = \frac{\sin 2\pi f_d T_s(m-i)}{2\pi f_d T_s(m-i)}e^{j2\pi f_d T_s(m-i)+j(\theta_n-\theta_l)}. \tag{2.13}$$

The JFPM signals satisfy the orthogonality condition if real the part of the correlation coefficient r is zero, that is

$$\begin{aligned} \Re\{r\} &= \frac{\sin 2\pi f_d T_s(m-i)}{2\pi f_d T_s(m-i)}\cos(2\pi f_d T_s(m-i)+(\theta_n-\theta_l)) \\ &= 0. \end{aligned} \tag{2.14}$$

Thus, in the case where the receiver has perfect knowledge of the signal phases (coherent detection) and when the number of phases is equal to two (i.e., $|\theta_n - \theta_l| = 0$ or π) , $\Re\{r\} = 0$ when the cosine term is zero, i.e., when the frequency separation between two signals $2f_d$ is such that

$$2f_d T_s = \frac{k}{2}, \qquad k \text{ any non zero integer.} \tag{2.15}$$

From (2.15) we observe that the orthogonality condition is met when the minimum frequency separation is such that $2f_dT_s = 0.5$.

In noncoherent detection (or coherent detection with $M_P > 2$), the phase information is not available (or used), the orthogonality condition must be fulfilled independently of the phase of the signals. In this case $\Re\{r\} = 0$ when the sine term is zero, i.e., the orthogonality condition is satisfied when the frequency separation between two signals satisfies

$$2f_dT_s = k, \qquad k \text{ any non zero integer.} \tag{2.16}$$

This means that the minimum frequency separation between two adjacent frequencies is such that $2f_dT_s = 1$.

An interesting relation obtained by observing (2.15) and (2.16) is

$$2f_dT_s = 2f_dk_FT_b\frac{k_F + k_P}{k_F} \tag{2.17}$$

The JFPM signals satisfy the orthogonality condition when the minimum frequency separation between two adjacent tones is $1/T_s$ (or $1/2T_s$). During each symbol time T_s, $(k_F + k_P)$ bits of information are transmitted. Only k_F bits are transmitted, however, during each symbol time $\bar{T}_s$ by M-ary FSK having the same number of tones $M_F = 2^{k_F}$. The symbol time of FSK must then be reduced to $\bar{T}_s = T_sk_F/(k_F + k_P)$ in order to maintain the same information bit rate. The minimum frequency separation between two adjacent tones in this equivalent FSK system is $1/\bar{T}_s$ (or $1/2\bar{T}_s$), and is $(k_F + k_P)/k_F$ wider than the JFPM tone separation of $1/T_s$ (or $1/2T_s$).

2.3 Power Spectral Density

A standard result of the power spectral density of a digitally modulated signal that is generated by a Markov chain is given by [49]. The power spectral density of

JFPM signals may be viewed as a special case of the result given in [49]; in which JFPM waveforms are Markov chain driven process for random memoryless choice of signals. For this class of signals, the source can be modeled as a degenerate case of a Markov source whose transition matrix P has the property $P^m = P$ for all $m \geq 1$, where P^m denotes the m-step transition matrix. The power spectral density of JFPM signals is given by [49, eq. 22], [45, p. 45]

$$\begin{aligned} \mathcal{S}(f) &= \frac{1}{T_s}\left[\sum_{l=1}^{M} p_l \left|S(f;\zeta_l,\lambda_l)\right|^2 - \left|\sum_{l=1}^{M} p_l S(f;\zeta_l,\lambda_l)\right|^2\right] \\ &+ \frac{1}{T_s^2}\left|\sum_{l=1}^{M} p_l S(f;\zeta_l,\lambda_l)\right|^2 \sum_{l=-\infty}^{\infty} \delta\left(f-\frac{l}{T_s}\right), \end{aligned} \tag{2.18}$$

where $S(f;\zeta_l,\lambda_l)$ is the Fourier transform of $s(t;\zeta_l,\lambda_l)$ and p_l is the probability of occurrence of $s(t;\zeta_l,\lambda_l)$.

Defining $U(f;\lambda_l)$ as the Fourier transform of $u(t;\lambda_l)$, and substituting $S(f;\zeta_l,\lambda_l) = \zeta_l U(f;\lambda_l)$ in (2.18) gives

$$\begin{aligned} \mathcal{S}(f) &= \frac{1}{T_s}\left[\sum_{l=1}^{M} p_l \left|\zeta_l U(f;\lambda_l)\right|^2 - \left|\sum_{l=1}^{M} p_l \zeta_l U(f;\lambda_l)\right|^2\right] \\ &+ \frac{1}{T_s^2}\left|\sum_{l=1}^{M} p_l \zeta_l U(f;\lambda_l)\right|^2 \sum_{l=-\infty}^{\infty} \delta\left(f-\frac{l}{T_s}\right). \end{aligned} \tag{2.19}$$

Using $U(f;\lambda_l) = G(f - f_d\lambda_l)$, $G(f)$ is the Fourier transform of $g(t)$, (2.19) can be written as

$$\begin{aligned} \mathcal{S}(f) &= \frac{1}{T_s}\left[\sum_{l=1}^{M} p_l \left|\zeta_l G(f - f_d\lambda_l)\right|^2 - \left|\sum_{l=1}^{M} p_l \zeta_l G(f - f_d\lambda_l)\right|^2\right] \\ &+ \frac{1}{T_s^2}\left|\sum_{l=1}^{M} p_l \zeta_l G(f - f_d\lambda_l)\right|^2 \sum_{l=-\infty}^{\infty} \delta\left(f-\frac{l}{T_s}\right). \end{aligned} \tag{2.20}$$

For equally probable symbols $p_l = 1/M$ for all l and when the number of phases used is greater than one, the last two term of (2.20) are vanish and the power spectral density of the JFPM signals given in (2.20) reduced to

$$\begin{aligned} \mathcal{S}(f) &= \frac{1}{MT_s}\sum_{l=1}^{M}|\zeta_l G(f-f_d\lambda_l)|^2 \\ &= \frac{1}{M_F T_s}\sum_{l=1}^{M_F}|G(f-f_d\lambda_l)|^2 \end{aligned} \tag{2.21}$$

Assuming that the complex envelope $g(t)$ is a rectangular pulse with unit amplitude and duration T_s, it follows that

$$|U(f;\lambda_l)|^2 = T_s^2\left(\frac{\sin\pi(f-f_d\lambda_l)T_s}{\pi(f-f_d\lambda_l)T_s}\right)^2. \tag{2.22}$$

By substituting (2.22) into (2.21), the power spectral density of the JFPM signals is found to be

$$\mathcal{S}(f) = \frac{1}{M_F T_s}\sum_{l=1}^{M_F}\left(\frac{\sin\pi(f-f_d\lambda_l)T_s}{\pi(f-f_d\lambda_l)T_s}\right)^2. \tag{2.23}$$

Thus the spectrum of JFPM does not contain a discrete spectral components but consists of a continuous spectrum whose shape depends only on the spectral characteristic of the signal pulse. The above analysis can be concluded by observing two factors which affect the shape of the signal spectrum, independently. The first factor is the shape of the complex envelope waveform $g(t)$. The second factor is the correlation of the sequence $\{\zeta_k\}$. When no spectral shaping is employed, and for frequencies far from the center frequency, the spectra of JFPM signals fall off at a rate proportional to the inverse of the frequency difference squared.

2.4 Bandwidth Efficiency

One of the important spectral properties of a communication system is bandwidth efficiency. Bandwidth efficiency, expressed in bit/s/Hz, is a measure of the so-called channel throughput, which can be defined as the information bit rate that can be transmitted per unit of bandwidth for a given modulation scheme with a specific acceptable bit error rate. This parameter shows how well the digital communication link makes use of the available channel bandwidth. To make a meaningful derivation of the bandwidth efficiency, it is convenient to derive it for a particular measure of signal bandwidth. Actually there is no unique measure of the signal bandwidth and the simplest and most popular measures of the signal bandwidth [45] are based on half power bandwidth, null-to-null bandwidth, minimum frequency separation bandwidth, fractional power containment bandwidth, bounded power spectral density bandwidth and equivalent noise bandwidth. In this section, the bandwidth efficiency based on minimum frequency separation bandwidth, null-to-null bandwidth and fractional power containment bandwidth are analyzed and numerically evaluated.

2.4.1 Bandwidth Efficiency Based on Minimum Frequency Separation Bandwidth

Orthogonality of JFPM waveforms, which are coherently detected, requires a minimum frequency separation $\Delta f = 2f_d$, where $2f_d = 1/2T_s$. In noncoherent detection, orthogonality requires a minimum frequency separation $\Delta f = 2f_d = 1/T_s$. In JFPM, the required carrier bandwidth will almost always be determined by its FSK part but not by the PSK part. Consequently, the required channel bandwidth for transmission can be approximated by [46, p. 254]

$$W = M_F \Delta f. \tag{2.24}$$

However, the bit rate is given by $R_b = \log_2 M/T_s = (\log_2 M_F + \log_2 M_P)/T_s$. Hence, for coherent JFPM the bandwidth efficiency is

$$\frac{R_b}{W} = \frac{2(\log_2 M_F + \log_2 M_P)}{M_F} \tag{2.25}$$

For noncoherent JFPM, the bandwidth efficiency is given by

$$\frac{R_b}{W} = \frac{\log_2 M_F + \log_2 M_P}{M_F} \tag{2.26}$$

The expressions given in (2.25) and (2.26) show that as the number of keying frequencies M_F increases, the bandwidth required for transmission also increases and the bandwidth efficiency decreases. If the number of keying phases M_P increases, the bandwidth required for transmission decreases and the bandwidth efficiency increases.

2.4.2 Bandwidth Efficiency Based on Null-to-Null Bandwidth

The null-to-null bandwidth W_{nn} represents the width of the main spectral lobe. According to (2.23), the first zero of the power spectral density $S(f)$ is determined by the term $l = M_F$, which is

$$\frac{\sin^2(\pi(f - f_d\lambda_{M_F})T_s)}{(\pi(f - f_d\lambda_{M_F})T_s)^2} \tag{2.27}$$

Considering only the first zero frequency (denoted as f_n), this can be found by letting

$$\pi(f_n - f_d\lambda_{M_F})T_s = \pi \tag{2.28}$$

or

$$f_n = \frac{1}{T_s} + f_d\lambda_{M_F} \tag{2.29}$$

The null-to-null bandwidth is

$$W_{nn} = 2f_n = \frac{2 + 2f_dT_s\lambda_{M_F}}{T_s} \tag{2.30}$$

using $\lambda_{M_F} = M_F - 1$ and $T_s = (\log_2 M_F + \log_2 M_P)/R_b$, then

$$W_{nn} = \frac{2 + 2f_dT_s(M_F - 1)}{\log_2 M_F + \log_2 M_P} R_b \tag{2.31}$$

For $2f_dT_s = 0.5$, the bandwidth efficiency is given by

$$\frac{R_b}{W_{nn}} = \frac{\log_2 M_F + \log_2 M_P}{2 + (M_F - 1)/2} \tag{2.32}$$

and for $2f_dT_s = 1$, the bandwidth efficiency is given by

$$\frac{R_b}{W_{nn}} = \frac{\log_2 M_F + \log_2 M_P}{M_F + 1} \tag{2.33}$$

2.4.3 Bandwidth Efficiency based on Fractional Power Containment Bandwidth

In practice, bandwidth efficiency depends entirely upon the roll-off factor of the filters used. As well, channel effects and adjacent channels interference must be included. However, the definition of the bandwidth efficiency may often be modified to cover such cases. From a practical point of view, the bandwidth efficiency of a modulated signal can be calculated in terms of fractional out-of-band power containment. If the total power is normalized to 1, the power contained in bandwidth B may be expressed as

$$\mu_{Bi} = \int_{-B/2}^{B/2} S(f)df. \tag{2.34}$$

Therefore, the fractional out of band power is then defined as

$$\mu_{Bo} = 1 - \mu_{Bi} = 1 - \int_{-B/2}^{B/2} S(f)df. \tag{2.35}$$

If the fractional out of band power containment defined in (2.35) is plotted against the bandwidth normalized by the bit rate (BT_b), bandwidth efficiency can be obtained directly for a given fractional power bandwidth.

2.5 Results and Comparisons

2.5.1 Spectral Characteristics

Our concern in this section is to calculate the power spectral density for different JFPM signal formats. As a short hand notation, the JFPM signal format that results from the combination of x-frequencies and y-phases is referred to as the xF/yP format. The power spectral density derived in (2.23) depends on the parameter $2f_dT_s$. For the JFPM waveforms with $2f_dT_s = 0.5$, substituting the values of λ_k from (2.6) into (2.23), we obtain

$$S(f) = \frac{T_s}{M_F} \sum_{k=1}^{M_F} \left(\frac{\sin \pi(fT_s - [2k - 1 - M_F]/4)}{\pi(fT_s - [2k - 1 - M_F]/4)} \right)^2 . \tag{2.36}$$

For JFPM waveforms with $2f_dT_s = 1$ and by substituting the values of λ_k from (2.6) into (2.23), we obtain

$$S(f) = \frac{T_s}{M_F} \sum_{k=1}^{M_F} \left(\frac{\sin \pi(fT_s - [2k - 1 - M_F]/2)}{\pi(fT_s - [2k - 1 - M_F]/2)} \right)^2 . \tag{2.37}$$

Our observation on (2.36) and (2.37) is that, when $M_F = 1$, the power spectral density of a JFPM signal is reduced to the power spectral density of an M_P-ary PSK signal.

The power spectral density (as a function of the normalized frequency fT_b) of JFPM waveforms with the M_FF/2P format (for $M_F = 1, 2, 4, 8, 16$ and $2f_dT_s = 0.5$) is plotted in Fig. 2.2. The same family of curves representing the power spectral density of JFPM waveforms with the M_FF/2P format when $2f_dT_s = 1$ is illustrated in Fig. 2.3. From Fig. 2.2 and Fig. 2.3, we observe that the main spectral lobe of JFPM with $2f_dT_s = 1$ is wider than that of JFPM with $2f_dT_s = 0.5$ for the same value of M_F. The power spectrum density of JFPM with M_FF/4P and M_FF/8P formats (for $M_F = 1, 2, 4, 8, 16$ and $2f_dT_s = 1$) is plotted versus fT_b in Fig. 2.4 and Fig. 2.5 respectively. From a comparison of Fig. 2.4 and Fig. 2.5, it is evident that for

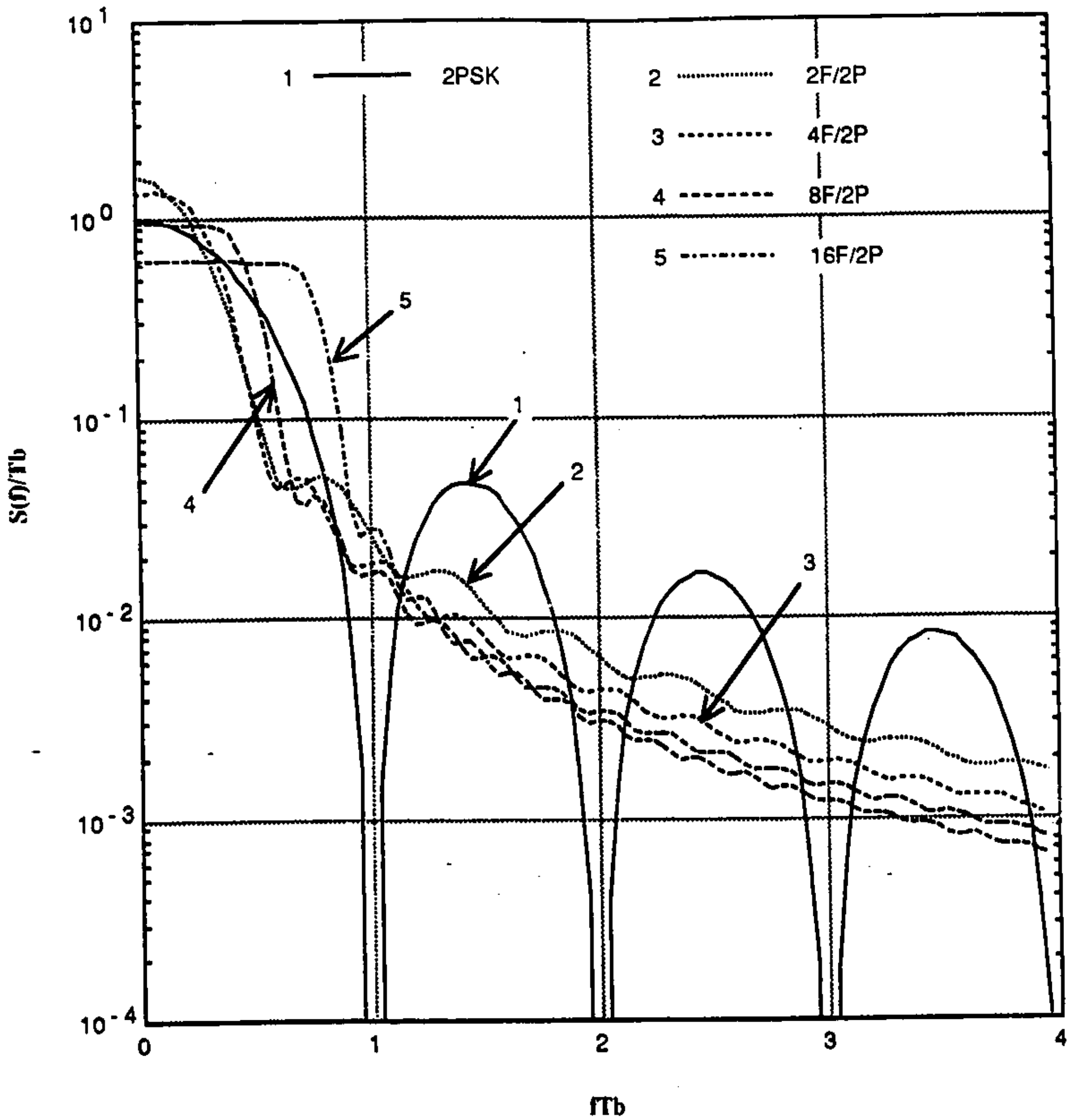

Figure 2.2 : Normalized power spectral density of a JFPM signal (with a combination M_FF/2P and $2f_dT_s = 0.5$) as a function of fT_b when M_F=1,2,4,8,16.

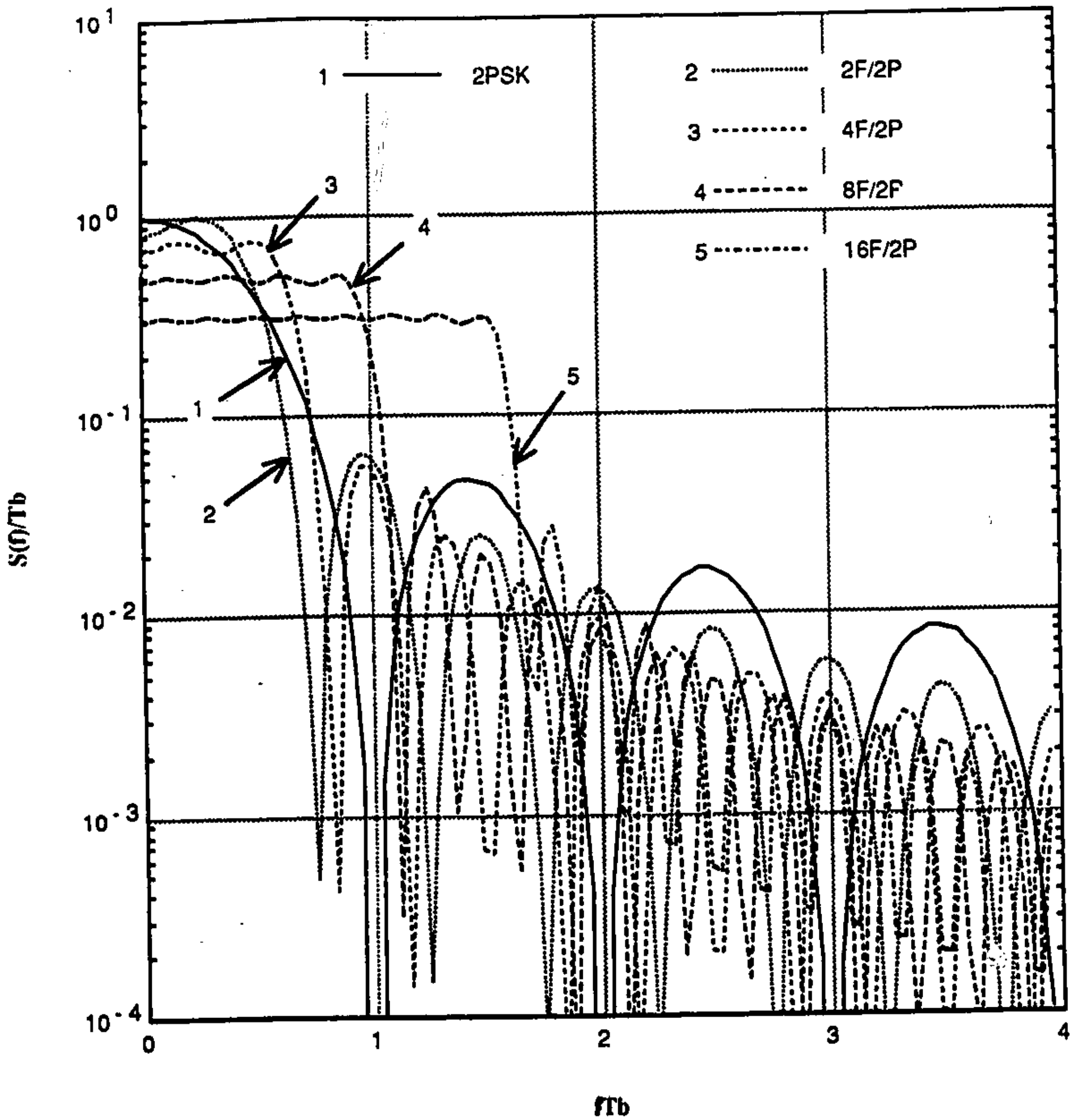

Figure 2.3 : Normalized power spectral density of a JFPM signal (with a combination $M_F F/2P$ and $2f_d T_s = 1$) as a function of fT_b when M_F=1,2,4,8,16.

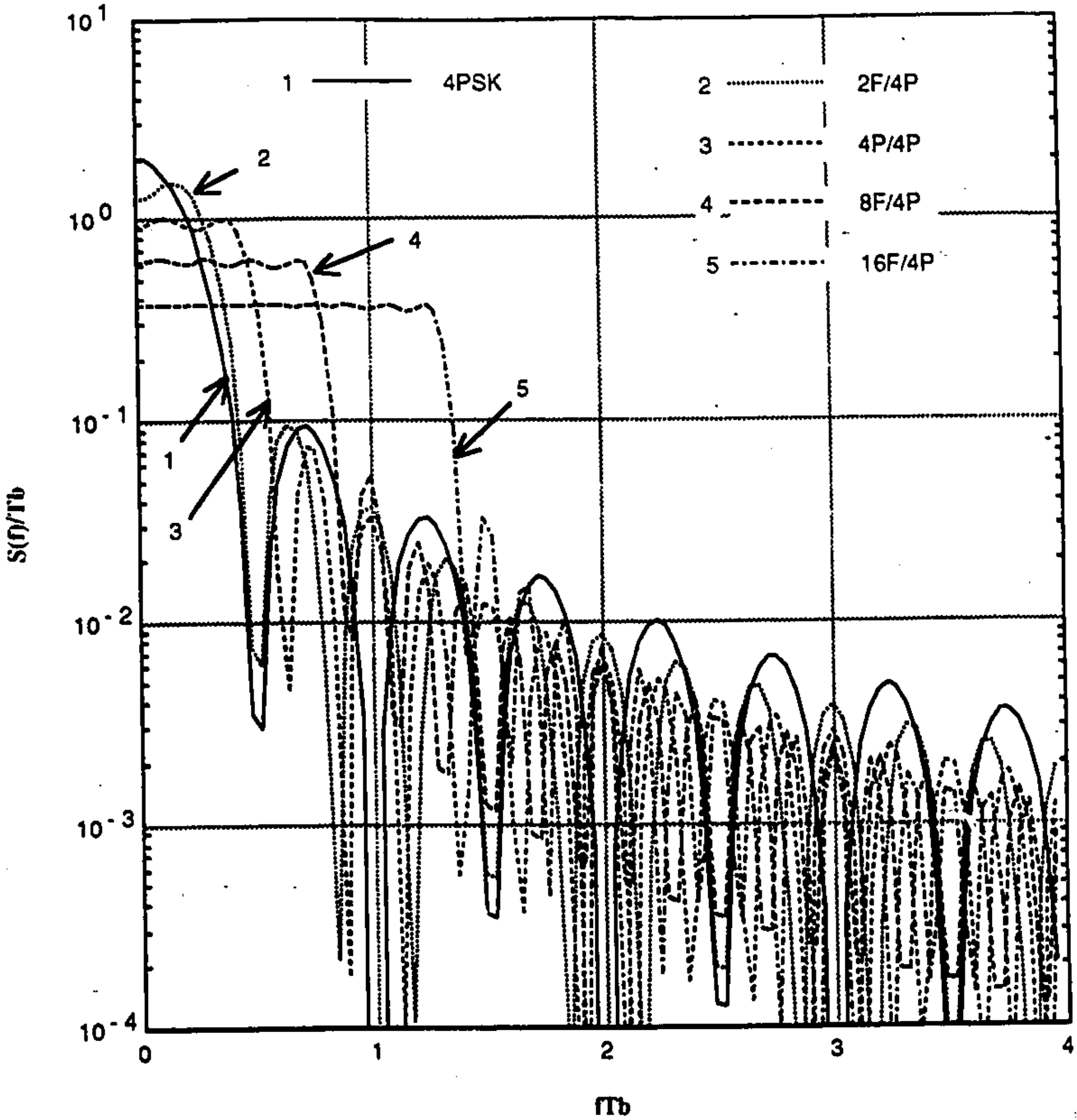

Figure 2.4 : Normalized power spectral density of a JFPM signal (with a combination $M_F F/4P$ and $2f_d T_s = 1$) as a function of fT_b when M_F=1,2,4,8,16.

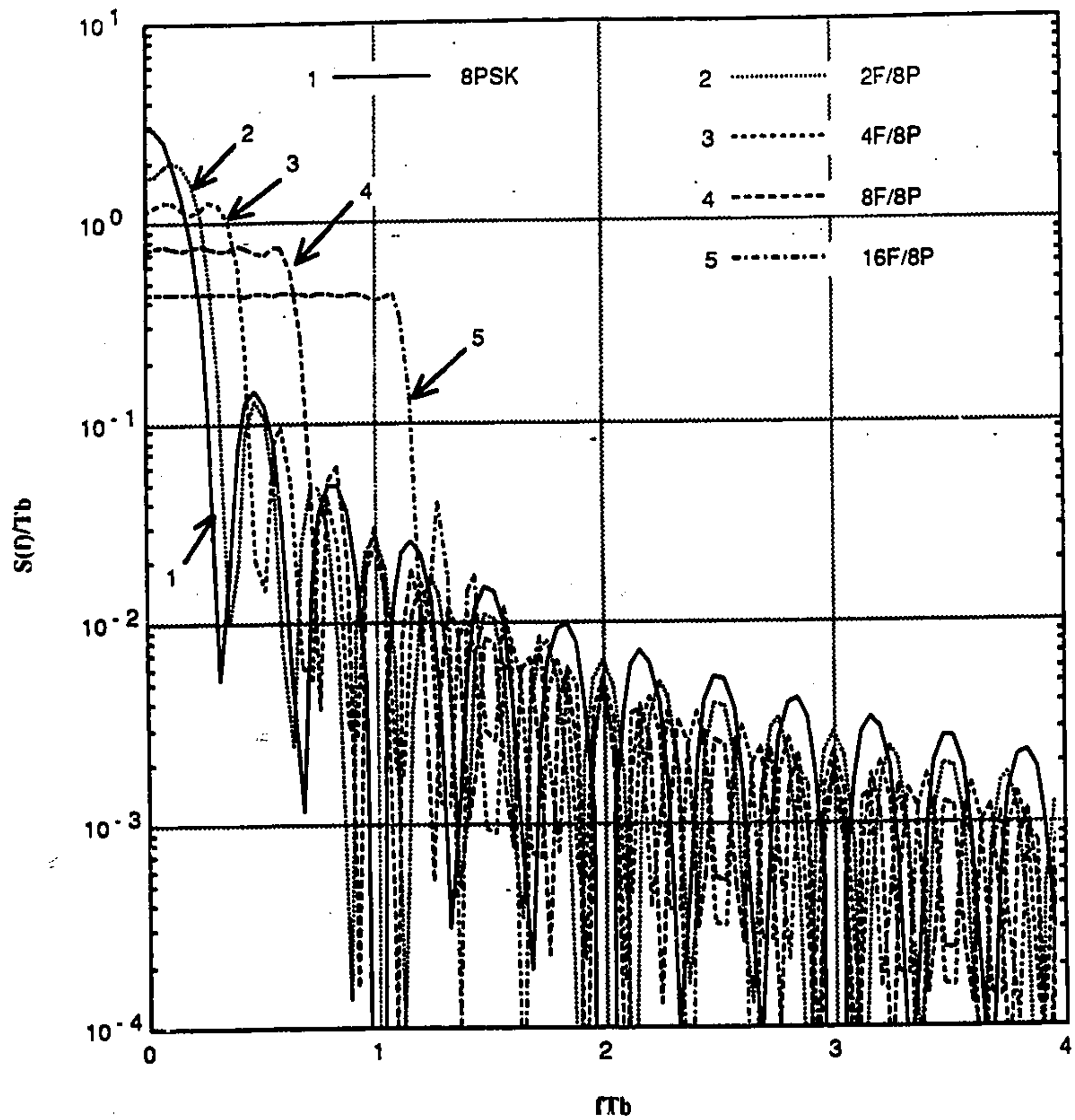

Figure 2.5 : Normalized power spectral density of a JFPM signal (with a combination $M_F F/8P$ and $2 f_d T_s = 1$) as a function of fT_b when M_F=1,2,4,8,16.

fixed M_P, and as M_F increases, the main spectral lobe widens, although a reduction in the out-of-band spectral tails is observed.

2.5.2 Bandwidth Efficiency

Bandwidth Efficiency Based on null-to-null Bandwidth

Numerical computations of the bandwidth efficiencies, based on the null-to-null bandwidth, for JFPM, M-ary PSK and MSK are given in Tables 2.1 and 2.2. From these data, we conclude that in terms of null-to-null bandwidth and for a given value of M the bandwidth efficiency of JFPM is less than that of PSK system and it is greater than the bandwidth efficiency of MSK system. Also, the bandwidth efficiency of JFPM with $2f_dT_s = 0.5$ is greater than that of JFPM with $2f_dT_s = 1$.

Table 2.1 : Comparison of null-to-null bandwidth efficiencies in bit/s/Hz for M-ary PSK, MSK and different JFPM formats with $2f_dT_s = 0.5$ (the value of $\eta_{nn} = R_b/W_{nn}$ for MSK is given in [16]).

–	$2f_dT_s = 0.5$				–	–
M	M_FF/2P	M_FF/4P	M_FF/8P	M_FF/16P	PSK	MSK
2	–	–	–	–	0.5	–
4	0.80	–	–	–	1.0	0.67
8	0.86	1.20	–	–	1.5	–
16	0.73	1.14	1.60	–	2.0	–
32	0.53	0.91	1.43	2.00	2.5	–
64	0.33	0.63	1.09	1.71	3.0	–

Bandwidth Efficiency Based on Fractional Power Containment Bandwidth

The fractional out-of-band power containment of JFPM with M_FF/2P format obtained by substituting (2.36) into (2.35) is plotted versus the normalized bandwidth BT_b in Fig. 2.6, for different values of M_F. The same family of curves for JFPM obtained by substituting (2.37) into (2.35) is plotted in Fig. 2.7. From this family

Table 2.2 : Comparison of null-to-null bandwidth efficiencies in bit/s/Hz for M-ary PSK, MSK and different JFPM formats with $2f_dT_s = 1$.

–	$2f_dT_s = 1.0$				–	–
M	M_FF/2P	M_FF/4P	M_FF/8P	M_FF/16P	PSK	MSK
2	–	–	–	–	0.5	–
4	0.67	–	–	–	1.0	0.67
8	0.60	1.00	–	–	1.5	–
16	0.44	0.80	1.33	–	2.0	–
32	0.29	0.55	1.00	1.66	2.5	–
64	0.18	0.35	0.67	1.20	3.0	–

of curves, we conclude that the normalized bandwidth of JFPM with $2f_dT_s = 0.5$ is smaller than that of JFPM with $2f_dT_s = 1$ for any given value of fractional out-of-band power containment.

The curves of fractional out-of-band power containment for JFPM with M_FF/4P and M_FF/8P formats obtained by substituting (2.37) into (2.35) are plotted versus the normalized bandwidth BT_b in Fig. 2.8 and Fig 2.9, respectively. From these and other plots we conclude that, for any fixed M_F and as the number of phases M_P increase, the bandwidth efficiency of JFPM is increased and the out-of-band spectral tails are reduced.

Numerical computations of the bandwidth efficiencies for JFPM, M_P-ary PSK and continuous phase FSK (CPFSK) are given in Table 2.3 and Table 2.4 for the bandwidth that contains 90% and 99% of the total power, respectively. Our observation of the data in Table 2.3 and Table 2.4 is that, by using JFPM, there are many possibilities for choosing the bandwidth efficiency of the desired system (as allowed in the design). In terms of 90% power bandwidth efficiency, one can observe that, for $M > 4$ the bandwidth efficiency of JFPM is greater than that of the CPFSK system with the same M. It can also be observed that, for any fixed value of M, the bandwidth efficiency of JFPM is smaller than that of the M-ary PSK system.

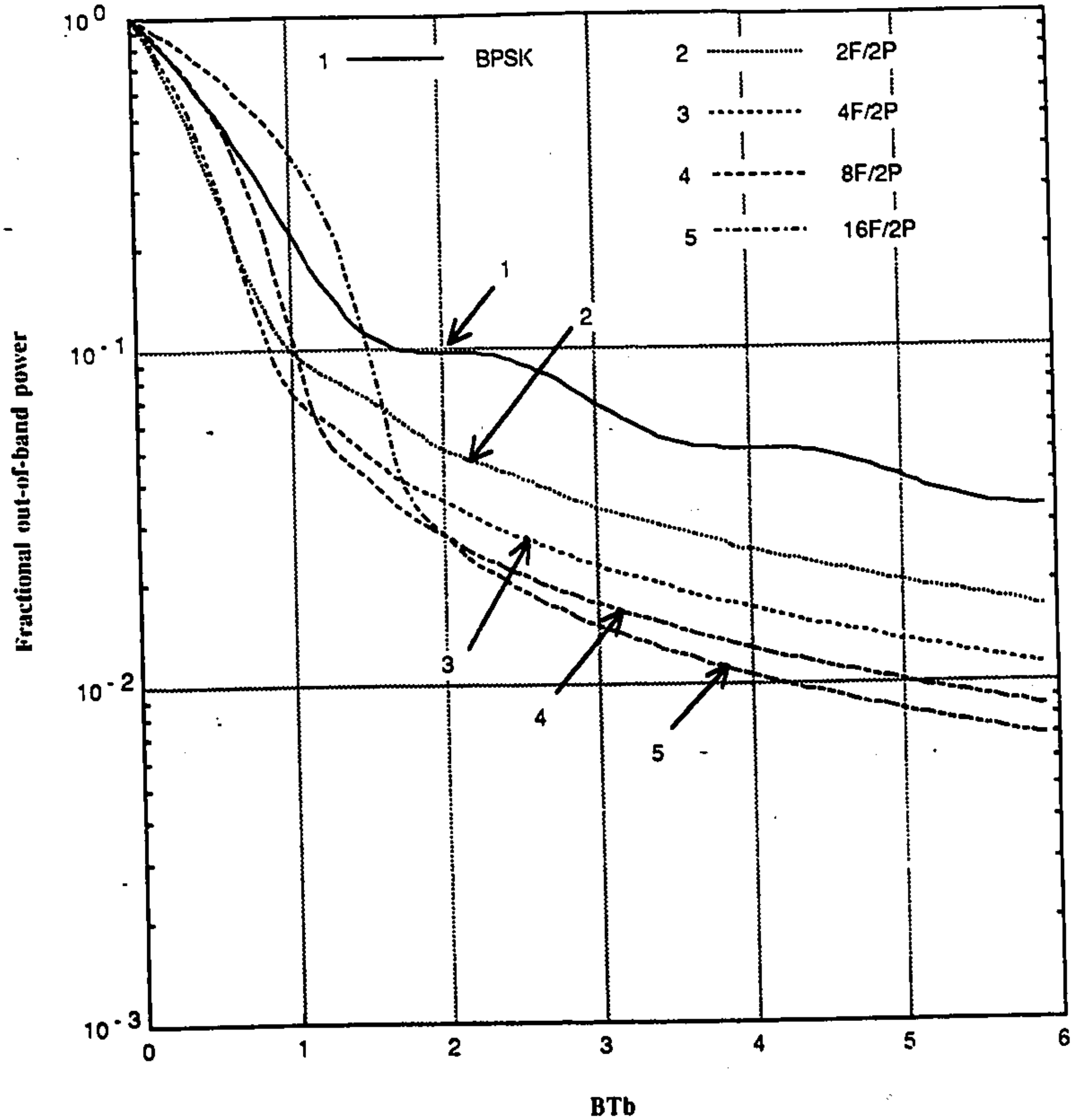

Figure 2.6 : Fractional out-of-band power of JFPM as a function BT_b with $M_F F/2P$ format when $M_F = 1, 2, 4, 8, 16$ $(2f_d T_s = 0.5)$.

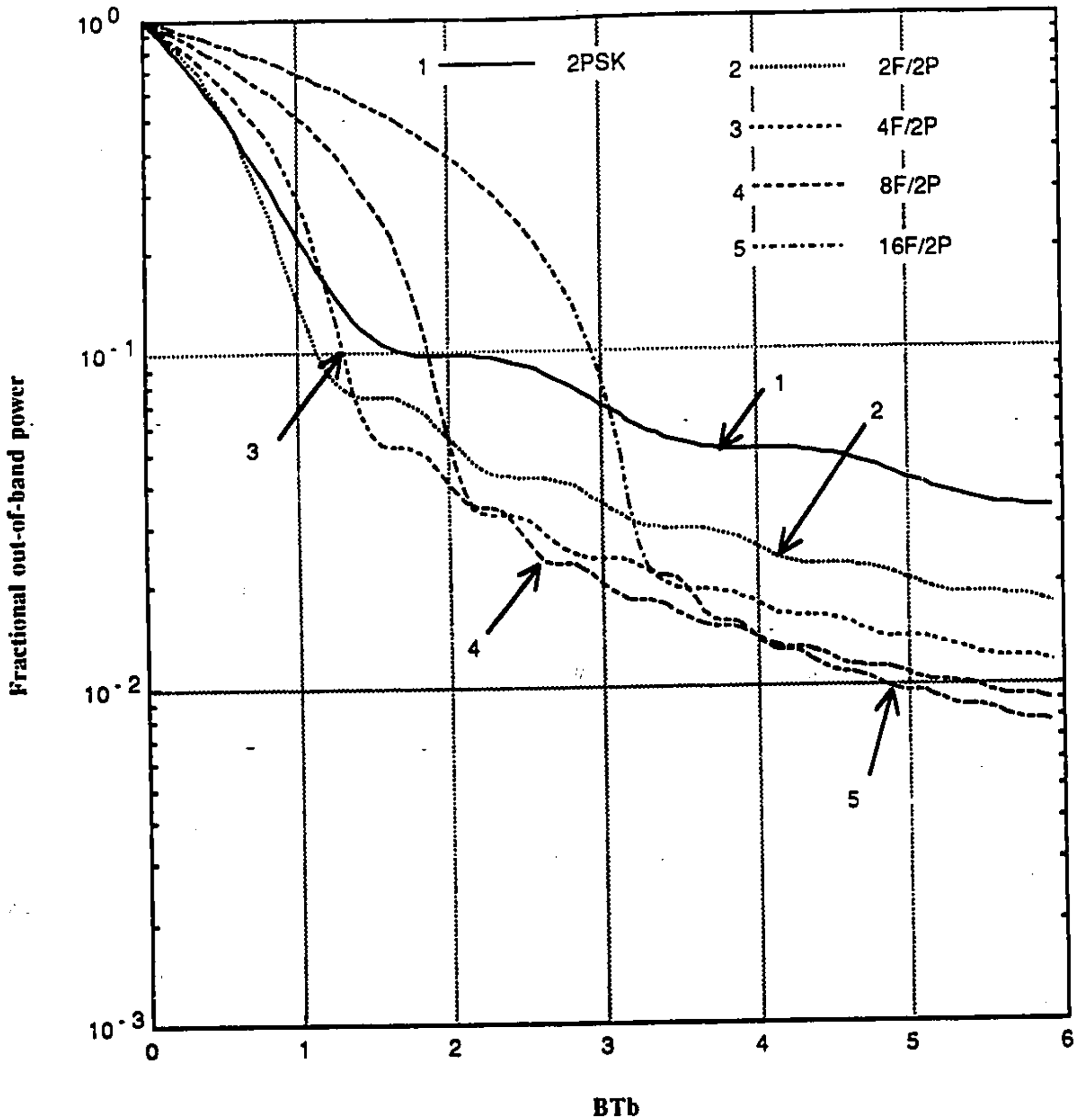

Figure 2.7 : Fractional out-of-band power of JFPM as a function BT_b with $M_F F/2P$ format when $M_F = 1, 2, 4, 8, 16$ $(2f_d T_s = 1)$.

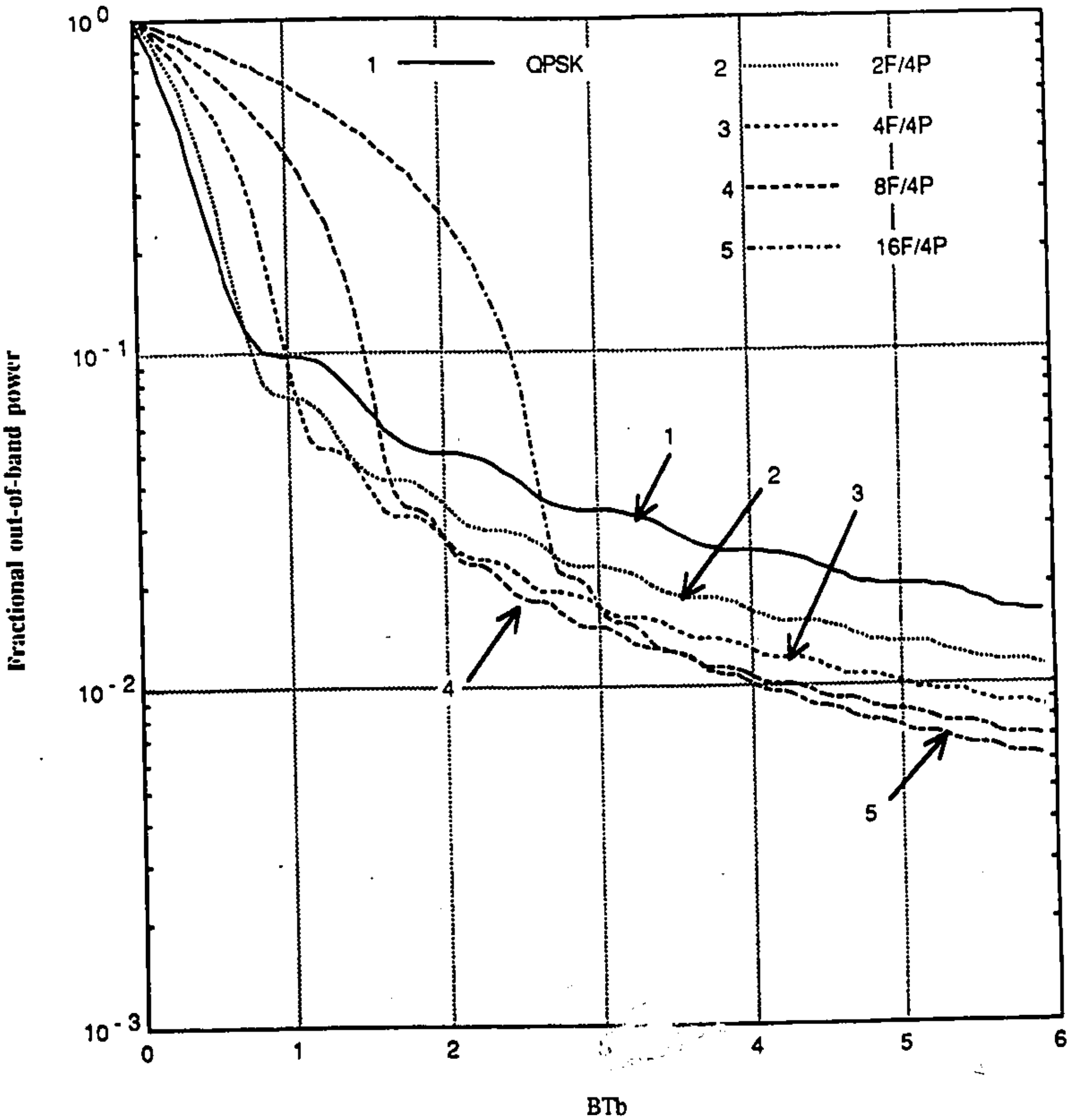

Figure 2.8 : Fractional out-of-band power of JFPM as a function BT_b with $M_F F/4P$ format when $M_F = 1, 2, 4, 8, 16$ $(2f_d T_s = 1)$.

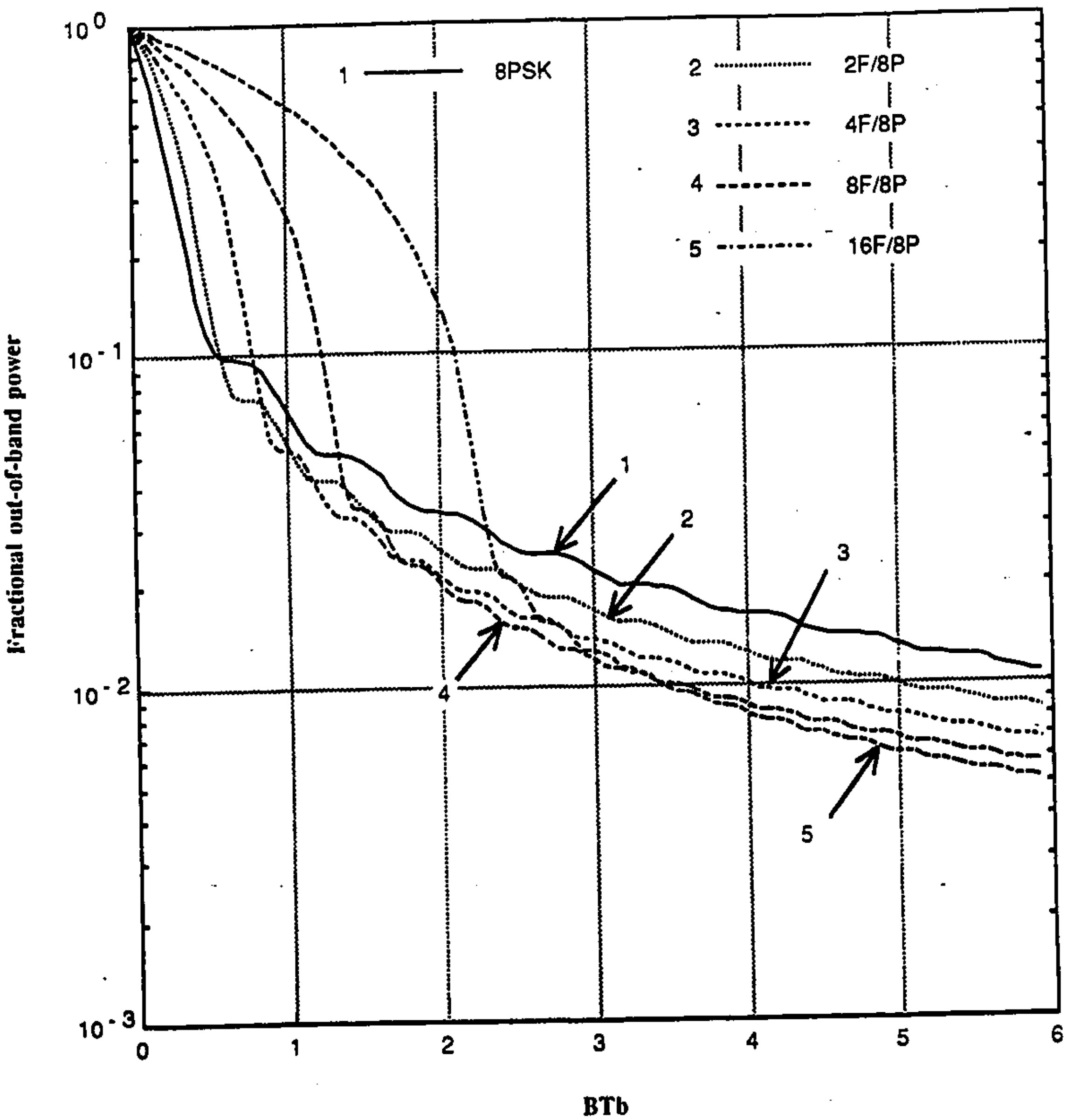

Figure 2.9 : Fractional out-of-band power of JFPM as a function BT_b with $M_F F/8P$ format when $M_F = 1, 2, 4, 8, 16$ $(2f_dT_s = 1)$.

In terms of 99% power bandwidth efficiency, our observation is that, the bandwidth efficiency for both JFPM and M-ary PSK are very close. However now, CPFSK is more bandwidth efficient than JFPM.

Table 2.3 : Comparison of 90% power bandwidth efficiencies in b/s/Hz for M-ary PSK, CPFSK and different JFPM formats (the values of $(1/BT_b)$ for the conventional M-ary CPFSK are given in [16] and [34]).

–	$2f_dT_s = 0.5$	$2f_dT_s = 1$				–	–
M	M_FF/2P	M_FF/2P	M_FF/4P	M_FF/8P	M_FF/16P	MPSK	CPFSK
2	–	–	–	–	–	0.591	1.250
4	0.993	0.877	–	–	–	1.188	1.180
8	1.156	0.764	1.317	–	–	1.789	–
16	0.967	0.535	1.018	1.756	–	2.398	0.560
32	0.662	0.340	0.669	1.273	2.197	2.900	–
64	0.408	0.206	0.408	0.803	1.528	3.470	0.210
128	0.241	0.121	0.241	0.476	0.937	4.070	–

Table 2.4 : Comparison of 99% power bandwidth efficiencies in b/s/Hz for M-ary PSK, CPFSK and different JFPM formats.

–	$2f_dT_s = 0.5$	$2f_dT_s = 1$				–	–
M	M_FF/2P	M_FF/2P	M_FF/4P	M_FF/8P	M_FF/16P	MPSK	CPFSK
2	–	–	–	–	–	0.052	0.830
4	0.105	0.101	–	–	–	0.104	0.790
8	0.156	0.150	0.153	–	–	0.150	–
16	0.202	0.194	0.201	0.207	–	0.210	0.470
32	0.240	0.208	0.244	0.252	0.271	0.250	–
64	0.249	0.174	0.250	0.294	0.305	0.300	–
128	0.202	0.110	0.204	0.292	0.344	0.350	–

2.6 Conclusions

In the first part of this chapter, a mathematical model of JFPM signals was presented. Such signals are characterized by relative simplicity in obtaining a large set of waveforms. The modulated signal has a constant-envelope and therefore is of interest for use in nonlinear and/or fading channels. We restricted our attention to the orthogonal JFPM signals. In this case, the minimum frequency separation between the two adjacent tones of JFPM signals is reduced compared to FSK signals that use the same number of tones. Thus, requiring less bandwidth for the same bit rate.

In the second part of this chapter, the power spectral density of JFPM signals was analyzed. This analysis concluded that the spectral density of JFPM does not contain discrete components (which waste power) and contains only continuous components which carry the information. The main factor affecting the shape of the signal spectrum is the complex envelope of the waveform.

Finally, the spectral efficiency of JFPM signal was studied. It can be concluded that the same bandwidth efficiency may be achieved by using different combinations of JFPM formats, which give the system designer a freedom of choice.

Chapter 3

Demodulation and Error Performance of JFPM Signals over AWGN Channels

3.1 Introduction

Evaluation of a digital modulation technique (EDMT) involves many parameters and constraints. The most important parameters of EDMT that are well known and used in the literature can be stated as: bit error rate (P_e), E_b/N_0, bandwidth efficiency and complexity. Therefore, the cost function of EDMT may be written as

$$\text{EDMT} = f(P_e, E_b/N_0, R/W, C) \tag{3.1}$$

where P_e is the performance target, E_b/N_0 is a measure of the power expenditure, R/W is a measure of the bandwidth required for a given data rate, and C is the complexity or the cost. The constraints on EDMT depend heavily on the applications and on the channels to be used where the power and the bandwidth are limited. Therefore, these constraints force the designer to seek to minimize the bit error rate, minimize the required power, maximize the bandwidth efficiency and minimize the complexity.

It should be noted that all of the EDMT parameters are related to each other. The bit error rate can be easily expressed in terms of E_b/N_0 and The complexity C is related to all of the other parameters.

The growing need for digital transmission demands efficient utilization of bandwidth and power. This has led to the search for power and bandwidth efficient modulation techniques for use in mobile and satellite channels. The preceding chapter considered the signal properties and the spectral efficiency of JFPM signals. Here, we study the bit error rate performance of JFPM signals.

This chapter is organized as follows. Section 3.2 describes the Transmission Model of JFPM signals. In Section 3.3, we review some previous research which covered the operation of the receiver structure and bit error rate performance of coherently detected JFPM signals in AWGN channels. In Section 3.4, the receiver structure of differentially detected JFPM signals is obtained and the probability of a bit error is analyzed. Finally, conclusions are drawn in Section 3.5.

3.2 Transmission Model

In JFPM modulation system, the transmitted signal in the k-th signaling interval is represented by

$$s_{mn}(t) = \sqrt{\frac{2E_s}{T_s}} \cos(2\pi f_m t + \theta^{(k)} + \varphi), \quad kT_s < t \leq (k+1)T_s \tag{3.2}$$

where φ is the initial phase introduced by the frequency synthesizer whose frequencies are such that their phase changes over an interval of T_s is a multiple of 2π. $\theta^{(k)}$ is the transmitted phase in the k-th signaling interval and its value depends on the type of detection to be employed. For coherent detection

$$\theta^{(k)} = \left[\theta_n \triangleq \frac{2\pi(n-1)}{M_P}\right] \qquad \text{for} \quad n = 1, ..., M_P.$$

For differential detection

$$\theta^{(k)} = \theta_n + \theta^{(k-1)} \quad \text{modulo } 2\pi,$$

where $\theta_n = 2\pi(n-1)/M_P$ is the differential phase to be transmitted in the k-th signaling interval and $\theta^{(k-1)}$ is the total accumulated phase (modulo 2π) until the end of $(k-1)$-th signaling interval.

Assume a nondistorting linear time-invariant channel with transfer function $H(f)$,

$$H(f) = e^{j\Omega(f)}. \tag{3.3}$$

In this channel there is no amplitude distortion and $\Omega(f)$ is a linear function of frequency, i.e. the channel delay, τ, is constant for all frequencies and

$$\Omega(f) = 2\pi f\tau. \tag{3.4}$$

The system noise $\nu(t)$ is an additive white Gaussian noise (AWGN) process with one-sided power spectral density N_0. It is further assumed that the intersymbol interference (ISI) from the adjacent symbols is negligible (this is especially true when the frequency spacing between successive symbols is large [32]).

If the waveform $s_{mn}(t)$ in (3.2) is transmitted, the received signal during the k-th symbol interval is given by

$$s_r(t) = \sqrt{\frac{2E_s}{T_s}} \cos(2\pi f_m t + \theta^{(k)} + \varphi + \Omega(f_m)) + \nu(t) \tag{3.5}$$

where $\Omega(f_m)$ is the phase introduced by the channel which is assumed to be constant for each frequency.

3.3 Performance with Coherent Detection

As mentioned in Chapter 1, the performance of coherently detected JFPM signals in an AWGN channel have been studied by [7]-[9]. However, it is perhaps worthwhile to review some of the previous work which covered the operation of the receiver structure and bit error rate performance. Hence, in this section we restrict our discussion to the optimum receiver structure and the bit error rate performance of JFPM.

3.3.1 Optimum Receiver

In coherent detection, the receiver needs a carrier reference whose phase is close to the phase of the incoming signal. If we assume that each of the JFPM waveforms is equiprobable, then the receiver producing the lowest possible average error rate is the maximum likelihood receiver which merely needs to correlate the received signal $s_r(t)$ with all possible $M_F \times M_P$ noiseless waveforms given in (2.7) and decide on the symbol that results in the largest correlation. The optimum receiver structure of JFPM signals is shown in Fig. 3.1.

It was shown in [9] that the symbol error probability of the coherently detected JFPM signals is given by

$$\begin{aligned} P_e(M) = 1 \quad - \quad & \frac{1}{\sqrt{\pi}} \int_0^{\infty} \operatorname{erf}\left(\omega \tan \frac{\pi}{M_P}\right) e^{-(\omega - \sqrt{\rho})^2} \\ \times \quad & \left[\frac{M_P}{\sqrt{\pi}} \int_0^{\omega} \operatorname{erf}\left(v \tan \frac{\pi}{M_P}\right) e^{-v^2} dv \right]^{M_F - 1} d\omega, \end{aligned} \tag{3.6}$$

where ρ denotes the signal-to-noise ratio for each k_s-bit defined as

$$\rho = \frac{E_s}{N_0} = \frac{ST_s}{N_0}. \tag{3.7}$$

E_s represents the received symbol energy, S is the signal power and $\operatorname{erf}(u)$ is the error function given by

$$\operatorname{erf}(u) = \frac{2}{\sqrt{\pi}} \int_0^u e^{-t^2} dt.$$

The relationship between the signal-to-noise ratio per symbol and the signal-to-noise

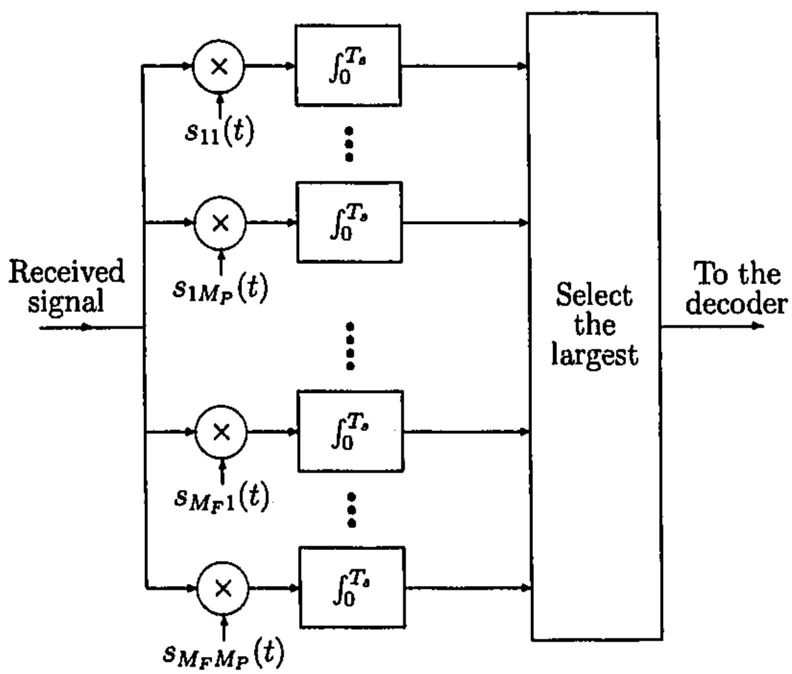

Figure 3.1 : The optimum cross-correlation-type coherent demodulator of the JFPM.

ratio per bit can be expressed as

$$\rho = k_s \rho_b = (k_F + k_P)\rho_b. \tag{3.8}$$

The special cases of $M_P = 2$ and $M_P = 4$, the error probability performance of an M-ary JFPM signal set of $M = M_F \times M_P$ signals is equivalent to that of biorthogonal signal set of M signals. That is

$$P_e(M) = 1 - \frac{1}{\sqrt{\pi}} \int_0^\infty [\text{erf}(\omega)]^{(M/2-1)} \, e^{-(\omega-\sqrt{\rho})^2} d\omega \tag{3.9}$$

For equiprobable and equal energy M-ary biorthogonal signals including $M_F F/2P$, the bit error probability is upper bounded in [16], [47] by

$$P_b(M) \leq \frac{M-2}{4} \text{erfc}\left(\sqrt{\frac{\rho}{2}}\right) + \frac{1}{2} \text{erfc}\left(\sqrt{\rho}\right) \tag{3.10}$$

Exact values of ρ_b required for a given $P_b(M)$ with biorthogonal signals sets are given in [47, Table 5.2], and are reproduced in Fig. 3.2 for various values of M.

3.3.2 Results of Coherent Detection

The two basic measures of performance in digital modulations are the bit error rate (BER) and the bandwidth efficiency. The probability of a bit error as a function of ρ_b has been plotted in Fig. 3.2 for M_FF/2P JFPM format when M_F=2,4,8,16. From this figure it can be observed that, for a given error probability, JFPM requires less power than BPSK and QPSK.

A comparison of JFPM with different modulation schemes based on the normalized data rate R_b/W versus ρ_b required to achieve 10^{-5} BER are tabulated in Table 3.1. In this table, the bandwidth efficiencies of JFPM with M_FF/2P are calculated by using (2.25) i.e., bandwidth efficiency based on minimum frequency separation bandwidth. As well, the bandwidth efficiency of M-ary PSK has been calculated using

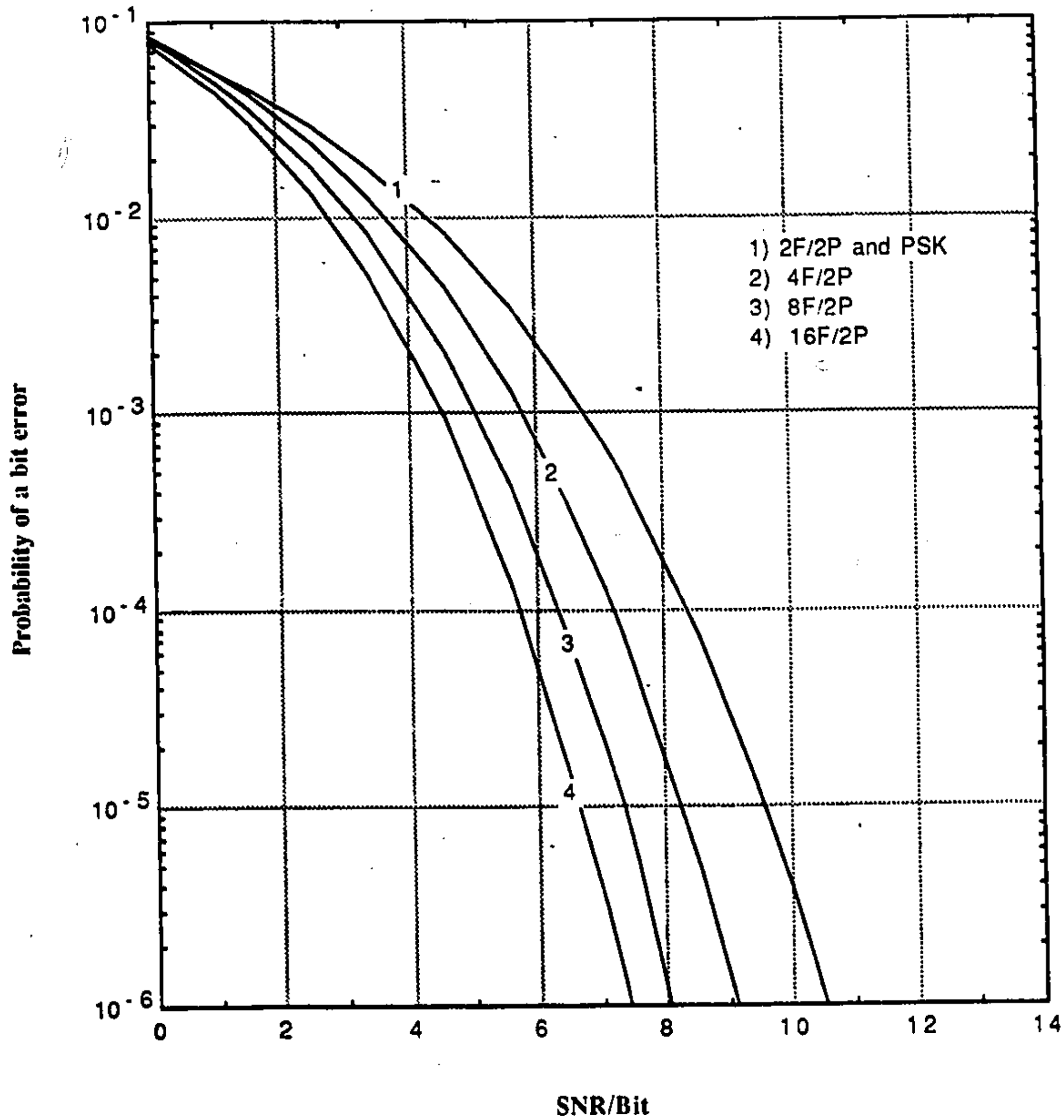

Figure 3.2 : Additive white Gaussian noise channel bit error probability of coherent JFPM with a combination $M_F F/2P$ when $M_F = 2, 4, 8, 16$.

the theoretical minimum bandwidth; in practice a wider bandwidth (a function of the roll-off factor of the filters employed) is occupied resulting in a smaller bandwidth efficiency. From the data in Table 3.1, it is clear that JFPM performs better than the

Table 3.1 : Power and bandwidth efficiencies, based on minimum frequency separation bandwidth, of coherent JFPM, M-ary PSK and coherent M-ary FSK in an AWGN channel. ($P_{eb} = 10^{-5}$, ρ_b in dB, R_b/W in bits/s/Hz)

–	M_FF/2P		M-ary PSK		M-ary FSK	
M	R_b/W	ρ_b	R_b/W	ρ_b	R_b/W	ρ_b
2	–	–	1.0	9.6	1.000	12.6
4	2.000	9.6	2.0	9.6	1.000	10.0
8	1.500	8.3	3.0	12.9	0.750	8.3
16	1.000	7.4	4.0	17.6	0.500	7.4
32	0.625	6.6	5.0	22.3	0.313	6.6
64	0.375	6.1	6.0	27.3	0.188	6.1

conventional M-ary FSK and M-ary PSK of comparable bandwidth efficiency. For example $R_b/W = 1.0$ bit/s/Hz can be obtained by the conventional BPSK, 2FSK and 4FSK or by the JFPM formats 8F/2P while requiring a ρ_b of 9.6, 12.6, 10.0 and 7.4 dB, respectively. In this particular example, JFPM signals provides power efficiency improvement up to 2.2 dB over BPSK and 5.2 dB over 2FSK.

Table 3.2 : Power and bandwidth efficiencies, based on 90% fractional power containment bandwidth, of coherent JFPM, M-ary PSK and coherent M-ary CPFSK with $2f_dT_s = 0.5$ in an AWGN channel. ($P_{eb} = 10^{-5}$, ρ_b in dB, μ_{90} in bits/s/Hz)

–	M_FF/2P		M-ary PSK		M-ary CPFSK	
M	μ_{90}	ρ_b	μ_{90}	ρ_b	μ_{90}	ρ_b
2	–	–	0.591	9.6	1.250	12.6
4	0.993	9.6	1.188	9.6	1.180	10.0
8	1.156	8.3	1.789	12.9	-	8.3
16	0.967	7.4	2.398	17.6	0.560	7.4
32	0.662	6.6	3.470	22.3	-	6.6
64	0.408	6.1	4.070	27.3	0.210	6.1

Table 3.3 : Power and bandwidth efficiencies, based on 99% fractional power containment bandwidth, of coherent JFPM, M-ary PSK and coherent M-ary CPFSK $2f_dT_s = 0.5$ in an AWGN channel. ($P_{eb} = 10^{-5}$, ρ_b in dB, μ_{99} in bits/s/Hz)

–	M_FF/2P		M-ary PSK		M-ary CPFSK	
M	μ_{99}	ρ_b	μ_{99}	ρ_b	μ_{99}	ρ_b
2	–	–	0.052	9.6	0.830	12.6
4	0.105	9.6	0.104	9.6	0.790	10.0
8	0.156	8.3	0.150	12.9	-	8.3
16	0.202	7.4	0.210	17.6	0.470	7.4
32	0.240	6.6	0.250	22.3	-	6.6
64	0.249	6.1	0.300	27.3	-	6.1

Finally, the power and bandwidth efficiencies of JFPM and the conventional schemes are compared, based on the bandwidth that captures 90% and 99% of the total power. Our observation of the data in Table 3.2 is that the bandwidth efficiency of M-ary PSK is greater than that of the JFPM and CPFSK, but there is a JFPM format whose bandwidth efficiency is very close to that of the M-ary PSK. From the data in Table 3.3, the bandwidth efficiency of JFPM is almost equal to that of the M-ary PSK, while JFPM requires less power than the M-ary PSK. Also, the bandwidth efficiency of JFPM with some formats is higher than that of CPFSK.

3.4 Performance with Differential Detection

In this section, we present the receiver structure and error rate performance of differentially encoded JFPM signals by first discussing the practical problem which it overcomes. In Section 3.3, it was assumed that the receiver was perfectly synchronized in frequency and had exact knowledge of the carrier reference phase. In practice, however, the carrier phase is extracted from the received signal by performing some nonlinear operation that introduces a phase ambiguity [46, p. 315]. In JFPM, this problem can be overcome by employing a differential phase-shift-keyed modulation and differentially coherent demodulation of the JFPM signal phase components.

3.4.1 Receiver Structure

The JFPM signal set consists of M_F subsets of polyphase signals, where the signals in each subset are orthogonal to signals in all other subsets. Because of the special form of this signal set, the differential detection of JFPM signals must be accomplished in two stages. In the first stage the signal set containing the transmitted frequency is estimated. This is the noncoherent FSK part. In the second stage, the phase difference between the present and the previous symbol is estimated. This is the differentially detected PSK (DPSK) part.

The receiver structure for differential detection of a JFPM signal set can take the form as given in Fig. 3.3. The receiver requires M_F noncoherent frequency detectors and a single differential phase detector. The FSK-part can work without any phase information; thus it is independent of the DPSK-part. However, the DPSK-part requires a knowledge of the transmitted frequency. For this purpose, the inputs to the DPSK-part are the one-symbol delayed signal and the estimate of the frequency provided by the FSK-part. This frequency estimate can be obtained from a reference signal generator driven by the output of the FSK-detector. The one symbol delay in the DPSK-part is later compensated in demultiplexing (bit combining) by introducing a one-symbol delay following the FSK detector.

A possible implementation of the one branch of the frequency detector and M_P-ary DPSK detector for the JFPM receiver are shown in Fig. 3.4 and Fig. 3.5. Another possible implementation of M_P-ary DPSK detector is illustrated in Fig. 3.6.

In the DPSK part of a JFPM receiver, the receiver employs two symbol interval in a symbol decision interval, each of the phases may or may not have been transmitted

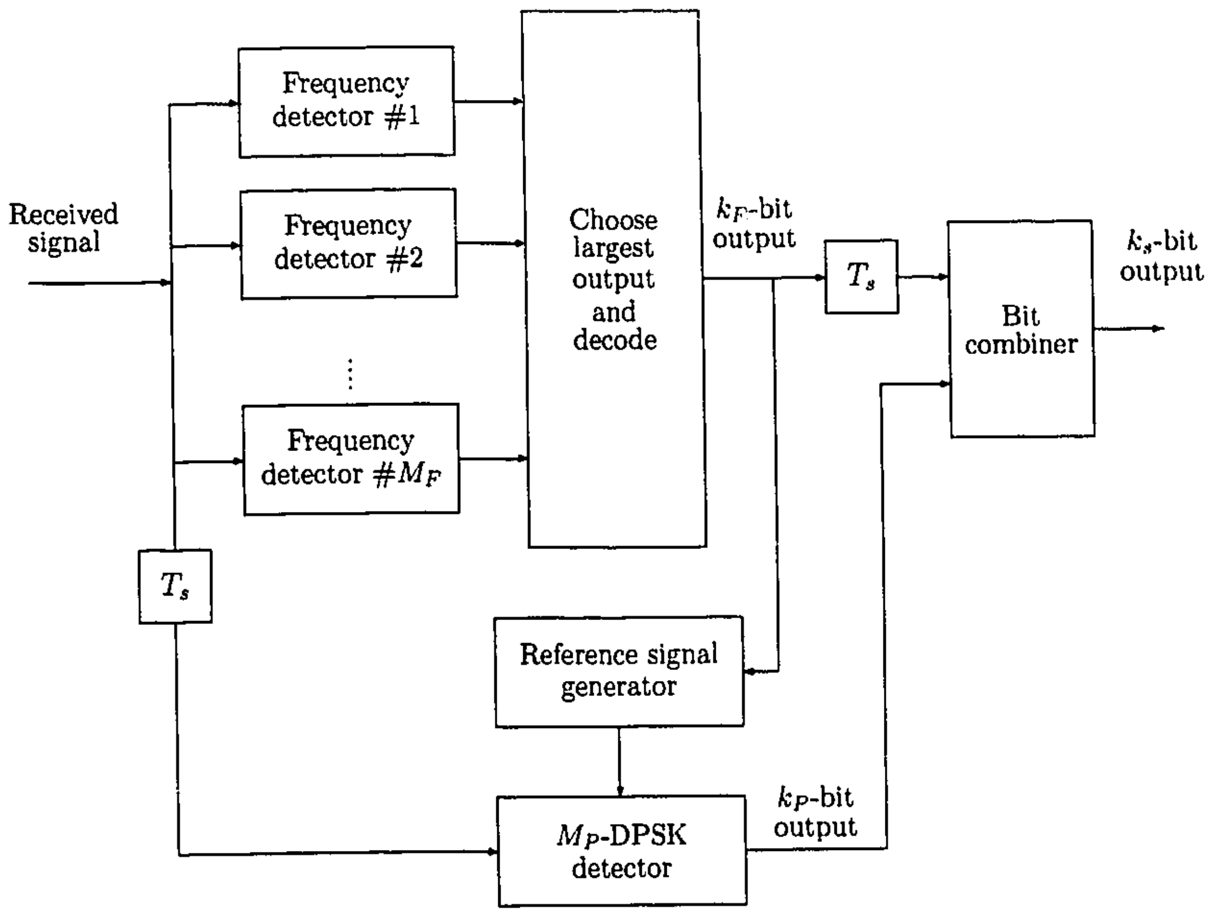

Figure 3.3 : Block diagram of differentially detected JFPM receiver.

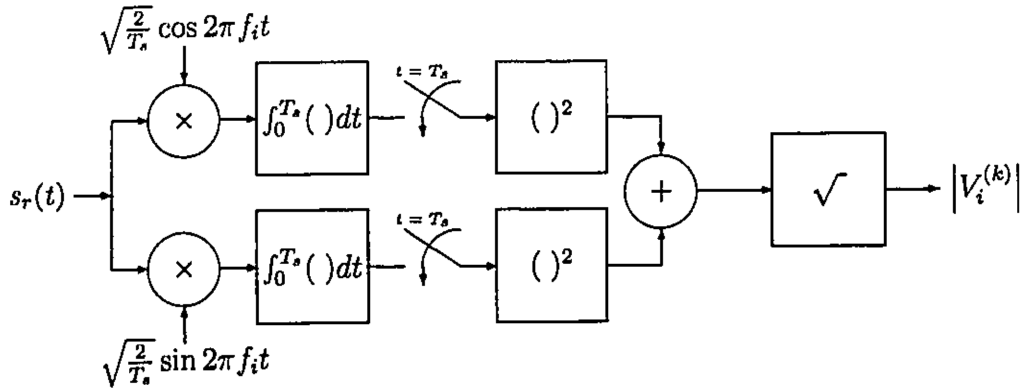

Figure 3.4 : Matched filter with square-law detector (frequency detector # i).

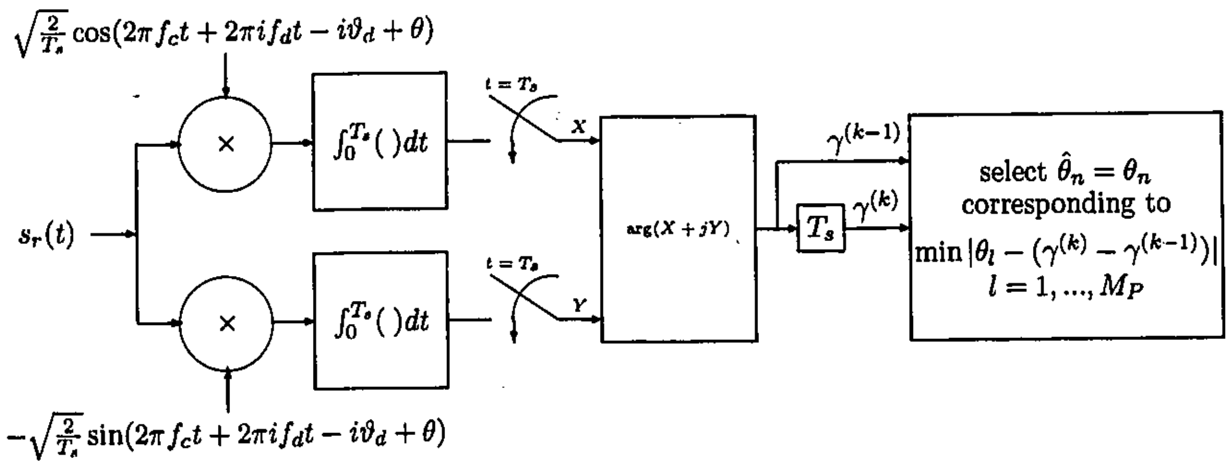

Figure 3.5 : Block diagram of a DPSK-part.

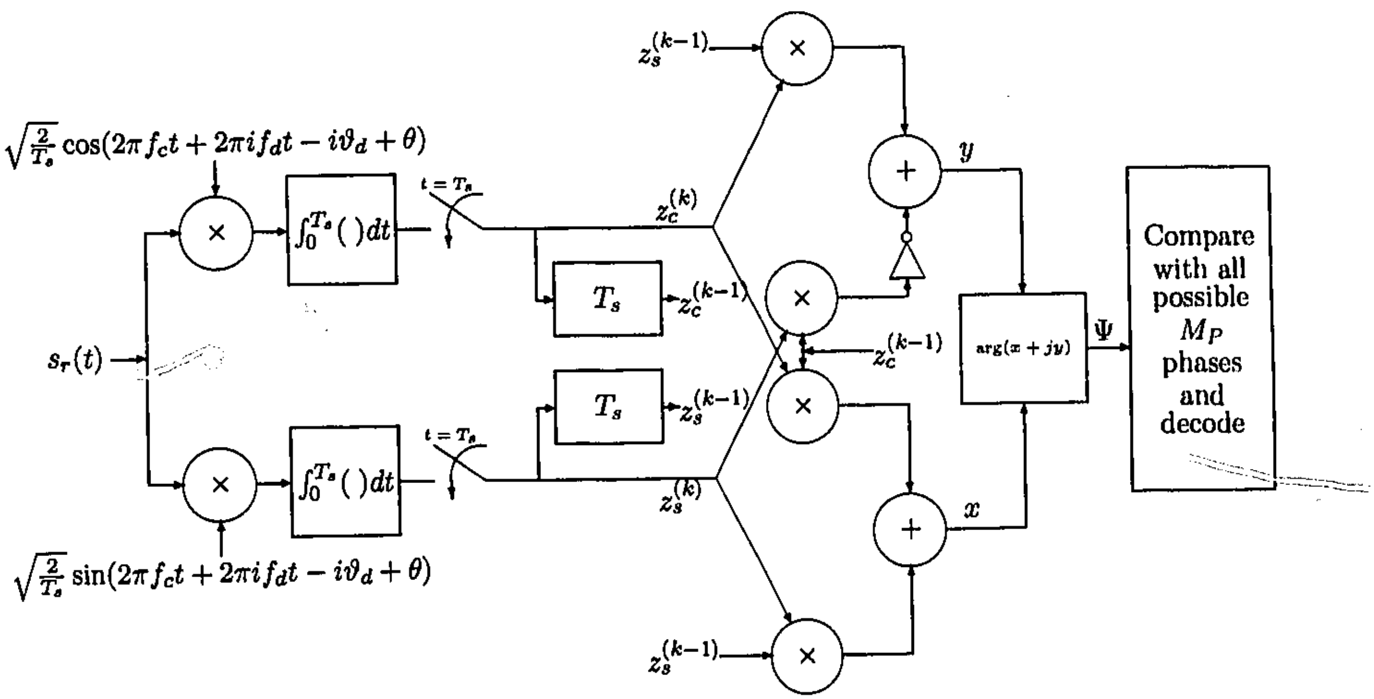

Figure 3.6 : Block diagram of a DPSK-part.

on the same carrier. Thus, in the presence of a channel phase distortion, i.e., $\Omega(f) \neq 0$, the phase shifts introduced by the channel for different frequencies are different. Our approach to solve this problem is to utilize an input from a time tracking loop in the receiver. Which is mainly employed for symbol timing recovery. In our case it also serves as a reference signal generator for estimating the frequency dependent phase shift.

For convenience, we rewrite the possible transmitted frequencies of (2.9) as

$$f_m = f_c + m f_d; \qquad \text{for} \quad m = \pm 1, \pm 3, ..., \pm(M_F - 1). \tag{3.11}$$

Then the received signal during the k-th symbol interval is given by

$$s_r(t) = \sqrt{\frac{2E_s}{T_s}} \cos(2\pi f_m t + \theta^{(k)} + \varphi + \Omega(f_m)) + \nu(t), \quad \text{for } kT_s \leq t \leq (k+1)T_s, \tag{3.12}$$

where $\Omega(f_m)$ is the phase introduced by the channel and is given by

$$\begin{aligned} \Omega(f_m) &= -2\pi f_c \tau - 2\pi m f_d \tau; \qquad \text{for} \quad m = \pm 1, \pm 2, ..., \pm(M_F - 1) \\ &= -\vartheta_c - m\vartheta_d \end{aligned} \tag{3.13}$$

where τ is the channel delay, $\vartheta_c = 2\pi f_c \tau$ and $\vartheta_d = 2\pi f_d \tau$.
If f_l $(l \neq m)$ is the transmitted tone in the $(k-1)$-th symbol interval, then the received signal can be written as

$$s_r(t) = \sqrt{\frac{2E_s}{T_s}} \cos(2\pi f_l t + \theta^{(k-1)} + \varphi + \Omega(f_l)) + \nu(t) \quad \text{for } (k-1)T_s \leq t \leq kT_s \tag{3.14}$$

where the phase introduced by the channel is given by

$$\begin{aligned} \Omega(f_l) &= -2\pi f_c \tau - 2\pi l f_d \tau; \qquad \text{for} \quad l = \pm 1, \pm 2, ..., \pm(M_F - 1) \\ &= -\vartheta_c - l\vartheta_d \end{aligned} \tag{3.15}$$

In the DPSK part, the decision on the transmitted phase is made by first computing the phase difference between the k-th and $(k-1)$-th signal intervals. This phase difference is then compared to all possible phases and the closest one is selected. From (3.12)-(3.15), we observe that, the phases φ and ϑ_c are common to all possible transmitted tones, and that differential detection can eliminate them. The indices m and l (f_m is the transmitted frequency in the k-th symbol and f_l is the transmitted frequency in the $(k-1)$-th symbol) are determined in the FSK part of the receiver. In addition, the start time of each symbol is estimated by the time tracking loop. As will be seen in the forthcoming analysis, the reference signal generator produces a signal with phase $m\vartheta_d$ for the symbol number k and $l\vartheta_d$ for the symbol number l.

To describe the operation of the reference signal generator, we first start describing the case when the system uses only two tones (i.e., 2F/M_PP). Then we generalize this method to a system employ M_F tones (i.e., M_FF/M_PP).

Fig. 3.7 shows the block diagram of the reference signal generator for the JFPM system with 2F/M_PP. The time tracking loop generates the signal $v(t) = \sum_{k=0}^{\infty} \delta(t - t_k)$, where t_k is the start time of the k-th symbol, i.e.,

$$t_k = kT_s - \tau. \tag{3.16}$$

In (3.16) τ is the delay time introduced by the channel. We assume that the channel delay τ is fixed for the duration of at least two symbol intervals.

The signal generator generates the signal $r_c(t) = \sum_{k=0}^{\infty} \cos(2\pi f_d[t - t_k])$. In a fixed signal interval the output of the signal generator is given by

$$\begin{aligned} r_c(t) &= \cos(2\pi f_d[t-\tau]) \\ &= \cos(2\pi f_d t - \vartheta_d) \end{aligned} \tag{3.17}$$

by using phase shift $\pi/2$ then we have

$$\begin{aligned} r_s(t) &= \sin(2\pi f_d[t-\tau]) \\ &= \sin(2\pi f_d t - \vartheta_d) \end{aligned} \tag{3.18}$$

The local oscillator generates, at frequency f_c, the tones

$$\begin{aligned} c_c(t) &= \cos(2\pi f_c t + \theta) \\ c_s(t) &= \sin(2\pi f_c t + \theta) \end{aligned} \tag{3.19}$$

where θ is a random phase. The output of the multipliers, $d_1(t)$ and $d_2(t)$ are given by

$$\begin{aligned} d_1(t) &= c_s(t) r_s(t) \\ &= \frac{1}{2}\cos(2\pi f_c t - 2\pi f_d t + \vartheta_d + \theta) \\ &- \frac{1}{2}\cos(2\pi f_c t + 2\pi f_d t - \vartheta_d + \theta) \end{aligned} \tag{3.20}$$

and

$$\begin{aligned} d_2(t) &= c_c(t) r_c(t) \\ &= \frac{1}{2}\cos(2\pi f_c t + 2\pi f_d t - \vartheta_d + \theta) \\ &+ \frac{1}{2}\cos(2\pi f_c t - 2\pi f_d t + \vartheta_d + \theta). \end{aligned} \tag{3.21}$$

By inverting the sign of $d_1(t)$ and using the adders, we get the waveforms $b_1(t)$ and $b_2(t)$ where,

$$\begin{aligned} b_1(t) &= d_2(t) - d_1(t) \\ &= \cos(2\pi f_c t + 2\pi f_d t - \vartheta_d + \theta) \end{aligned} \tag{3.22}$$

and

$$\begin{aligned} b_2(t) &= d_2(t) + d_1(t) \\ &= \cos(2\pi f_c t - 2\pi f_d t + \vartheta_d + \theta), \end{aligned} \tag{3.23}$$

which are the waveforms needed for the differential detector. The frequency selector select either $b_1(t)$ or $b_2(t)$ based on the estimated frequency at the output of the frequency detector.

Fig. 3.8 shows the block diagram of the reference signal generator for the JFPM system with M_FF/M_PP. The signal generator generates the signals

$$
\begin{aligned}
r_{ci}(t) &= \cos(2\pi i f_d[t-\tau]) \qquad \text{for} \quad i = 1, 3, ..., (M_F - 1) \\
&= \cos(2\pi i f_d t - i\vartheta_d)
\end{aligned} \tag{3.24}
$$

by using phase shift $\pi/2$ then we have

$$
\begin{aligned}
r_{si}(t) &= \sin(2\pi i f_d[t-\tau]) \qquad \text{for} \quad i = 1, 3, ..., (M_F - 1) \\
&= \sin(2\pi i f_d t - i\vartheta_d)
\end{aligned} \tag{3.25}
$$

The local oscillator generates, at frequency f_c, the tones given in (3.19). By following a procedure similar to that leading to $d_1(t), d_2(t), b_1(t)$ and $b_2(t)$ in the 2F/M_PP case, we obtain

$$
\begin{aligned}
d_{1i}(t) &= \frac{1}{2}\cos(2\pi f_c t - 2\pi i f_d t + i\vartheta_d + \theta) \\
&- \frac{1}{2}\cos(2\pi f_c t + 2\pi i f_d t - i\vartheta_d + \theta) \quad \text{for } i = 1, 3, ..., (M_F - 1)
\end{aligned} \tag{3.26}
$$

$$
\begin{aligned}
d_{2i}(t) &= \frac{1}{2}\cos(2\pi f_c t + 2\pi i f_d t - i\vartheta_d + \theta) \\
&+ \frac{1}{2}\cos(2\pi f_c t - 2\pi i f_d t + i\vartheta_d + \theta), \quad \text{for } i = 1, 3, ..., (M_F - 1)
\end{aligned} \tag{3.27}
$$

$$
b_{1i}(t) = \cos(2\pi f_c t + 2\pi i f_d t - i\vartheta_d + \theta) \qquad \text{for} \quad i = 1, 3, ..., (M_F - 1) \tag{3.28}
$$

and

$$
b_{2i}(t) = \cos(2\pi f_c t - 2\pi i f_d t + i\vartheta_d + \theta), \qquad \text{for} \quad i = 1, 3, ..., (M_F - 1) \tag{3.29}
$$

The frequency selector select either $b_{1i}(t)$ or $b_{2i}(t)$ for $i = 1, 3, ..., (M_F - 1)$ based on the estimated frequency at the output of the frequency detector.

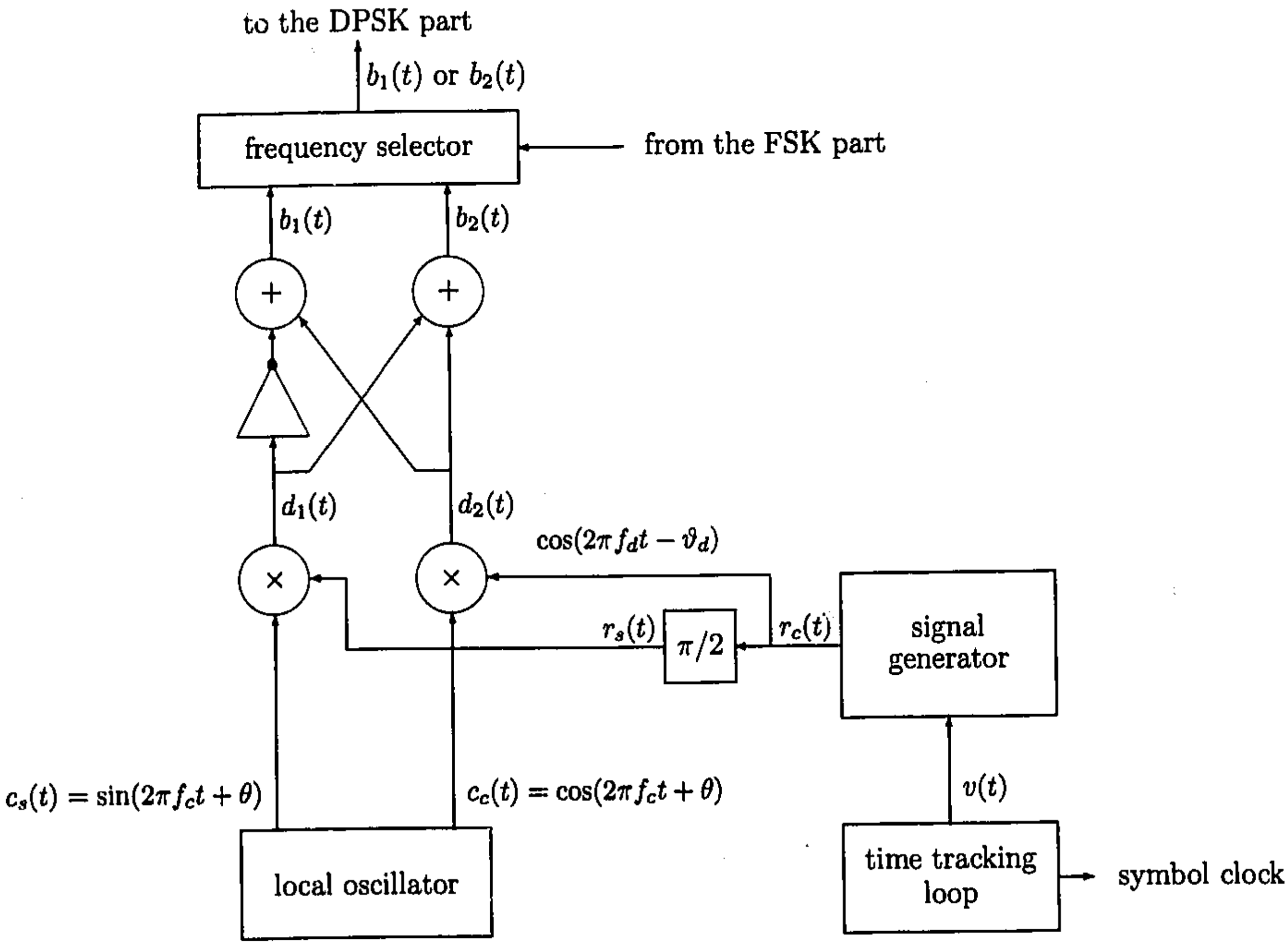

Figure 3.7 : Block diagram of a reference signal generator for JFPM with 2F/M_PP

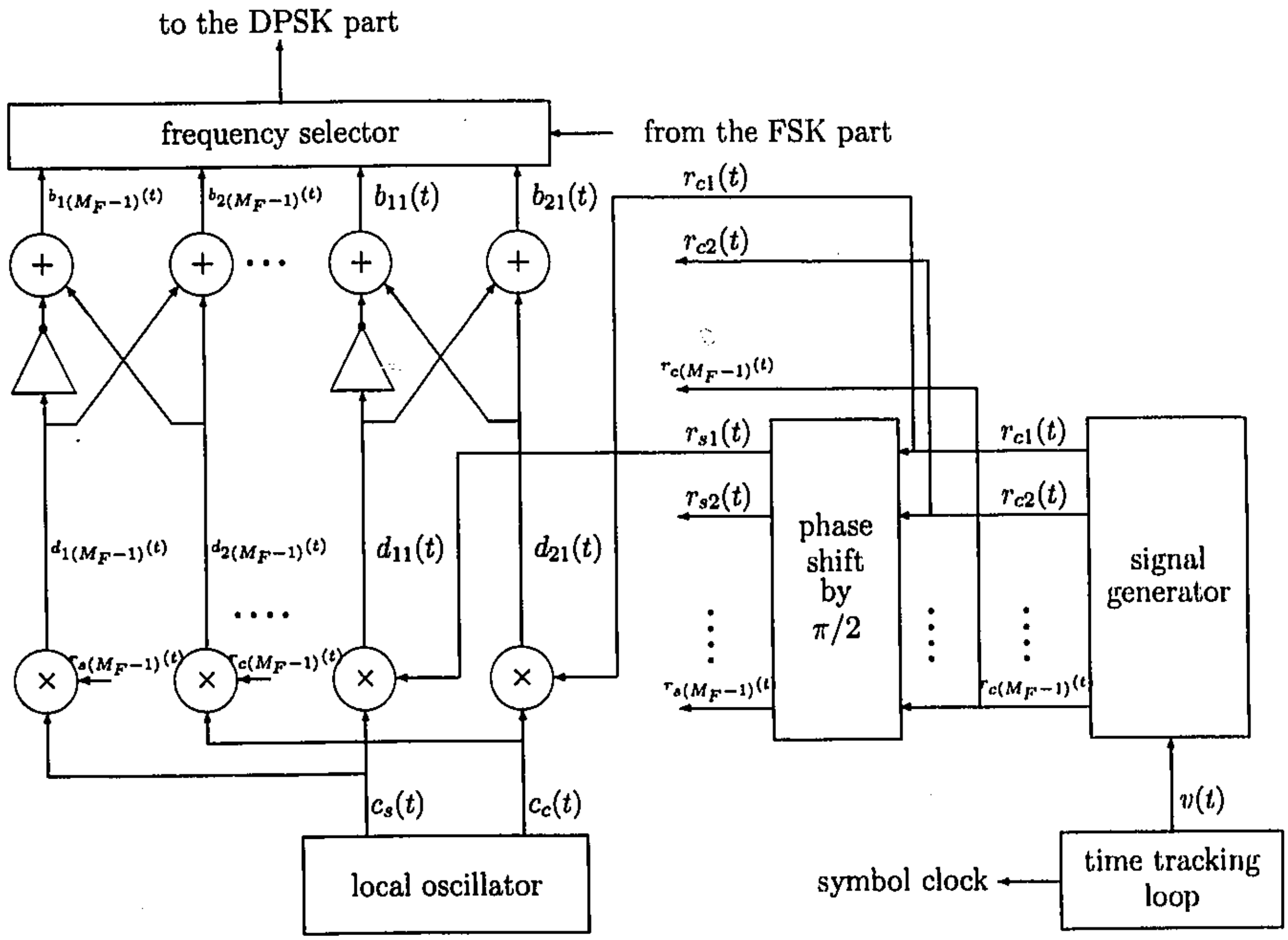

Figure 3.8 : Block diagram of a reference signal generator

3.4.2 Error Probability Performance

Assuming $s_{mn}(t)$ is the transmitted signal, a correct decision from the receiving system of Fig. 3.3 is made if $\left|V_m^{(k)}\right|$ is chosen such that

$$\left|V_m^{(k)}\right| = \max_{l\in\{1,\dots,M_F\}} \left[\left|V_l^{(k)}\right|\right] \tag{3.30}$$

and the phase θ_n satisfies the following

$$\min_{l\in\{1,\dots,M_P\}} \left[\left|\theta_l - \left(\gamma^{(k)} - \gamma^{(k-1)}\right)\right|\right], \tag{3.31}$$

where

$\left|V_l^{(k)}\right|$ denotes the output of the envelope detector l in the k-th signaling interval,

$\gamma^{(k)}$ is the estimate phase of the incoming signal in the k-th signaling interval at the output of the inverse tangent circuit,

$\gamma^{(k-1)}$ is the estimate phase of the incoming signal in the $(k-1)$-th signaling interval at the output of the inverse tangent circuit, and

θ_l for $l = 1, \dots, M_P$ denotes any of the M_P possible phases.

In the absence of noise, the index l where (3.30) is satisfied should be equal to the index m of the transmitted signal $s_{mn}(t)$ and the index l where (3.31) is satisfied should be equal to the index n of $s_{mn}(t)$.

The decision variables $V_l^{(k)}$, $\gamma^{(k)}$ and $\gamma^{(k-1)}$ can be written as

$$V_l^{(k)} = \begin{cases} \left(\sqrt{E_s}\cos(\theta^{(k)}+\varphi+\Omega(f_m))+N_{cm}\right)+j\left(\sqrt{E_s}\sin(\theta^{(k)}+\varphi+\Omega(f_m))+N_{sm}\right) & l = m \\ N_{cl}+jN_{sl} & l \neq m, \end{cases} \tag{3.32}$$

$$\gamma^{(k)} = \arctan\left[\frac{\sqrt{E_s}\sin(\theta^{(k)} + \varphi - \vartheta_c - \theta) + N_s}{\sqrt{E_s}\cos(\theta^{(k)} + \varphi - \vartheta_c - \theta) + N_c}\right] \tag{3.33}$$

and

$$\gamma^{(k-1)} = \arctan\left[\frac{\sqrt{E_s}\sin(\theta^{(k-1)} + \varphi - \vartheta_c - \theta) + N_s}{\sqrt{E_s}\cos(\theta^{(k-1)} + \varphi - \vartheta_c - \theta) + N_c}\right]. \tag{3.34}$$

The noise components N_c, N_s, N_{cl} and N_{sl} for $l = 1, 2, ... M_F$ are independent Gaussian random variables, where

$$N_c = \sqrt{\frac{2}{T_s}} \int_0^{T_s} \nu(t) \cos(2\pi f_l t + \theta - l\vartheta_d) dt, \tag{3.35}$$

$$N_s = -\sqrt{\frac{2}{T_s}} \int_0^{T_s} \nu(t) \sin(2\pi f_l t + \theta - l\vartheta_d) dt, \tag{3.36}$$

$$N_{cl} = \sqrt{\frac{2}{T_s}} \int_0^{T_s} \nu(t) \cos(2\pi f_l t) dt, \tag{3.37}$$

and

$$N_{sl} = -\sqrt{\frac{2}{T_s}} \int_0^{T_s} \nu(t) \sin(2\pi f_l t) dt. \tag{3.38}$$

The probability of a correct decision for the receiving system is equal to the probability that $\left|V_m^{(k)}\right| = \max\left[\left|V_l^{(k)}\right|\right]$ for $l = 1, ..., M_F$ times the probability of the event that the measured phase difference $\left(\gamma^{(k)} - \gamma^{(k-1)}\right)$ differs by less than π/M_P in absolute value from the phase difference $\left(\theta^{(k)} - \theta^{(k-1)}\right)$ of the transmitted signals, given that $\left|V_m^{(k)}\right| = \max\left[\left|V_l^{(k)}\right|\right]$ for $l = 1, ..., M_F$. That is,

$$\begin{aligned} P_c &= \text{Prob}\left(\left|V_m^{(k)}\right| = \max_{l\in\{1,...,M_F\}}\left[\left|V_l^{(k)}\right|\right]\right) \\ &\times \text{Prob}\left(|\psi| = \left|\left(\gamma^{(k)} - \gamma^{(k-1)}\right) - \left(\theta^{(k)} - \theta^{(k-1)}\right)\right| < \frac{\pi}{M_P}\left|\left|V_m^{(k)}\right| = \max_{l\in\{1,...,M_F\}}\left[\left|V_l^{(k)}\right|\right]\right.\right). \end{aligned} \tag{3.39}$$

The Prob $\left(\left|V_m^{(k)}\right| = \max\left[\left|V_l^{(k)}\right|\right]\right)$ for $l = 1, ..., M_F$ is equal to the probability that a correct decision is made on the transmitted tone at the output of the frequency detectors. For convenience, the squared envelope is normalized by $2/N_0$. It was shown in [45] that the decision variables $\left|V_i^{(k)}\right|$ for $i = 1, ..., M_F$ are mutually statistically independent and the probability density function of the envelope $\left|V_i^{(k)}\right|$ conditioned on the transmitted signal $s_{mn}(t)$ is given by

$$p_{\left|V_i^{(k)}\right| \big| s_{mn}}(\alpha|s_{mn}) = \begin{cases} \alpha e^{-(\alpha^2+2\rho)/2} I_0(\alpha\sqrt{2\rho}) & i = m, \alpha \geq 0 \\ \alpha e^{-\alpha^2/2} & i \neq m, \alpha \geq 0, \end{cases} \tag{3.40}$$

where ρ denotes the signal-to-noise ratio for k_s-bits, defined as $\rho = E_s/N_0$, I_0, is the zeroth-order modified Bessel function of the first kind. By using (3.40), the probability of correct decision being made on the transmitted tone can be expressed as

$$\begin{aligned} P_{c,FSK} &= \int_0^\infty \alpha e^{-(\alpha^2+2\rho)/2} I_0(\alpha\sqrt{2\rho}) \left[1 - e^{-\alpha^2/2}\right]^{M_F-1} d\alpha \\ &= \frac{1}{M_F} \sum_{i=1}^{M_F} (-1)^{i+1} \begin{pmatrix} M_F \\ i \end{pmatrix} e^{-\rho\left(\frac{i-1}{i}\right)}. \end{aligned} \tag{3.41}$$

The Prob$\left(|\psi| < \pi/M_P \,\middle|\, \left|V_m^{(k)}\right| = \max\left[\left|V_l^{(k)}\right|\right]\right)$ for $l = 1, ..., M_F$ as given in (3.39) is equal to the probability that the transmitted phase is chosen correctly at the output of the phase estimators, given that a correct decision is made on the transmitted frequency at the output of the frequency detectors. Thus, the phase difference ψ can be viewed as being the phase difference between two vectors perturbed by Gaussian noise [48]. In [48] the Prob($\psi_{min} \leq \psi \leq \psi_{max}$) was expressed in terms of an auxiliary function $F(\psi)$ as

$$\text{Prob}(\psi_{min} \leq \psi \leq \psi_{max}) = \begin{cases} F(\psi_{max}) - F(\psi_{min}) + 1 & \psi_{min} < 0 < \psi_{max} \\ F(\psi_{max}) - F(\psi_{min}) & \psi_{min} > 0, \text{or}\, \psi_{max} < 0, \end{cases} \tag{3.42}$$

where $F(\psi)$ is given by

$$F_\psi(\psi) = -\frac{\sin(\psi)}{4\pi} \int_{\pi/2}^{\pi/2} \frac{e^{-\rho(1-\cos(\psi)\cos(u))}}{1-\cos(\psi)\cos(u)} du. \tag{3.43}$$

The probability of correct decision for the phase, given that the transmitted frequency is estimated correctly, can be expressed as

$$\begin{aligned} P_{c,PSK|FSK} &= F(\pi/M_P) - F(-\pi/M_P) + 1 \\ &= 1 - \frac{\sin(\pi/M_P)}{2\pi} \int_{-\pi/2}^{\pi/2} \frac{e^{-\rho(1-\cos(\pi/M_P)\cos(u))}}{1-\cos(\pi/M_P)\cos(u)} du. \end{aligned} \tag{3.44}$$

Substituting (3.41) and (3.44) in (3.39), the symbol error of the differentially detected JFPM signals, which is $P_e(M) = 1 - P_c$, can be expressed as

$$\begin{aligned} P_e(M) = 1 - \left(1 - \frac{\sin(\pi/M_P)}{2\pi} \int_{-\pi/2}^{\pi/2} \frac{e^{-\rho(1-\cos(\pi/M_P)\cos(u))}}{1-\cos(\pi/M_P)\cos(u)} du\right) \\ \times \frac{1}{M_F} \sum_{i=1}^{M_F} (-1)^{i+1} \binom{M_F}{i} e^{-\rho\left(\frac{i-1}{i}\right)}. \end{aligned} \tag{3.45}$$

For $M = 4$ (i.e., $M_F = 2$ and $M_P = 2$) the expression given in (3.45) can be written as

$$\begin{aligned} P_e(M) &= 1 - \left(1 - \frac{1}{2\pi} \int_{-\pi/2}^{\pi/2} e^{-\rho} du\right) \left(1 - \frac{1}{2} e^{-\rho/2}\right) \\ &= 1 - \left(1 - \frac{1}{2} e^{-\rho}\right) \left(1 - \frac{1}{2} e^{-\rho/2}\right). \end{aligned} \tag{3.46}$$

After some manipulations the symbol error probability given in (3.46) becomes

$$P_e(4) = \frac{1}{2} e^{-\rho/2} \left[1 + e^{-\rho/2} - \frac{1}{2} e^{-\rho}\right]. \tag{3.47}$$

For $M = 2M_F$ (i.e., $M_P = 2$) the symbol error probability expression given in (3.45) can be written as

$$P_e(M) = 1 - \left(1 - \frac{1}{2} e^{-\rho}\right) \frac{1}{M_F} \sum_{i=1}^{M_F} (-1)^{i+1} \binom{M_F}{i} e^{-\rho\left(\frac{i-1}{i}\right)}. \tag{3.48}$$

In general, the integral expression given in (3.45) cannot be written in a closed form when $M_P > 2$.

The Probability of a Bit Error

In JFPM signal detection, a two step decision process is necessary to establish which signal was received. The relationship between the bit probability and the symbol error probability of the JFPM signal set is not related in the same way as it is for orthogonal signals or polyphase signals. This is so because of the two kinds of symbol errors that can occur. The first type of error occurs when the transmitted tone is chosen incorrectly, causing at least one bit error in the $k_F + k_P$ bits of the selected symbol. The second kind of symbol error may occur when the transmitted tone is selected correctly, but there is an error in the selection of the transmitted phase. This symbol error can cause at least one bit error out of k_P bits in the $k_F + k_P$ bits of the selected symbol. In the receiver of Fig. 3.3, a symbol error occurs if the frequency is incorrectly chosen in the first stage. If the frequency is correctly chosen, an error occurs in the second stage if the differential phase is incorrectly estimated. Hence the probability of error is

$$P_e(M) = P_{e,FSK} + (1 - P_{e,FSK})P_{e,PSK|FSK} \tag{3.49}$$

where $P_{e,FSK}$ is the probability of an erroneous noncoherent decision on the frequency in the FSK-part (first stage) and $P_{e,PSK|FSK}$ is the probability of an incorrect decision on the phase in the DPSK-part (second stage) given that the noncoherent decision of the FSK-part was correct.

By using (3.41) the probability of an erroneous noncoherent decision on the frequency in the first stage may be given in the form

$$\begin{aligned} P_{e,FSK} &= 1 - P_{c,FSK} \\ &= \frac{1}{M_F}\sum_{i=2}^{M_F}(-1)^i \binom{M_F}{i} e^{-\rho\left(\frac{i-1}{i}\right)} \end{aligned} \tag{3.50}$$

which is the well-known performance of a noncoherently demodulated M_F-ary FSK signals [46, p. 296].

Recall the relationship between the symbol signal-to-noise ratio ρ and the bit signal-to-noise ratio ρ_b

$$\rho = k_s\rho_b = (k_F + k_P)\rho_b. \tag{3.51}$$

An interesting relation can be found by observing (3.50), (3.51), where at certain ρ_b, the combined M_F-ary FSK (i.e., JFPM) perform better than the conventional M_F-ary FSK by an improvement factor I_F, where

$$I_F = \frac{k_s}{k_F} = \frac{k_F + k_P}{k_F} = 1 + \frac{k_P}{k_F} \tag{3.52}$$

This result means that the error rate performance curve of $P_{e,FSK}$ moves left by $10\log_{10} I_F$ dB (in comparison to FSK system that use same number of tones).

Using the probability of an incorrect decision on the phase given that the noncoherent decision on the frequency was correct is given by

$$\begin{aligned} P_{e,PSK|FSK} &= 1 - P_{c,PSK|FSK} \\ &= \frac{\sin(\pi/M_P)}{2\pi}\int_{-\pi/2}^{\pi/2}\frac{e^{-\rho(1-\cos(\pi/M_P)\cos(u))}}{1-\cos(\pi/M_P)\cos(u)}du \end{aligned} \tag{3.53}$$

which is the ideal performance of M_P-ary DPSK signals [48].

For $M_P = 2$, it is possible to evaluate the integral given in (3.53) in a closed form, and the result is given by

$$P_{e,PSK|FSK} = \frac{1}{2}e^{-\rho} \tag{3.54}$$

For $M_P > 2$ the approximation of (3.53) is

$$P_{e,PSK|FSK} \simeq \sqrt{\frac{1+\cos(\pi/M_P)}{2\cos(\pi/M_P)}}\operatorname{erfc}\left(\sqrt{\rho[1-\cos(\pi/M_P)]}\right) \tag{3.55}$$

where $\mathrm{erfc}(u)$ is the complementary error function

$$\mathrm{erfc}(u) = \frac{2}{\sqrt{\pi}} \int_{u}^{\infty} e^{-t^2} dt. \tag{3.56}$$

The combined M_P-ary DPSK outperforms the conventional M_P-ary DPSK by an improvement factor I_P, where

$$I_P = \frac{k_s}{k_P} = \frac{k_F + k_P}{k_P} = 1 + \frac{k_F}{k_P} \tag{3.57}$$

It seems worthwhile here to observe (3.57), where the symbol error probability curve of the DPSK-part of the joint receiver (i.e., $P_{e,PSK|FSK}$) moves left by $10\log_{10} I_P$ dB (in comparison to DPSK system that use same number of phases).

The easiest way of relating the symbol error to bit error probability is to assume that the transmitted k_s-bit word corresponds to all zeros (see Fig. 3.9), and then find the probability of 1's in an incorrect decision. If the symbol error is due to an incorrect decision on the frequency, then there are $(M_F - 1)M_P = (M - M_P)$ equally likely incorrect k_s-bit patterns. In the M_P patterns with the correct frequency, the number of 1's is $k_P M_P/2$. Hence, the total number of 1's in the incorrect patterns is $(Mk_s/2) - (M_P k_P/2)$. By taking the ratio of 1's to the total number of bits in the frequency incorrect part, we find the probability of bit error due to an error in the first stage (P_{b1}) as

$$P_{b1} = \frac{k_s M - k_P M_P}{2k_s(M - M_P)} P_{e,FSK}. \tag{3.58}$$

When a symbol error is due to an error in the DPSK part, k_F bits of k_s-bit pattern are correct, and the decision affects the k_P bits for the phase. A phase error in a Gray coded system is well approximated by a one bit error in k_P-bits (Gray code is used only for the k_P-bits). Hence the probability of bit error due to an error in the

$$
\begin{array}{ll}
\multicolumn{2}{c}{\overbrace{\overbrace{000\cdots0}^{k_F\text{-bit}}\qquad\overbrace{000\cdots0}^{k_P\text{-bit}}}^{k_s\text{-bit}}} \\
000\cdots0 & 000\cdots1 \\
\vdots & \vdots \\
000\cdots0 & 111\cdots0 \\
000\cdots0 & 111\cdots1
\end{array}
$$

$$
\text{set \# 2 of } M_P \text{ patterns} \left\{
\begin{array}{ll}
000\cdots1 & 000\cdots0 \\
000\cdots1 & 000\cdots1 \\
\vdots & \vdots \\
000\cdots1 & 111\cdots0 \\
000\cdots1 & 111\cdots1
\end{array}\right.
$$

$$
\begin{array}{ll}
\vdots & \vdots
\end{array}
$$

$$
\text{set \# } i \text{ of } M_P \text{ patterns} \left\{
\begin{array}{ll}
010\cdots1 & 000\cdots0 \\
010\cdots1 & 000\cdots1 \\
\vdots & \vdots \\
010\cdots1 & 111\cdots0 \\
010\cdots1 & 111\cdots1
\end{array}\right.
$$

$$
\begin{array}{ll}
\vdots & \vdots
\end{array}
$$

$$
\text{set \# } M_F \left\{
\begin{array}{ll}
111\cdots1 & 000\cdots0 \\
111\cdots1 & 000\cdots1 \\
\vdots & \vdots \\
111\cdots1 & 111\cdots0 \\
111\cdots1 & 111\cdots1
\end{array}\right.
$$

Figure 3.9 : JFPM bit patterns

second stage (P_{b2}) is

$$P_{b2} \simeq \frac{1}{k_s}(1 - P_{e,FSK})P_{e,DPSK|FSK}. \tag{3.59}$$

Using (3.58) and (3.59), the total bit error probability for JFPM signal set is given by

$$\begin{aligned} P_b(M) &= P_{b1} + P_{b2} \\ &\simeq \frac{k_s M - k_P M_P}{2k_s(M - M_P)} P_{FSK} + \frac{1}{k_s}(1 - P_{FSK})P_{DPSK|FSK}. \end{aligned} \tag{3.60}$$

By substituting the expressions of P_{FSK} and $P_{DPSK|FSK}$ given in (3.50) and (3.53) into (3.49), the bit error probability expression can be obtained as

$$\begin{aligned} P_b(M) &\simeq \frac{k_s M - k_P M_P}{2k_s(M - M_P)} \cdot \frac{1}{M_F} \sum_{i=2}^{M_F} (-1)^i \binom{M_F}{i} e^{-\rho\left(\frac{i-1}{i}\right)} \\ &+ \frac{1}{k_s} \left\{ 1 - \frac{1}{M_F} \sum_{i=2}^{M_F} (-1)^i \binom{M_F}{i} e^{-\rho\left(\frac{i-1}{i}\right)} \right\} \\ &\times \left\{ \frac{\sin(\pi/M_P)}{2\pi} \int_{-\pi/2}^{\pi/2} \frac{e^{-\rho[1-\cos(\pi/M_P)\cos u]}}{1 - \cos(\pi/M_P)\cos u} du \right\}. \end{aligned} \tag{3.61}$$

The bit error probability obtained by (3.61) is evaluated numerically for different values of M_F and M_P and the results are presented in the next section.

3.4.3 Results of Differential Detection

The bit error probability as a function of ρ_b has been calculated by using (3.61) and the results have been plotted in Fig. 3.10, Fig. 3.11 and Fig. 3.12 for M_FF/2P, M_FF/4P and M_FF/8P respectively when M_F=2,4,8,16. We also added the curves for the conventional noncoherent FSK and DPSK systems. From these figures it can be observed that, for a given error probability and with the same signal set size M, JFPM with a combination M_FF/2P requires less power than M-ary DPSK and M-ary FSK. JFPM with a combination M_FF/4P also requires less power than M-ary DPSK but it needs more power than M-ary FSK at bit error rate less than 3×10^{-3}. In addition JFPM with M_FF/8P requires less power than M-ary DPSK but it needs more power than the conventional FSK system. Another important property of JFPM with M_FF/4P is observed from Fig. 3.11, where JFPM curves crossover the conventional FSK curves when the two systems have the same signal set size. The reason for these crossover points is that the bit error rate curves of the conventional FSK system fall down faster than that of the conventional DPSK system. In JFPM the bit error rate is limited by either FSK-part or DPSK-part (whichever one can provide the higher bit error rate). Therefore crossover points can occur.

The comparisons of JFPM and the conventional schemes are made in terms of power efficiency (i.e., required signal-to-noise ratio per bit to achieve a given bit error rate) and bandwidth efficiency (i.e., R_b/W which is in bit/s/Hz). The comparison between JFPM, M-ary FSK and M-ary DPSK, based on the bandwidth efficiency R_b/W versus ρ_b required to achieve 10^{-5} BER, are tabulated in Table 3.4. The bandwidth efficiencies of JFPM and M-ary FSK are calculated by using (2.26), which are realistic values. The theoretical bandwidth efficiency of M-ary DPSK is also tabulated by using (2.26) when $M_F = 1$. For a practical M-ary DPSK system, these theoretical values should be divided by $(1+\alpha)$ to account for the non-minimum bandwidth of practical filters, with α representing the roll-off factor $(0 < \alpha < 1)$.

From the data in Table 3.4, we observe that the same bandwidth efficiency can be achieved by using different combinations of JFPM schemes. For example, $R_b/W = 1.0$ bits/s/Hz can be obtained by conventional 2-DPSK, or by JFPM with combinations 2F/2P or 4F/4P while requiring an ρ_b of 10.34, 10.22 and 8.63 dB respectively to achieve a bit error rate of 10^{-5}. In this particular example, using a more complex

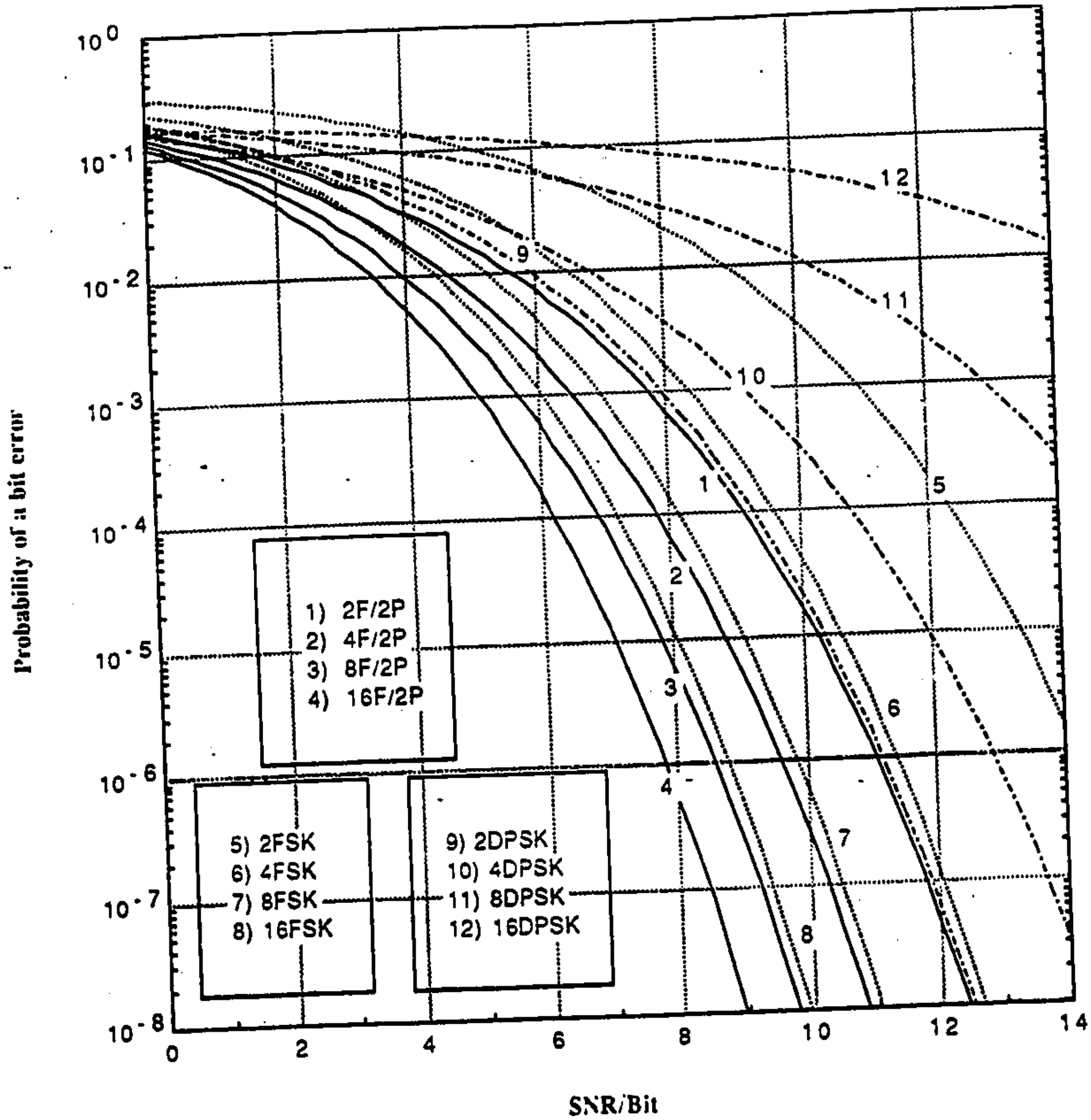

Figure 3.10 : Bit error rate performance of DPSK, noncoherent FSK and differentially detected JFPM in AWGN channel when $M_P = 2$ and $M_F = 2, 4, 8, 16$ (JFPM with a combination $M_F F/2P$).

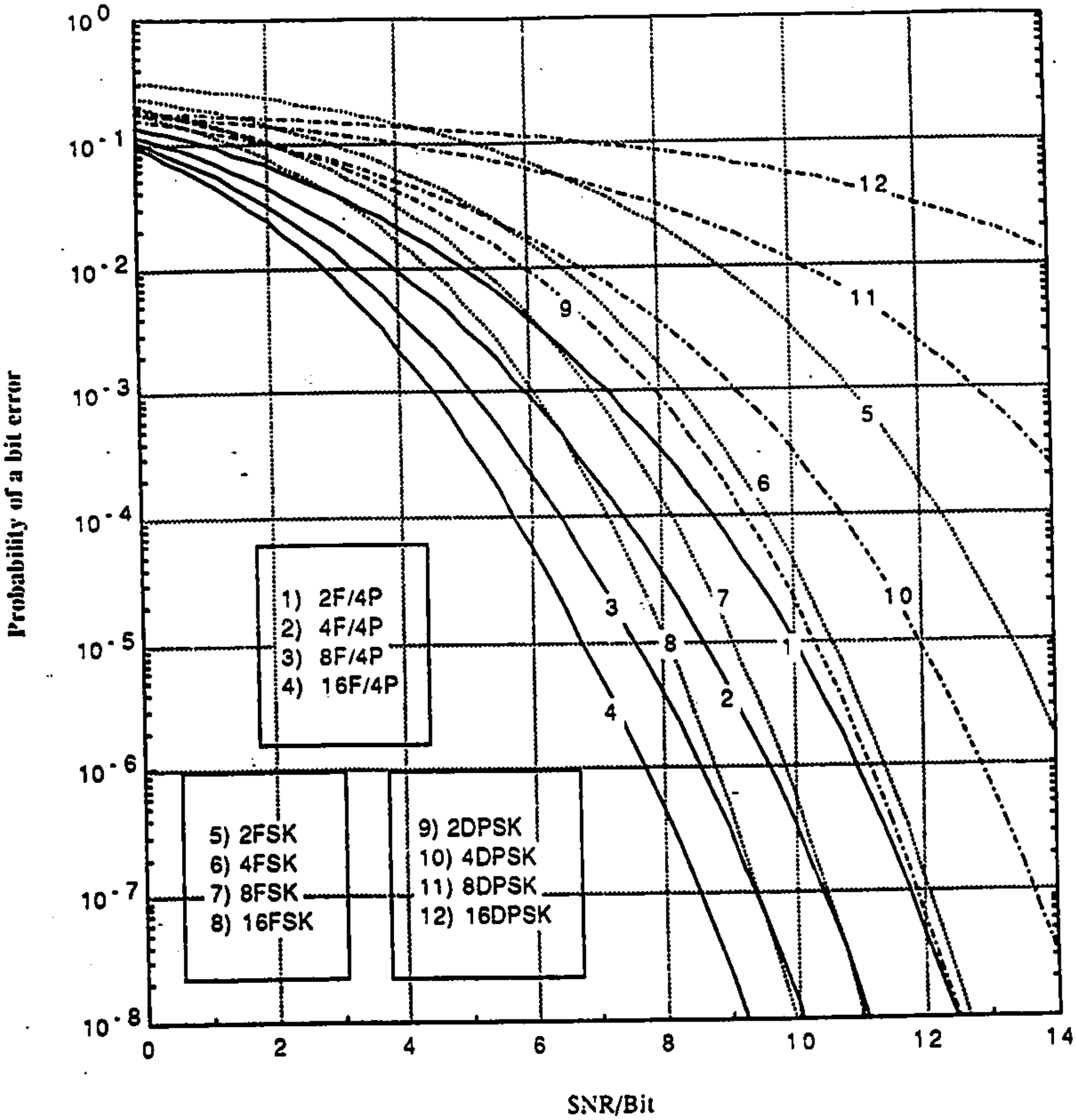

Figure 3.11 : Bit error rate performance of DPSK, noncoherent FSK and differentially detected JFPM in AWGN channel when $M_P = 4$ and $M_F = 2, 4, 8, 16$ (JFPM with a combination M_FF/4P).

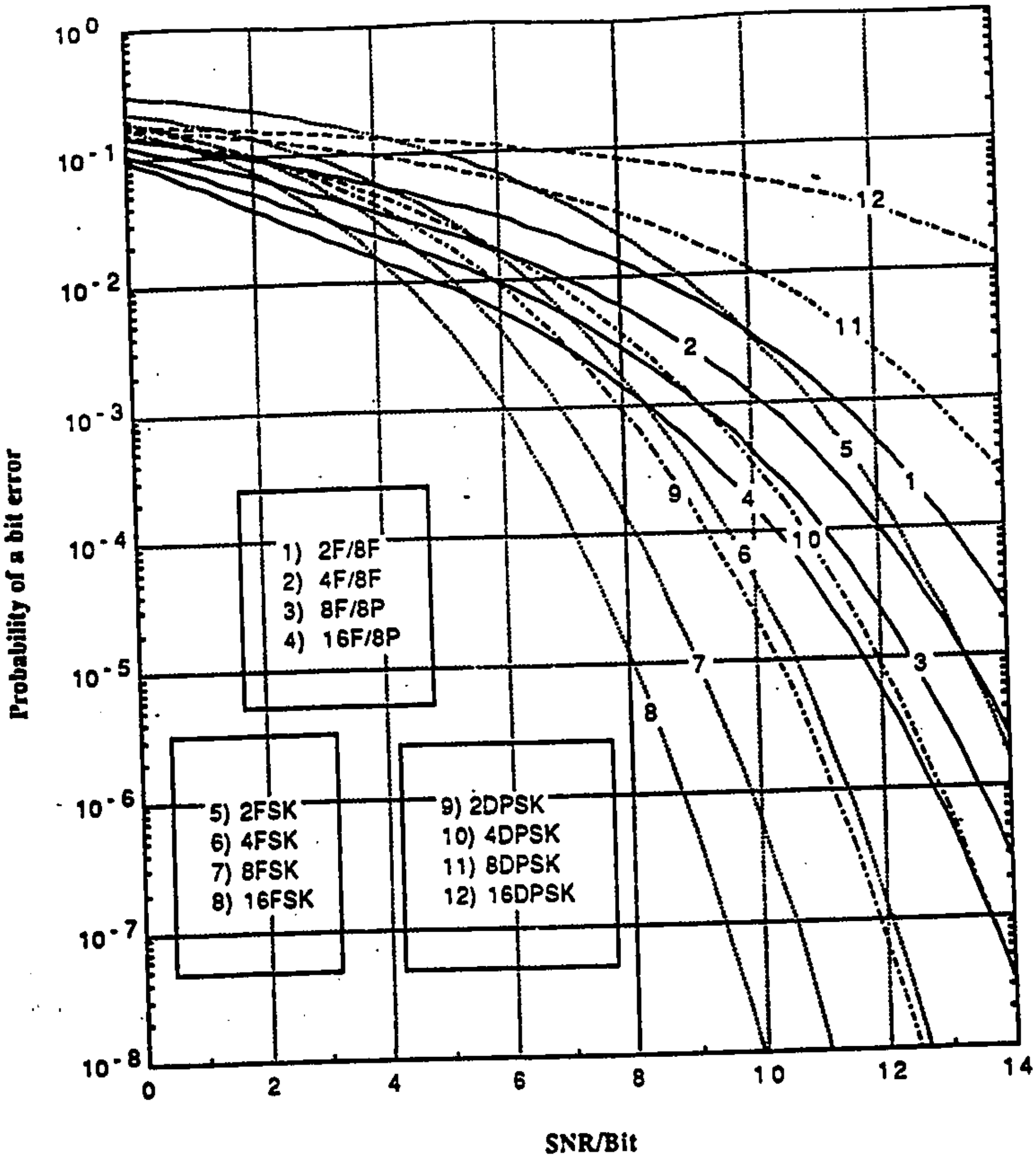

Figure 3.12 : Bit error rate performance of DPSK, noncoherent FSK and differentially detected JFPM in AWGN channel when $M_P = 8$ and $M_F = 2, 4, 8, 16$ (JFPM with a combination $M_F F/8P$).

configuration provides up to 1.71 dB power efficiency improvement over 2-DPSK. Another example where JFPM provides power efficiency at a given bandwidth efficiency, occurs when $R_b/W = 0.5$ JFPM with a combination 2F/8P performs better than 2-FSK and 4-FSK system by 5.52 and 2.78 dB respectively. There are also cases where JFPM provides power and bandwidth efficiency over the conventional M-ary FSK system, as an example M_FF/2P. Finally, JFPM with all frequency and phase combinations, provides power efficiency over the conventional M-ary DPSK system.

Table 3.4 : Power and bandwidth efficiencies of differentially detected M-ary JFPM, M-ary DPSK and noncoherent M-ary FSK. ($P_{eb} = 10^{-5}$, ρ_b in dB, $\eta = R_b/W$ in bits/s/Hz)

–	M_FF/2P		M_FF/4P		M_FF/8P		M-ary DPSK		M-ary FSK	
M	η	ρ_b	η	ρ_b	η	ρ_b	η	ρ_b	η	ρ_b
2	–	–	–	–	–	–	1.0	10.34	0.500	13.35
4	1.000	10.22	–	–	–	–	2.0	11.96	0.500	10.61
8	0.750	8.81	1.500	10.01	–	–	3.0	15.82	0.375	9.09
16	0.500	7.83	1.000	8.63	2.000	14.43	4.0	20.40	0.250	8.08
32	0.313	7.10	0.625	7.59	1.250	13.35	5.0	25.34	0.156	7.33
64	0.188	6.49	0.375	6.78	0.750	12.47	6.0	30.47	0.094	6.56

A further advantage of using JFPM appears when the comparisons are based on the bandwidth that contains 90% and 99% of the total power, our observation of the data in Table 3.5 is that the bandwidth efficiency of M-ary DPSK is greater than that of the JFPM, but there is a combination of JFPM where its bandwidth efficiency is very close to M-ary DPSK. In general, JFPM requires less power than M-ary DPSK. A specific example illustrating this point can be obtained by observing that JFPM with 4F/4P and the conventional 4-DPSK have approximately the same bandwidth efficiency in terms of the bandwidth that contains 90% of the total power, however in terms of power efficiency JFPM outperforms 4-DPSK by 3.33 dB at a BER=10^{-5}. From the data in Table 3.6, the bandwidth efficiency of JFPM is almost equal to that of the M-ary DPSK, and JFPM requires less power than M-ary DPSK. As an example JFPM with 8F/8P and the conventional 64-DPSK have approximately the same bandwidth efficiency in terms of the bandwidth that contains 99% of the total power, but JFPM outperforms 64-DPSK by 18 dB at BER=10^5.

Table 3.5 : Power and bandwidth efficiencies based on 90% fractional power containment bandwidth of differentially detected M-ary JFPM and M-ary DPSK. ($P_{eb} = 10^{-5}$, ρ_b in dB, μ_{90} in bits/s/Hz)

–	M_FF/2P		M_FF/4P		M_FF/8P		M-ary DPSK	
M	μ_{90}	ρ_b	μ_{90}	ρ_b	μ_{90}	ρ_b	μ_{90}	ρ_b
2	–	–	–	–	–	–	0.591	10.34
4	0.877	10.22	–	–	–	–	1.188	11.96
8	0.764	8.81	1.317	10.01	–	–	1.789	15.82
16	0.535	7.83	1.018	8.63	1.756	14.43	2.398	20.40
32	0.340	7.10	0.669	7.59	1.273	13.35	2.900	25.34
64	0.206	6.49	0.408	6.78	0.803	12.47	3.470	30.47

Table 3.6 : Power and bandwidth efficiencies based on 99% fractional power containment bandwidth of differentially detected M-ary JFPM and M-ary DPSK. ($P_{eb} = 10^{-5}$, ρ_b in dB, μ_{99} in bits/s/Hz)

–	M_FF/2P		M_FF/4P		M_FF/8P		M-ary DPSK	
M	μ_{99}	ρ_b	μ_{99}	ρ_b	μ_{99}	ρ_b	μ_{99}	ρ_b
2	–	–	–	–	–	–	0.052	10.34
4	0.101	10.22	–	–	–	–	0.104	11.96
8	0.150	8.81	0.153	10.01	–	–	0.150	15.82
16	0.194	7.83	0.201	8.63	0.207	14.43	0.210	20.40
32	0.208	7.10	0.244	7.59	0.252	13.35	0.250	25.34
64	0.174	6.49	0.250	6.78	0.294	12.47	0.300	30.47

3.4.4 Simulation Results

For the validation of the analytical results presented in Chapter 3, we also performed some simulation. For this purpose we chose the simplest JFPM format, i.e., 2F/2P, and considered the AWGN channel performance.

Fig. 3.13 show the average bit error probability for JFPM with 2F/2P, also the analytical P_b is added. The number of symbols simulated is 10^5 when $\rho_b < 8$, and 10^6 when $\rho_b \geq 8$. The confidence interval is chosen to be 95%.

The simulation steps of the computer program are as follows.

1. initialization; read: k_F, k_P, ρ_b and the number of generated bits N.
2. generate random binary data.
3. differentially encoded the k_P bit.
4. generate Gaussian distributed random variables.
5. generate received samples.
6. estimate the frequency.
7. generate reference signal to the DPSK part.
8. count error in FSK part e_F.
9. count error in the DPSK part e_P.
10. $P_b = (e_F + e_P)/N$.

From Fig. 3.13 we observe that, the two curves of the average bit error probability for both analytical and simulation results are so close for high ρ_b and there is a small difference at low ρ_b. The reason of this is due to Gray coded approximation that is used in system analysis.

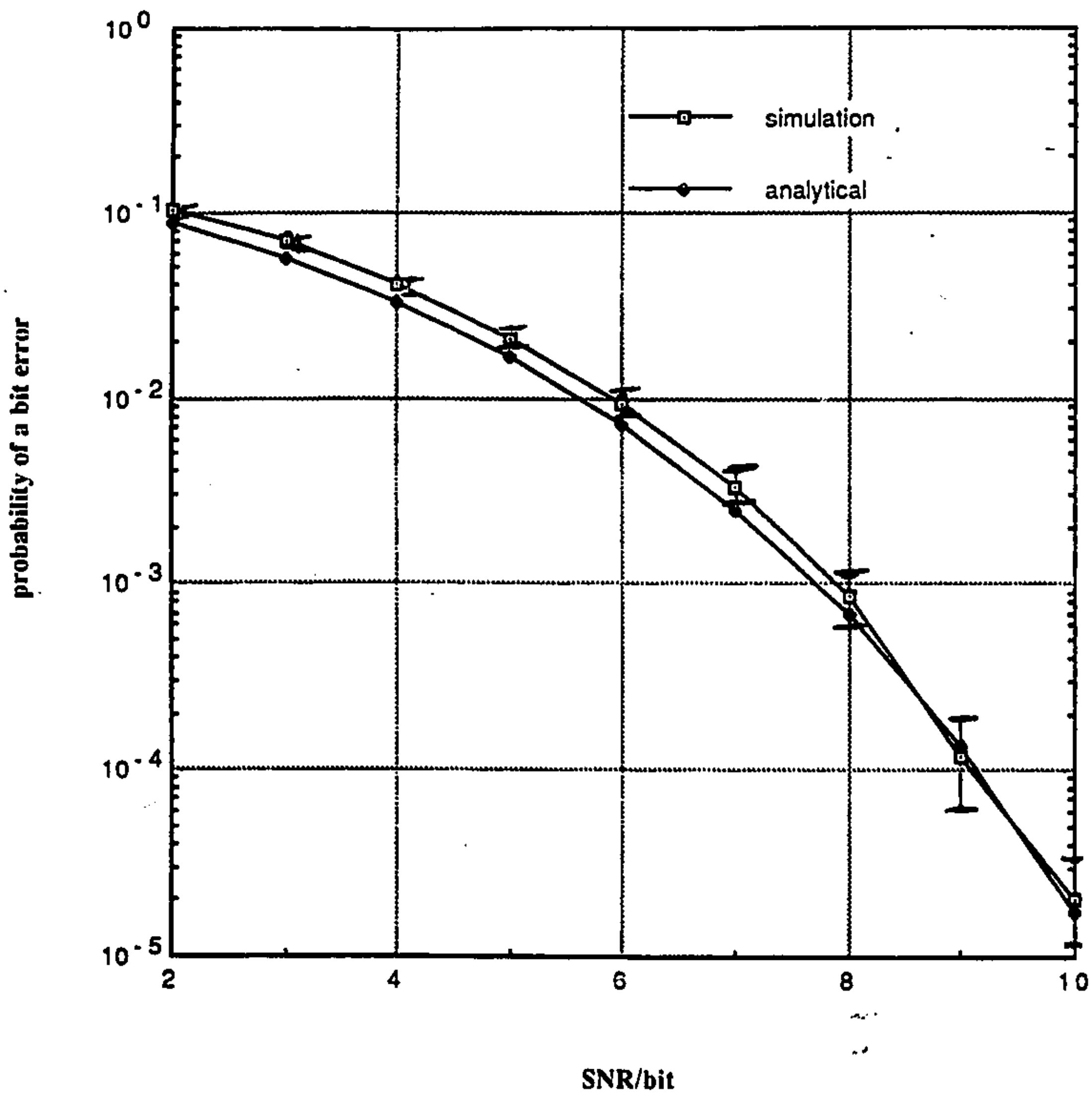

Figure 3.13 : Bit error rate performance of differentially detected JFPM with 2F/2P in AWGN channel obtained by simulation and also analysis.

3.5 Conclusions

In this chapter, the performance of JFPM signals over AWGN channels was studied. A differential receiver structure for JFPM signals was introduced and a simple equivalent receiver was obtained. The probability of error was analyzed and a bit error rate expression was obtained. The results showed that JFPM can perform better than M-ary DPSK and M-ary FSK systems of a comparable bandwidth efficiency. It was also concluded that, this modulation technique includes many formats which may be classified as an bandwidth efficient or power efficient modulation technique.

Chapter 4

Performance of Joint Frequency-Phase Modulation over Rayleigh Fading Channels

4.1 Introduction

In mobile radio communication systems, the received signal frequently undergoes multipath fading. In a typical urban situation, where the mobile users are not within a clear line-of-sight of the transmitting antenna, the received signal at the mobile user is the sum of many random amplitude and random phase signals. The probability density function of the envelope of the multipath faded signal usually has a Rayleigh distribution, and is therefore referred to as a Rayleigh channel [50, 51].

This chapter presents the performance of JFPM over Rayleigh fading channels with coherent and differential demodulation. Bit error rate performance is evaluated using diversity techniques over Rayleigh fading channels. Results show that JFPM performs better than conventional noncoherent M-ary FSK and M-ary DPSK of comparable bandwidth efficiency.

The organization of the chapter is as follows: In Section 4.2, the channel model under consideration is described. Section 4.3 presents the receiver structures and the performance analysis for coherent detection of JFPM signals. The performance analysis for differential detection is given in Section 4.4. The probability of error rate performance for JFPM signals using diversity techniques for multipath fading channels is evaluated in Section 4.5. Numerical results of error rate performance evaluation as a function of the average signal-to-noise ratio are presented in Section 4.6. Finally, the conclusions are stated in Section 4.7.

4.2 Channel Model

We are interested in the performance of the receiver in determining the frequency f_m and the phase θ_n of the transmitted signal given in (2.7) when it is transmitted over a multipath fading channel. The channel, we have assumed, can be represented as having the equivalent low-pass (complex) impulse response of [46]

$$h(\tau, t) = \sum_k \alpha_k(t) e^{-j2\pi f_c \tau_k(t)} \delta\left[\tau - \tau_k(t)\right] \tag{4.1}$$

where $\alpha_k(t)$ is the attenuation of the received signal due to the k-th path and $\tau_k(t)$ is the propagation delay for the k-th path. In (4.1) τ represents the usual channel response (propagation delay) variable, while the t-dependence indicates that the very structure of the impulse response changes with time. The impulse response of the time-varying multipath channel when the number of paths is large can be approximated by a complex Gaussian random process. This means that when the channel impulse response is modeled as a zero mean Gaussian random process, the envelope of the impulse response $|h(\tau, t)|$ at any time instant is a Rayleigh-distributed random variable.

When a single tone is transmitted through a discrete multipath channel given in

(4.1), the received signal in the absence of noise takes the form

$$s_r(t) = \sum_k \alpha_k(t) e^{-j2\pi f_c \tau_k(t)} = \sum_k \alpha_k(t) e^{-j\phi_k(t)}. \tag{4.2}$$

The observed received phasor is the sum of several phasors, with amplitudes $\alpha_k(t)$ and phases $\phi_k(t)$, where $\phi_k(t) = 2\pi f_c \tau_k(t)$. The value of $\phi_k(t)$ changes randomly over the interval $(-\pi, \pi)$. Based on the central limit theorem, the received signal $s_r(t)$ can be modeled as a complex-valued Gaussian random process [46, 52].

Usually, channel attenuation and phase changes are caused by inhomogeneities in the propagation medium. If the channel attenuation and phase change slowly so that they can be treated as constant over each symbol duration, the channel is said to be slowly fading. Furthermore, if the coherence bandwidth of the channel (which can be defined as the reciprocal of the multipath delay spread of the channel T_m) is small in comparison to the transmitted signal bandwidth, the channel is called frequency-selective.

In most mobile applications and for transmission rates not exceeding a few hundred kbit/s, the mobile communication channel can be classified as slowly-fading and nonfrequency selective [53, 54]. In this chapter, our analysis will be based on this channel model, and in a given symbol interval we will assume that the channel attenuation and phase shift are constant and can be denoted as α and ϕ.

4.3 Performance of Coherent JFPM

In this section, the error rate performance of coherently detected JFPM signals transmitted over slowly fading frequency-nonselective channels is evaluated and the receiver structure is described.

If the waveform $s_{mn}(t)$ described in (3.2) is transmitted over a frequency nonselective, slow Rayleigh-fading channel, the received signal during the k-th symbol interval is given by

$$s_r(t) = \alpha e^{-j\phi}\beta_{kmn}(t) + \nu(t) \qquad kT_s \le t < (k+1)T_s \tag{4.3}$$

where $\beta_{kmn}(t)$ denote the equivalent low-pass waveform of the mn-th signal transmitted during the k-th symbol interval, defined as

$$\beta_{kmn}(t) = \sqrt{2S}e^{j(2\pi f_d \lambda_m t + \theta^{(k)})},$$

$\alpha e^{-j\phi}$ represents the attenuation and phase shift introduced by the channel and $\nu(t)$ is a zero-mean complex-valued white Gaussian noise process with autocorrelation function $\phi_\nu(\tau) = \mathcal{E}\{\nu^*(t)\nu(t+\tau)\} = 2N_0\delta(\tau)$ where N_0 is the value of the power spectral density of the original bandpass noise process.

In coherent detection, it is assumed that the correct estimates of all the phases and frequencies are available at the receiver. The block diagram of the coherent receiver may be implemented as shown in Fig. 3.1. To determine the error probability of the JFPM receiver, conditional error probability for a given channel attenuation α is evaluated first. The resulting expression is then averaged over the probability density function of the channel attenuation. It was shown in (3.6) that the conditional symbol error probability of the coherently detected JFPM is

$$\begin{aligned} P_e(\rho) = 1 \; - \; & \frac{1}{\sqrt{\pi}}\int_0^\infty \operatorname{erf}\left(\upsilon \tan\frac{\pi}{M_P}\right) e^{[-(\upsilon-\sqrt{\rho})^2]} \\ \times \; & \left[\frac{M_P}{\sqrt{\pi}}\int_0^\upsilon \operatorname{erf}\left(\zeta \tan\frac{\pi}{M_P}\right) e^{-\zeta^2} d\zeta\right]^{M_F-1} d\upsilon, \end{aligned} \tag{4.4}$$

where ρ denotes the signal-to-noise ratio for each k_s-bit, defined as

$$\rho = \frac{\alpha^2 E_s}{N_0} = \frac{\alpha^2 S T_s}{N_0}. \tag{4.5}$$

To obtain the probability of symbol error $P_e(M)$, we must average $P_e(\rho)$ of (4.4) over the probability density function (pdf) of ρ, i.e.,

$$P_e(M) = \int_0^\infty P_e(\rho) f_\rho(\rho) d\rho, \tag{4.6}$$

where $f_\rho(\rho)$ denotes the pdf of the random variable ρ. When α is Rayleigh-distributed, ρ has a Chi-square-distribution and its pdf is given by

$$f_\rho(\rho) = \frac{1}{\bar{\rho}} e^{-\rho/\bar{\rho}}, \qquad \rho \geq 0; \tag{4.7}$$

where $\bar{\rho}$ represents the expected value of ρ, i.e.,

$$\bar{\rho} = \frac{E_s}{N_0} \mathcal{E}\left\{\alpha^2\right\} \tag{4.8}$$

where $\mathcal{E}\{\ \}$ denotes the expected value of the quantity in the brackets. Using (4.4) and (4.7), the symbol error probability in (4.6) can be written as

$$\begin{aligned} P_e(M) &= 1 - \frac{1}{\bar{\rho}} \int_0^\infty e^{-\rho/\bar{\rho}} \left[\frac{1}{\sqrt{\pi}} \int_0^\infty \operatorname{erf}\left(v \tan\frac{\pi}{M_P}\right) e^{[-(v-\sqrt{\rho})^2]} g(v) dv\right] d\rho \\ &= 1 - \frac{1}{\bar{\rho}\sqrt{\pi}} \int_0^\infty \operatorname{erf}\left(v \tan\frac{\pi}{M_P}\right) g(v) \left[\int_0^\infty e^{-(v-\sqrt{\rho})^2 - \rho/\bar{\rho}} d\rho\right] dv, \end{aligned} \tag{4.9}$$

where

$$g(v) = \left[\frac{M_P}{\sqrt{\pi}} \int_0^v e^{-\zeta^2} \operatorname{erf}\left(\zeta \tan\frac{\pi}{M_P}\right) d\zeta\right]^{M_P-1}. \tag{4.10}$$

The last integral in (4.9) can be evaluated to give

$$\begin{aligned} z(v) &= \int_0^\infty e^{-(v-\sqrt{\rho})^2 - \rho/\bar{\rho}} d\rho \\ &= e^{-v^2}\left[\sqrt{\pi\varepsilon^3 v^2} e^{\varepsilon v^2} \operatorname{erfc}\left(-\sqrt{\varepsilon v^2}\right) + \varepsilon\right], \end{aligned} \tag{4.11}$$

where

$$\varepsilon = \frac{\bar{\rho}}{1+\bar{\rho}}.$$

Hence, the symbol error probability in (4.9) can be written in the form of

$$P_e(M) = 1 - \frac{1}{\bar{\rho}\sqrt{\pi}} \int_0^{\infty} \operatorname{erf}\left(v \tan \frac{\pi}{M_P}\right) g(v) z(v) dv, \tag{4.12}$$

where $g(v)$ and $z(v)$ are as given in (4.10) and (4.11).

4.4 Performance with Differential Detection

In this section, we consider the problem of finding the probability of error performance with differential detection of JFPM signals over frequency-nonselective and slow Rayleigh fading channels. The block diagram of the receiver employed is given in Fig. 3.3. The receiver requires M_F noncoherent frequency detectors and a single differential phase detector.

To obtain the error performance of the JFPM receiver in the frequency nonselective slow Rayleigh-fading channel, we first evaluate the conditional error probability for each part of the receiver for a given channel attenuation α. The resulting expression for each part is then averaged over the probability density function of the channel attenuation. Finally, the symbol error probability $P_e(M)$ of the joint receiver can be obtained by applying (3.49), which is the probability of either FSK-part or DPSK-part being in error.

Now let us find the probability of an erroneous noncoherent decision on the frequency in the FSK-part of the joint receiver $P_{e,FSK}$. It was shown in (3.50) that the probability of an erroneous noncoherent decision on the frequency for a fixed channel attenuation α (i.e., $P_{e,FSK}(\rho)$) is equal to

$$P_{e,FSK}(\rho) = \frac{1}{M_F} \sum_{i=2}^{M_F} (-1)^i \begin{pmatrix} M_F \\ i \end{pmatrix} e^{-\rho\left(\frac{i-1}{i}\right)}. \tag{4.13}$$

Averaging the probability of error given in (4.13) over the pdf of ρ per (4.7) and by using (4.6), the probability of an erroneous noncoherent decision on the frequency,

$P_{e,FSK}$ is found as

$$P_{e,FSK} = \sum_{k=1}^{M_F-1} (-1)^{k+1} \frac{1}{k\bar{\rho}+k+1} \binom{M_F-1}{k}. \tag{4.14}$$

It is desirable to obtain the symbol error probability in terms of the average signal-to-noise ratio per bit $\bar{\rho}_b$. The relationship between the average signal-to-noise ratio per symbol and average signal-to-noise ratio per bit is given by

$$\bar{\rho} = k_s\bar{\rho}_b = (k_F + k_P)\bar{\rho}_b. \tag{4.15}$$

From (4.15) we observe an improvement on the average signal-to-noise ratio per bit by a factor I_F for the FSK-part of the JFPM over the conventional FSK, where I_F was given in (3.52).

For the DPSK-part, the probability of an incorrect decision on the phase in the DPSK-part given that the noncoherent decision of the FSK-part was correct for a fixed channel attenuation α (i.e., $P_{e,PSK|FSK}(\rho)$) is given in (3.53) and it is equal to

$$P_{e,PSK|FSK}(\rho) = \frac{\sin(\pi/M_P)}{2\pi} \int_{-\pi/2}^{\pi/2} \frac{e^{-\rho[1-\cos(\pi/M_P)\cos u]}}{1-\cos(\pi/M_P)\cos u} du \tag{4.16}$$

Averaging the probability of error given in (4.16) over the pdf of ρ per (4.7) and by using some trigonometry, the probability of an incorrect decision on the phase in the DPSK-part given that the noncoherent decision of the FSK-part was correct (i.e., $P_{e,PSK|FSK}$) when the signal was transmitted over a frequency nonselective, slow Rayleigh-fading channel is found as

$$P_{e,PSK|FSK} = \frac{M_P-1}{M_P} - \frac{\varepsilon\sin(\pi/M_P)}{\pi\sqrt{1-\varepsilon^2\cos^2(\pi/M_P)}} \cot^{-1}\left[\frac{-\varepsilon\cos(\pi/M_P)}{\sqrt{1-\varepsilon^2\cos^2(\pi/M_P)}}\right] \tag{4.17}$$

where $\varepsilon = \bar{\rho}/(1+\bar{\rho})$. The improvement factor for the DPSK-part of the JFPM receiver over the conventional M_P-ary DPSK is equal to I_P, where I_P is given in (3.57).

The symbol error probability for the JFPM signals can be written by substituting (4.14) and (4.17) into (3.30), and it is given by

$$
\begin{aligned}
P_e(M) &= \sum_{k=1}^{M_F-1} (-1)^{k+1} \frac{1}{k\bar{\rho}+k+1} \binom{M_F-1}{k} + \sum_{k=0}^{M_F-1} (-1)^{k} \frac{1}{k\bar{\rho}+k+1} \binom{M_F-1}{k} \\
&\times \left\{ \frac{M_P-1}{M_P} - \frac{\varepsilon \sin(\pi/M_P)}{\pi\sqrt{1-\varepsilon^2\cos^2(\pi/M_P)}} \cot^{-1}\left[\frac{-\varepsilon\cos(\pi/M_P)}{\sqrt{1-\varepsilon^2\cos^2(\pi/M_P)}} \right] \right\}. \qquad (4.18)
\end{aligned}
$$

The bit error probability expression for the JFPM signals obtained by substituting (4.14) and (4.17) into (3.60) can be written as

$$
\begin{aligned}
P_b(M) &= \frac{k_s M - k_P M_P}{2k_s(M-M_P)} \sum_{k=1}^{M_F-1} (-1)^{k+1} \frac{1}{k\bar{\rho}+k+1} \binom{M_F-1}{k} \\
&+ \frac{1}{k_s} \sum_{k=0}^{M_F-1} (-1)^{k} \frac{1}{k\bar{\rho}+k+1} \binom{M_F-1}{k} \qquad (4.19) \\
&\times \left\{ \frac{M_P-1}{M_P} - \frac{\varepsilon \sin(\pi/M_P)}{\pi\sqrt{1-\varepsilon^2\cos^2(\pi/M_P)}} \cot^{-1}\left[\frac{-\varepsilon\cos(\pi/M_P)}{\sqrt{1-\varepsilon^2\cos^2(\pi/M_P)}} \right] \right\}.
\end{aligned}
$$

The bit error probability expression given in (4.19) is evaluated numerically for different values of M_F and M_P and the results are presented in Section 6.

4.5 Diversity Combining Techniques

If several independent copies of a faded signal are available at the receiver, the probability that all these signals experiencing large fades simultaneously is much lower than that of a single copy, and a well designed system can take advantage of the diversity. Several ways of obtaining independent or nearly independent signals to apply diversity combining have been discussed in [52] and [53]. In the generic diversity reception which we will discuss, the diversity can be as a result of time, frequency or space diversity introduced in to the system.

4.5.1 Diversity Receiver Structure

In this section, we introduce a diversity receiver structure for JFPM signals, when the signal in (3.2) is transmitted over a Rayleigh fading channels, with L diversity branches. Each of the L branches is characterized by an equivalent low-pass impulse response $h_k(t) = \alpha_k e^{-j\phi_k}\delta(t - t_k)$ for $k = 1, 2, ..., L$. For simplicity, nonselective fading on each diversity channel is assumed. The time instants t_k, $k = 1, 2, ..., L$ are assumed to be uniformly distributed over the interval $(0, 2T_s)$. It is also assumed that the L diversity branches are mutually independent, each having Rayleigh-distributed envelope statistics. The transmitted signal on each branch is independently corrupted by an additive white Gaussian noise process. The equivalent low-pass received signal during the time interval $kT_s < t < (k+1)T_s$ for the l-th branch can be expressed in the form

$$s_r^{(l)}(t) = \alpha_l e^{-j\phi_l}\beta_{kmn}^{(l)}(t) + \nu_l(t) \qquad l = 1, 2, ..., L \tag{4.20}$$

where $\beta_{kmn}^{(l)}(t)$ represents the mn-th signal transmitted during the k-th time interval in the l-th channel, $\nu_l(t)$ is a zero mean complex-valued white Gaussian noise process with power spectral density N_0. It is assumed that α_l and ϕ_l are independent for $l = 1, 2, ..., L$.

For coherent detection, a maximal-ratio combiner is optimum [46] but it assumes perfect knowledge of the channel parameters $\{\alpha_k e^{-j\phi_k}\}$. In differential detection, channel parameter estimation is done implicitly. In a slowly fading channel, differential detection effectively achieves maximal-ratio combining by weighing the present received signal sample with a one-symbol delayed version of itself and then linearly combining different diversity paths [64]. In noncoherent detection of the FSK-part, the channel parameters are not known and square-law combining is optimum [46, 52].

A block diagram describing the diversity system in a multipath fading channel is shown in Fig. 4.1. Where a two-stage decision process is used to establish which signal is received. It is possible to determine the subset of the transmitted signal from the frequency of the signal. This can be accomplished in the first stage by using noncoherent detection with a square law combiner. After the frequency, the phase of the signal should be determined. The diversity receiver for the differential phase detection linearly combines different diversity paths as shown in [64]. The one symbol delay at the input of the DPSK-part is later compensated in demultiplexing by introducing a one-symbol delay following the FSK detector.

4.5.2 Analysis of Performance

The error rate performance for the noncoherent FSK-part of the JFPM receiver will now be determined. The FSK-part of the joint receiver employs square-law combining. The symbol error probability of the M_F-ary FSK-part in the joint receiver when square-law combining is employed was found in [46] and it is equal to

$$\begin{aligned} P_{e,FSK} &= \frac{1}{(L-1)!} \sum_{k=1}^{M_F-1} (-1)^{k+1} \frac{1}{(k\bar{\rho}_c + k + 1)^L} \binom{M_F - 1}{k} \\ &\times \sum_{n=0}^{k(L-1)} \sigma_{nk} (L+n-1)! \left(\frac{\bar{\rho}_c + 1}{k\bar{\rho}_c + k + 1} \right)^n \end{aligned} \tag{4.21}$$

where σ_{nk} is the set of coefficients in the following equation

$$\left(\sum_{n=0}^{L-1} \frac{x^n}{n!} \right)^k = \sum_{n=0}^{k(L-1)} \sigma_{nk} x^n \tag{4.22}$$

and $\bar{\rho}_c = \mathcal{E}\left\{\alpha_k^2\right\} E_s/N_0$ denotes the average signal-to-noise ratio per diversity channel. The relationship between the average signal-to-noise ratio per diversity channel and the average signal-to-noise ratio per bit is defined as

$$\bar{\rho}_b = \frac{L\bar{\rho}_c}{k_F + k_P} \tag{4.23}$$

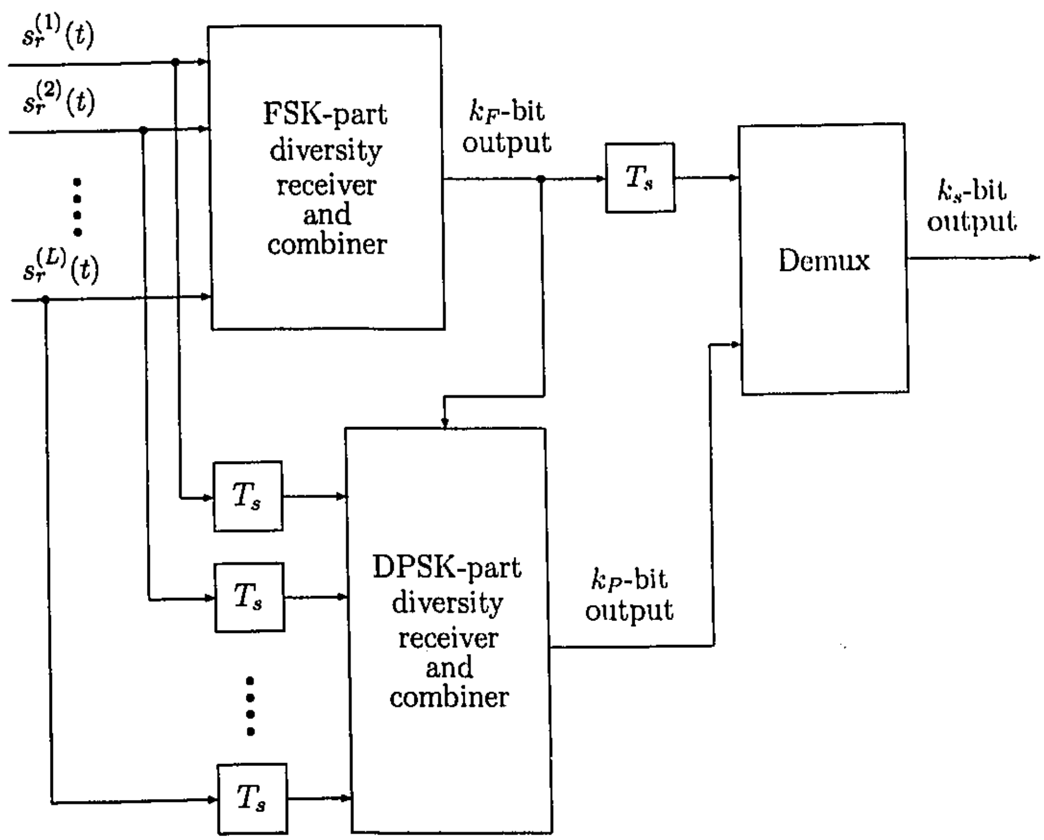

Figure 4.1 : Block diagram of diversity receiver for JFPM.

Having obtained the error rate performance with diversity reception for the M_F-ary FSK-part of the joint receiver, we turn our attention to the performance of differential detection of M_P-ary PSK signals. it was shown in [46] that the symbol error probability of the M_P-ary DPSK signals is equal to

$$
\begin{aligned}
P_{e,PSK|FSK} &= \frac{(-1)^{L-1}(1-\Omega^2)^L}{\pi\,(L-1)!}\left\{\frac{\partial^{L-1}}{\partial x^{L-1}}\left[\frac{1}{x-\Omega^2}\left(\frac{\pi}{M_P}(M_P-1)\right.\right.\right.\\
&- \left.\left.\left.\frac{\Omega\sin(\pi/M_P)}{\sqrt{x-\Omega^2\cos^2(\pi/M_P)}}\cot^{-1}\left[\frac{-\Omega\cos(\pi/M_P)}{\sqrt{x-\Omega^2\cos^2(\pi/M_P)}}\right]\right)\right]\right\}_{x=1} \quad (4.24)
\end{aligned}
$$

where $\Omega=\bar{\rho}_c/(1+\bar{\rho}_c)$ and $\bar{\rho}_c$ is the average signal-to-noise ratio per diversity channel. The symbol error probability of the diversity receiver can be found by substituting (4.21) and (4.24) into (3.30), and is given by

$$
\begin{aligned}
P_e(M) &= \frac{1}{(L-1)!}\sum_{k=1}^{M_F-1}(-1)^{k+1}\frac{1}{(k\bar{\rho}_c+k+1)^L}\binom{M_F-1}{k}\\
&\times \sum_{n=0}^{k(L-1)}\sigma_{nk}\,(L+n-1)!\left(\frac{\bar{\rho}_c+1}{k\bar{\rho}_c+k+1}\right)^n\\
&+ \left[\left\{\frac{1}{(L-1)!}\sum_{k=0}^{M_F-1}(-1)^k\frac{1}{(k\bar{\rho}_c+k+1)^L}\binom{M_F-1}{k}\right.\right.\\
&\times \left.\sum_{n=0}^{k(L-1)}\sigma_{nk}\,(L+n-1)!\left(\frac{\bar{\rho}_c+1}{k\bar{\rho}_c+k+1}\right)^n\right\}\\
&\times \left\{\frac{(-1)^{L-1}(1-\Omega^2)^L}{\pi\,(L-1)!}\left\{\frac{\partial^{L-1}}{\partial x^{L-1}}\left[\frac{1}{x-\Omega^2}\left(\frac{\pi}{M_P}(M_P-1)\right.\right.\right.\right.\\
&- \left.\left.\left.\left.\left.\frac{\Omega\sin(\pi/M_P)}{\sqrt{x-\Omega^2\cos^2(\pi/M_P)}}\cot^{-1}\left[\frac{-\Omega\cos(\pi/M_P)}{\sqrt{x-\Omega^2\cos^2(\pi/M_P)}}\right]\right)\right]\right\}_{x=1}\right\}\right] \quad (4.25)
\end{aligned}
$$

The bit error probability obtained by substituting (4.21) and (4.24) into (3.60) is evaluated numerically for different values of M_F and M_P and the results are presented in Section 6.

4.6 Performance Results and Comparisons

Based on the equations developed in the previous sections, we now present the performance of JFPM in a slowly fading nonfrequency selective Rayleigh channel and demonstrate the improvements achieved by using diversity combining. When diversity reception is used, it is assumed that the L diversity channels fade, independently.

The performance of JFPM in a frequency nonselective, slow Rayleigh fading channel has been numerically evaluated. In Fig. 4.2, we plotted the curves for $M_P = 2$ and $M_F = 2, 4, 8, 16$ which have been obtained directly from (4.19) and by substituting (4.21) and (4.24) into (3.60). We also added the curves for the conventional noncoherent FSK and DPSK systems. The curves when there is no diversity reception indicate that Rayleigh fading greatly degrades the performance and increasing the number of frequencies does not yield any appreciable improvement. To obtain a BER of 10^{-4}, the required $\bar{\rho}_b$ is about 40 dB, which is at least 30 dB more than the requirement for an AWGN channel (see Chapter 3). When 2 branch diversity ($L = 2$) is employed, significant performance gain (more than 15 dB) is achieved. In Fig. 4.3, we plotted a similar set of curves when $M_P = 4$ and $M_F = 2, 4, 8, 16$. The comparison of Fig. 4.2 and Fig. 4.3 indicates that in a Rayleigh fading channel $M_P = 2$ and $M_P = 4$ yield very close BER performances. Hence, the selection of the appropriate M_P and M_F would be based on the bandwidth efficiency versus complexity tradeoff.

The performance of various JFPM, noncoherent FSK and DPSK schemes can also be compared with the aid of Table 4.1 and Table 4.2. In Table 4.1 we present the energy per bit to noise density ratio (in dB) required to achieve a BER of 10^{-4} when the systems do not use diversity reception. We note that in this case, the required $\bar{\rho}_b$ is between 35.3 dB and 37.61 dB. Although the difference is small, JFPM schemes

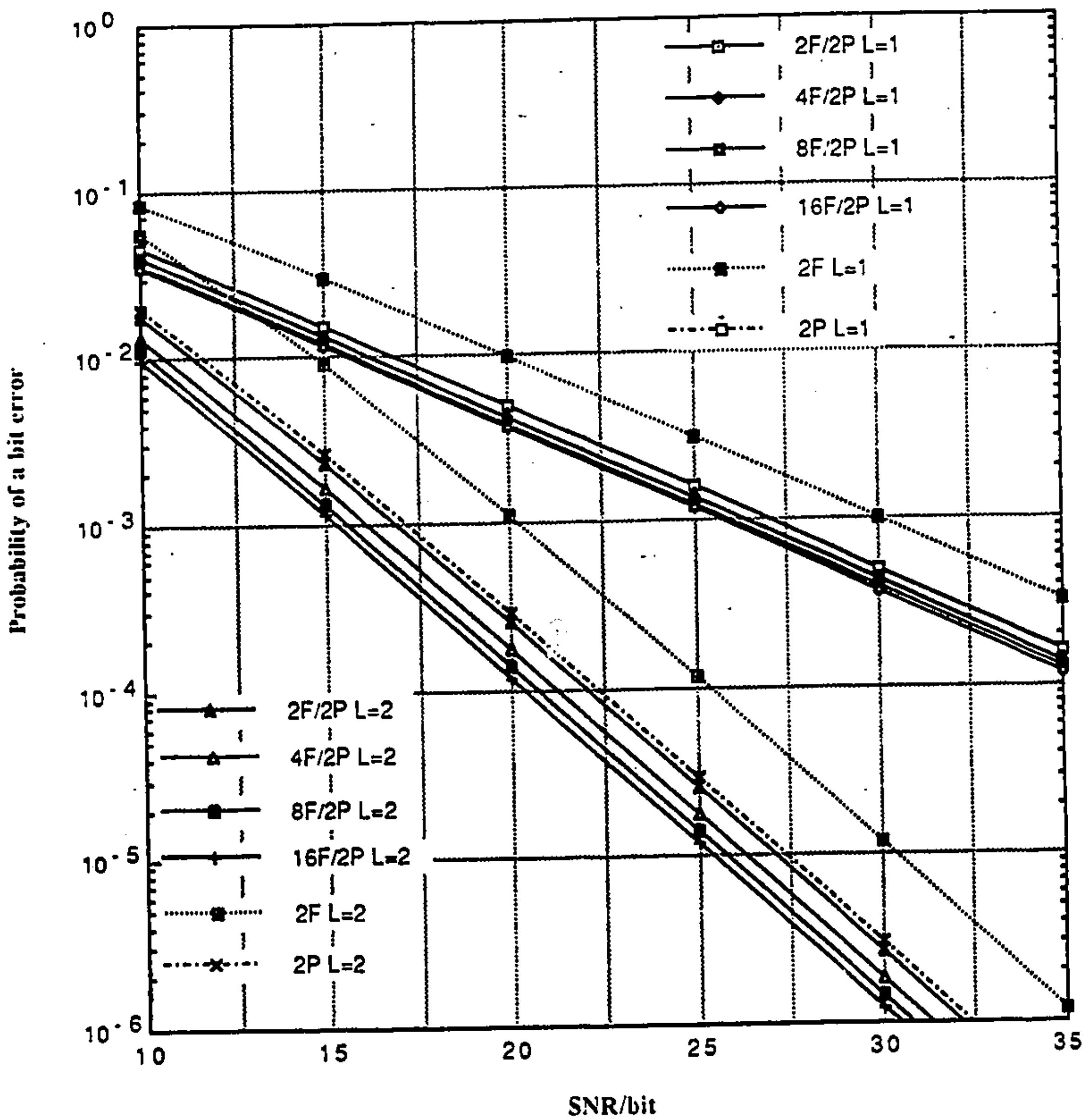

Figure 4.2 : Bit error rate performance of DPSK (P), noncoherent FSK (F) and differentially detected JFPM in Rayleigh fading channel when $M_P = 2$ and $M_F = 2, 4, 8, 16$, and diversity order $L = 1, 2$.

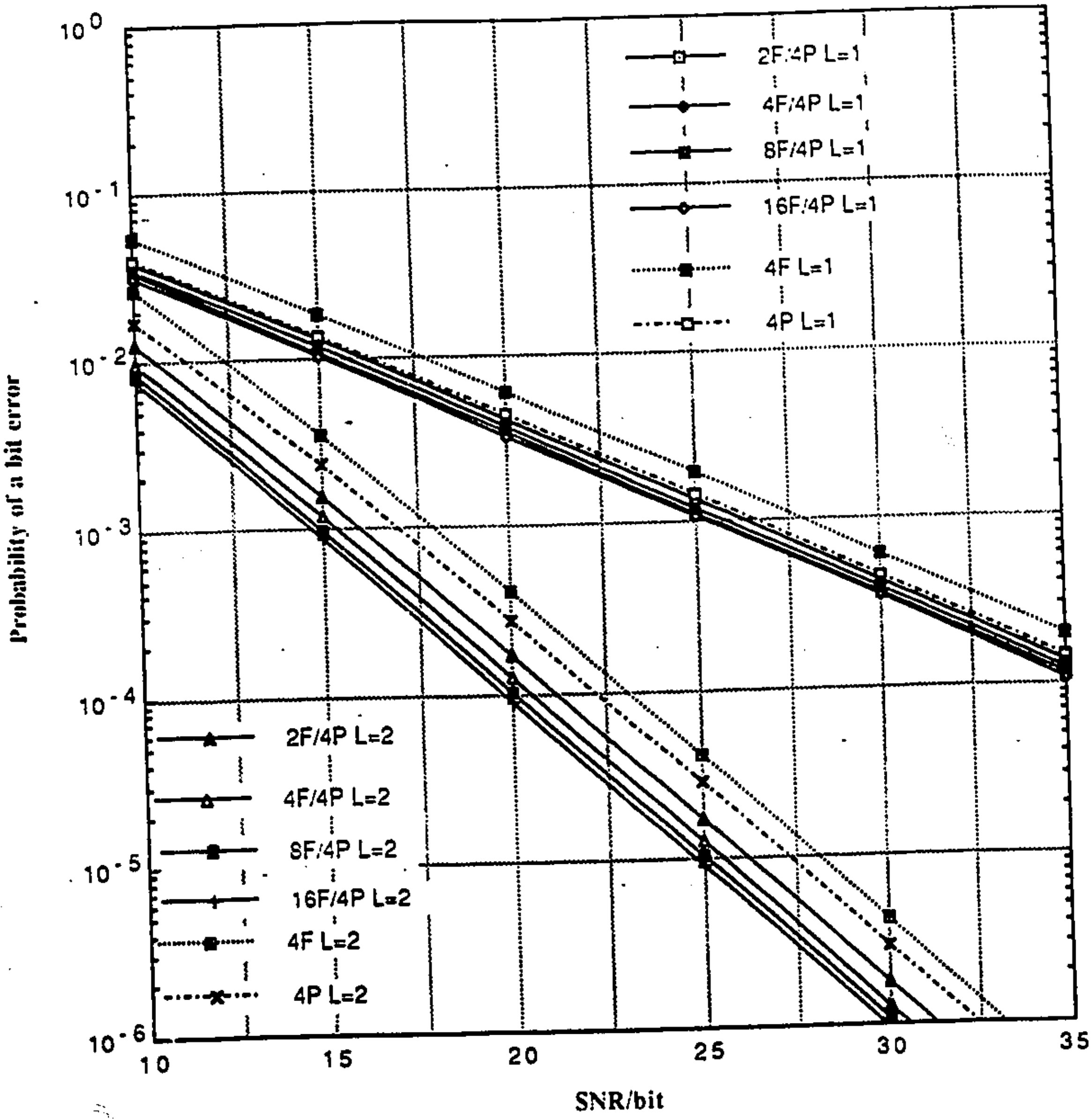

Figure 4.3 : Bit error rate performance of DPSK (P), noncoherent FSK (F) and differentially detected JFPM in Rayleigh fading channel when $M_P = 4$ and $M_F =$ 2, 4, 8, 16, and diversity order $L = 1, 2$.

Table 4.1 : A comparison of differentially detected JFPM, noncoherent FSK and DPSK in terms of bandwidth efficiency R_b/W (in b/s/Hz) and energy per bit to noise density ratio $\bar{\rho}_b$ (in dB) required to achieve a bit error rate of 10^{-4} in a Rayleigh channel (no diversity).

M_F \ M_P	1 (FSK)	2	4	8	-
1 (DPSK)	–	1	2	3	R_b/W
	–	36.99	36.58	38.74	$\bar{\rho}_b$
2	0.5	1	1.5	2	R_b/W
	40	36.98	36.27	37.61	$\bar{\rho}_b$
4	0.5	0.75	1	1.25	R_b/W
	37.86	36.32	35.80	36.78	$\bar{\rho}_b$
8	0.375	0.5	0.625	0.75	R_b/W
	36.94	35.91	35.49	36.21	$\bar{\rho}_b$
16	0.25	0.3125	0.375	0.4375	R_b/W
	36.46	35.67	35.30	35.83	$\bar{\rho}_b$

Table 4.2 : A comparison of differentially detected JFPM, noncoherent FSK and DPSK in terms of bandwidth efficiency R_b/W (in b/s/Hz) and energy per bit to noise density ratio $\bar{\rho}_b$ (in dB) required to achieve a bit error rate of 10^{-4} in a Rayleigh channel (with second order diversity).

M_F \ M_P	1 (FSK)	2	4	8	-
1 (DPSK)	–	1	2	3	R_b/W
	–	22.33	22.23	24.98	$\bar{\rho}_b$
2	0.5	1	1.5	2	R_b/W
	25.34	22.03	21.15	23.32	$\bar{\rho}_b$
4	0.5	0.75	1	1.25	R_b/W
	23.06	21.23	20.47	22.14	$\bar{\rho}_b$
8	0.375	0.5	0.625	0.75	R_b/W
	21.96	20.71	20.05	21.29	$\bar{\rho}_b$
16	0.25	0.3125	0.375	0.4375	R_b/W
	21.32	20.36	19.78	20.67	$\bar{\rho}_b$

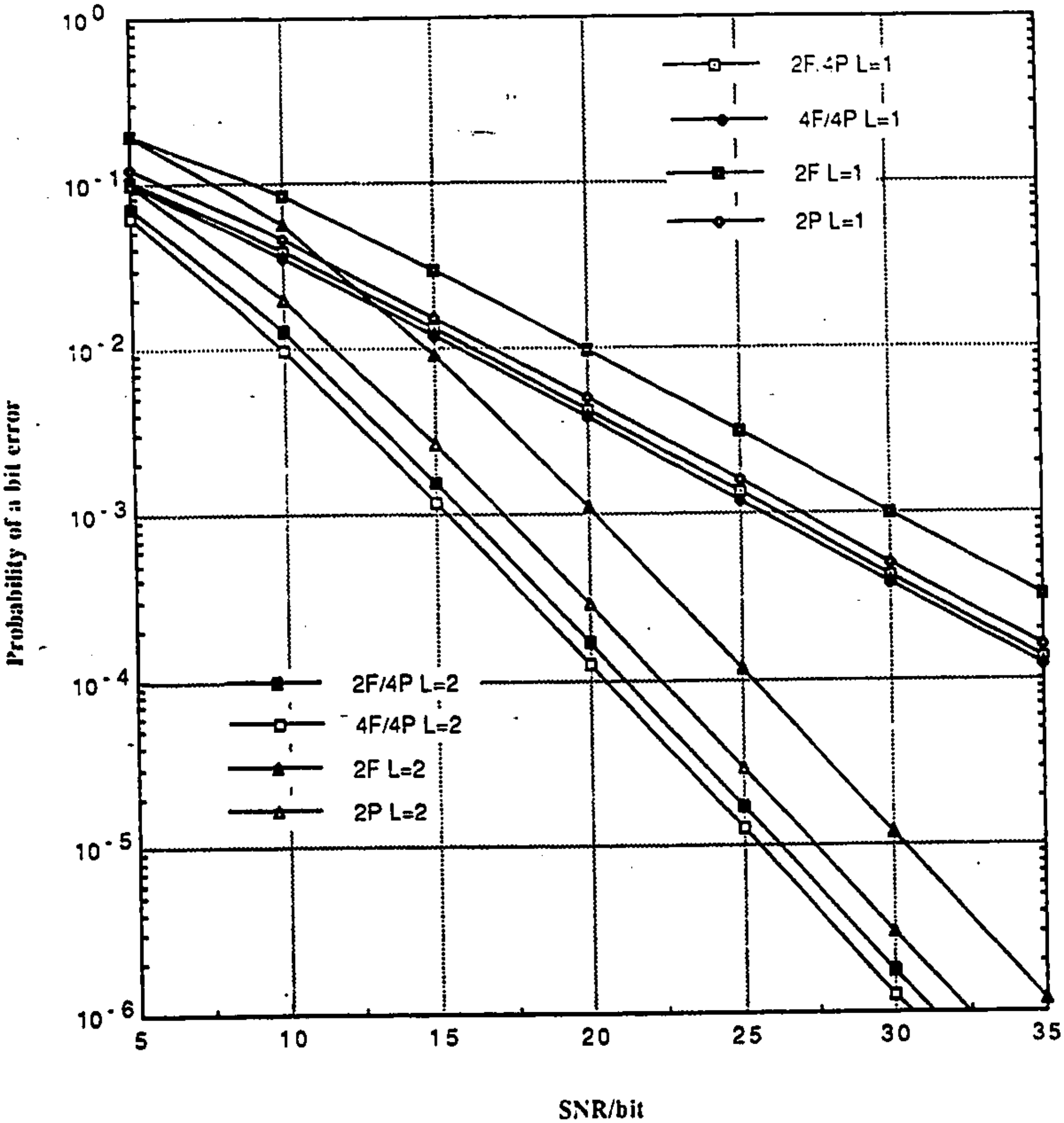

Figure 4.4 : Performance comparison of two differentially detected JFPM schemes with binary DPSK and binary FSK in Rayleigh fading channel with diversity order $L = 1, 2$ (note that JFPM provides power and bandwidth efficiency at the same time over the conventional noncoherent binary FSK and binary DPSK schemes).

using four phases perform better than their two-phase counterparts. In Table 4.2, $\bar{\rho}_b$ required with two-branch diversity is given. The values of $\bar{\rho}_b$ now range from 19.78 dB (16F/4P) to 24.98 dB (8-DPSK). Note that with diversity, JFPM schemes with four phases perform slightly better than their two-phase counterparts.

A comparison of two JFPM schemes, namely 2F/4P and 4F/4P that provide power and bandwidth efficiency at the same time over the conventional noncoherent binary FSK and binary DPSK schemes is shown in Fig. 4.4, when all the systems use single and double branch diversity. It is clear from this figure that with diversity, the improvement in JFPM schemes is greater.

4.7 Conclusions

It has been shown that JFPM schemes, by combining FSK and PSK properties in desirable proportions, can provide a good combination of bandwidth efficiency of PSK as the number of phases increases and the power efficiency of FSK as the number of frequencies increases. By developing probability of error expressions over nonselective slow fading Rayleigh channels and evaluating these expressions, we have shown that they retain these properties in Rayleigh fading channels. Assuming statistical independence of the diversity channels, we have analyzed the diversity combining reception of JFPM and shown that significant performance improvements can be achieved compared with the conventional systems and non-diversity. For a given M, the improvements of JFPM system over FSK and PSK systems are accompanied by a slight increase in the complexity of the transmitter and the receiver.

Chapter 5

The Spread Spectrum Frequency Hopped/JFPM System

5.1 Introduction

Spread spectrum techniques are widely used in mobile communications because of their capability to counteract multipath fading and their suitability to multiple access. Direct Sequence (DS) and Frequency Hopped (FH) techniques offer different advantages accompanied by different weaknesses. In this chapter, only the FH systems are considered. The modulation technique usually employed is either noncoherently detected M-ary FSK (FH/M-ary FSK) [18]-[19], [58]-[61] or differentially detected M-ary PSK (FH/M-ary DPSK) [20]-[30].

FH systems are classified as slow frequency hopping (SFH) and fast frequency hopping (FFH). For a given spread bandwidth and hop rate, a slow frequency hopping system can support higher data rates than a fast frequency hopping system. On the other hand, FFH systems are more resistant to the effects of multipath fading and partial band jamming. Improvements in the performance of FH systems can be achieved by employing modulation techniques more powerful than basic FSK or basic DPSK. For this purpose, we have investigated the impact of using combined modulation techniques.

In the first part of this chapter, a performance analysis of SFH/JFPM system is given in the presence of broadband and partial-band noise jamming. The worst case jamming strategy is evaluated. The results show that under these jamming conditions, the FH/JFPM performs better than the FH/M-ary DPSK and FH/M-ary FSK systems. It is also shown that for a given channel bandwidth and data rate, the FH/JFPM system has more processing gain than its FSK or DPSK counterparts. In the second part of this chapter, the performance of FFH/JFPM system over multipath Rayleigh fading channels is studied. A receiver structure for FFH/JFPM system is introduced and the probability of error is analyzed. The results show that the FFH/JFPM system performs better than the conventional FFH systems.

In Section 5.2, the properties of the transmitted signal and the frequency hopped system model are described. Section 5.3 presents the receiver structures and the performance analysis of SFH/JFPM signals in broadband and partial-band noise jamming, where the probability of error expressions are obtained and the optimal jamming strategy is evaluated. Section 5.4 describes the mechanism of the FFH/JFPM system. A receiver structure for FFH/JFPM signals is introduced and the performance analysis of this system over Rayleigh fading channels is obtained. Finally, the conclusions are stated in Section 5.5.

5.2 The Frequency-Hopped/JFPM System

In this section, a description of the frequency hopped system model and the transmitted signals of a FH/JFPM is given.

A block diagram of a frequency-hopping spread spectrum transmitter and receiver is shown in Fig. 5.1. The JFPM signal at the output of the modulator is translated in frequency by an amount determined and controlled by the PN code generator, which in turn is used to drive a frequency synthesizer. The modulated signal is mixed by the synthesized frequency and transmitted over the channel. In the receiver, the incoming signal is mixed with the synthesized signal identical to the one at the transmitter. If the PN code generators in the transmitter and receiver are in synchronized, the signal at the output of the mixer is demodulated in the usual fashion by passing the signal through the JFPM receiver.

The frequency-time plane of the frequency hopping JFPM signal is illustrated in Fig. 5.2. The available channel bandwidth β_{ss} is partitioned into q contiguous frequency slots of bandwidth $\beta_{ch} = \beta_{ss}/q$, and each frequency slot is subdivided into M_F frequency bins. The frequency separation between two adjacent bins is given by

$$\beta_{bin} = \frac{\beta_{ch}}{M_F} = \frac{\beta_{ss}}{qM_F} \tag{5.1}$$

This implies that the number of bins in the available channel bandwidth $N = qM_F$. On a given hop, to satisfy the orthogonality condition needed for the noncoherent detection, the JFPM tones must be separated in frequency by an integer multiple of $\beta_{bin} = 1/T_s$.

The processing gain may be defined as a measure of the anti-jam capability of the spread spectrum system [18, vol. I, p. 138; vol. II, p. 66] and can be expressed as

$$PG = \frac{\beta_{ss}}{R_b}. \tag{5.2}$$

The hopping from one frequency band to another is determined by a PN sequence. The transmission time is subdivided into slots of duration T_h (hop-duration). The relationship between the symbol duration T_s and the hop-duration $T_h = 1/R_h$ is given by

$$L = \frac{T_s}{T_h} = \frac{R_h}{R_s}. \tag{5.3}$$

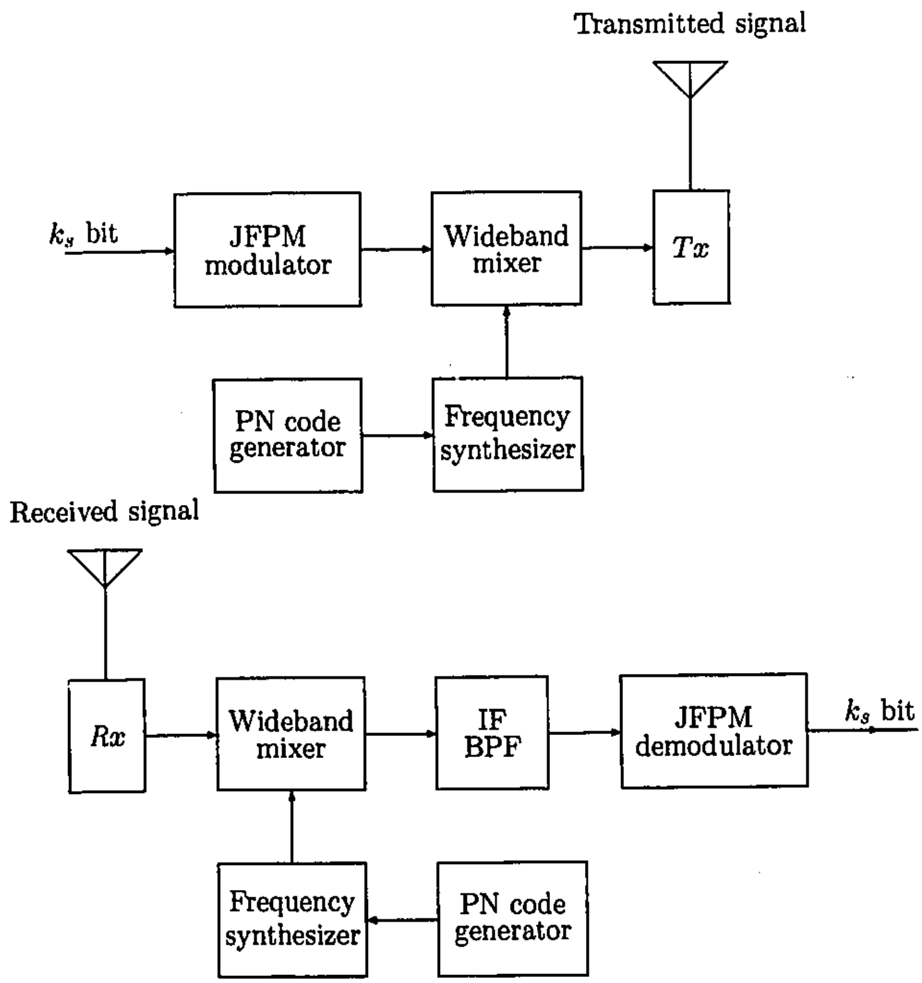

Figure 5.1 : Block diagram of a FH/JFPM system.

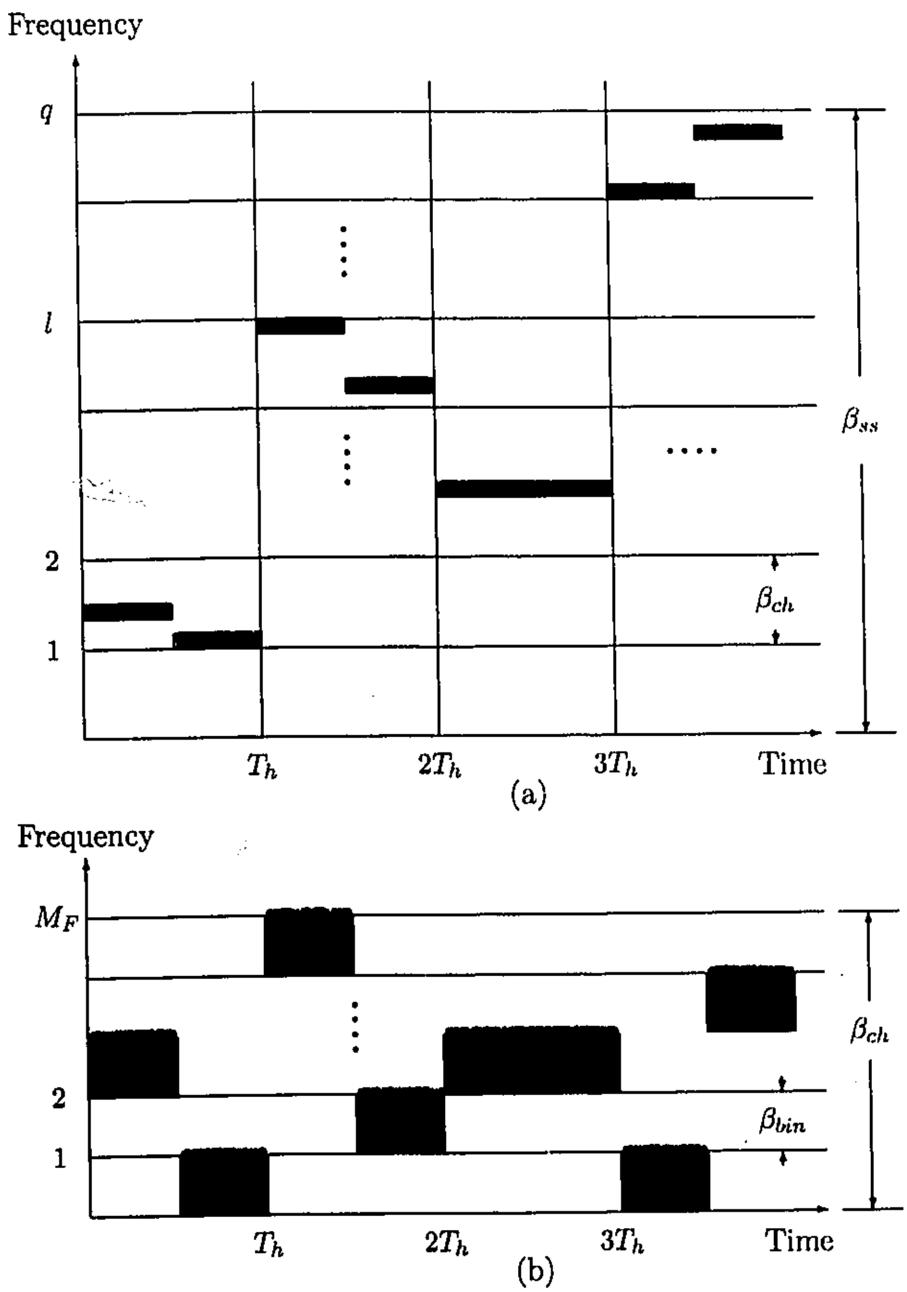

Figure 5.2 : Frequency-hopping signal in the Frequency-Time plane of (a) transmitted signal for FH/JFPM spread spectrum system; (b) a receiver dehopped signal at the input of a JFPM demodulator. When $T_h = 2T_s$ i.e., $L = 1/2$, SFH).

If $L \geq 1$, there are L hops per symbol duration, and it is called fast frequency hopping. If $L < 1$, there are multiple symbols per hop, and it is called slow frequency hopping. It is generally assumed that for fast frequency hopping L is an integer; and for slow frequency hopping $1/L$ is an integer.

An interesting interpretation of the performance characteristic for the FH/JFPM signals is obtained by expressing the relation given in (5.3) in terms of R_h/R_b, where

$$\begin{aligned} L &= \frac{k_F T_b}{T_h} + \frac{k_P T_b}{T_h} \\ &= \log_2 M_F \frac{R_h}{R_b} + \log_2 M_P \frac{R_h}{R_b}. \end{aligned} \tag{5.4}$$

The parameter L is important when the received signal frequently undergoes multipath fading, and in antijam applications to limit the effect of interference. It is interesting to observe from (5.4) that, the first part of this equation relates the diversity level L and the ratio R_h/R_b through the number of FSK tones per channel, whereas the second part relates the diversity level L and the ratio R_h/R_b through the number of phases used to form the JFPM signals. Therefore, for a given value of the bit rate and the hop rate, in FH/JFPM the diversity level L can be controlled by changing either M_F or M_P. In fading channels, as the diversity level L increases, the error rate decreases. The price to be paid for this improvement in a given value of the hop rate is a reduction in the data rate available for each user. In FH/JFPM, the diversity level L as given in (5.4) may be written in the form

$$L = k_F \frac{k_F + k_P}{k_F} \frac{R_h}{R_b} \tag{5.5}$$

In comparison to the conventional FH systems that use the same number of tones, from (5.5) it can be concluded that, the diversity level could be increased without changing the hop rate and the data rate.

In FH/JFPM system, the transmitted signal during the l-th frequency hopped slot can be expressed as

$$s_{mn}^{(l)}(t) = \sqrt{2S}\cos(2\pi(f_m + f_{h_l})t + \theta^{(k)}) \quad \text{for } l = 1, 2, ..., q, \tag{5.6}$$

where $\theta^{(k)} = \theta_n + \theta^{(k-1)}$ is the signal phase to be transmitted in the k-th signaling interval, θ_n is the differential phase to be transmitted and $\theta^{(k-1)}$ is the total accumulated phase (modulo 2π) until the end of $(k-1)$-th signaling interval. In (5.6) f_m is one of the M_F modulated tones at the output of the JFPM modulator and f_{h_l} is the frequency of the hopped slot. If slow frequency hopping is assumed, the transmitted tone $f_m + f_{h_l}$ is constant in the interval $kT_s \leq t \leq (k+1)T_s$. If fast frequency hopping is employed, the frequency $f_m + f_{h_l}$ is constant during each hop $kT_h \leq t \leq (k+1)T_h$.

5.3 Performance of SFH/JFPM Signals

When the waveform $s_{mn}^{(l)}(t)$ in (5.6) is transmitted over the channel, the received waveform is

$$r^{(l)}(t) = \sqrt{2S}\cos(2\pi(f_m + f_{h_l})t + \theta^{(k)} + \Omega[f_m + f_{h_l}]) + n_j(t) \tag{5.7}$$

where $n_j(t)$ is the jamming noise or interference and $\Omega(f_m + f_{h_l})$ is the phase introduced by the channel which is assumed to be constant within a frequency bin, i.e., $\Omega(f_m + f_{h_l}) = 2\pi(f_m + f_{h_l})\tau$ where τ is the channel delay.

In this work, we investigate the determination of the frequency f_m and the phase θ_n by passing the dehopped signal through a differentially detected JFPM receiver. The block diagram of the receiver structure is shown in Fig. 3.3. To obtain the symbol error rate performance of the joint receiver, we assume that the data symbols are independent, equiprobable and during a symbol duration the values of the phase angle $\theta_{(k)}$ and the frequency f_m do not change.

Two types of jamming interference are considered in examining the performance of FH/JFPM: broadband noise jamming, and partial-band noise jamming.

5.3.1 Broadband Jamming

In the case of broadband noise jamming, $n_j(t)$ in (5.7) is characterized as Gaussian distributed with zero mean and one-sided power spectral density of

$$N_j = \frac{J}{\beta_{ss}} \tag{5.8}$$

where J is the average jamming power. If slow frequency hopping is employed and the receiver hopping pattern synchronized with the transmitter hopping pattern. The symbol error probability for the FSK-part of the joint receiver is the same as the symbol error probability for noncoherent detection of conventional M_F-ary orthogonal signals. As shown in Section (3.5.2) the symbol error performance of this part of the joint receiver is given in (3.50), where ρ in (3.50) now denotes the symbol signal energy-to-jamming noise density ratio and it is defined as

$$\rho = \frac{E_s}{N_j} = \frac{S}{R_s N_j} \tag{5.9}$$

where E_s represents the received symbol energy. Substituting (5.8) into (5.9), the symbol signal-to-jamming noise ratio becomes

$$\rho = \frac{\beta_{ss}/R_s}{J/S}. \tag{5.10}$$

Recall that each symbol consists of k_s binary digits and the number of bits that can be represented by a set of M-ary JFPM signals is $\log_2 M = k_F + k_P$. A convenient way to express the signal-to-jamming noise ratio is in terms of the processing gain. The symbol signal-to-jamming noise ratio in (5.10) may be expressed as

$$\rho = \frac{(k_F + k_P)\beta_{ss}/R_b}{J/S}$$

$$
\begin{aligned}
&= \frac{k_F(\beta_{ss}/R_b)(k_F+k_P)/k_F}{J/S} \\
&= \frac{k_F PG_F}{J/S} \cdot \frac{k_F+k_P}{k_F} \qquad (5.11)
\end{aligned}
$$

where PG_F denotes the processing gain of the conventional FH/M_F-ary FSK system. The last expression in (5.11) means that, for a given channel bandwidth and data rate the processing gain of the combined FH/M_F-ary FSK signals (i.e., the FSK part of JFPM) shows an improvement over the conventional FH/M_F-ary FSK signals by a factor I_F, where I_F is defined in (3.52). Clearly, the processing gain of the FSK-part of the FH/JFPM system may be written as

$$PG_{FSK} = PG_F I_F \qquad (5.12)$$

Let us now analyze the DPSK-part of the joint receiver. The differential phase to be estimated depends on the frequency that is estimated in the same symbol. Under the assumption that the transmitted tone is estimated correctly, the symbol error probability of the M_P-DPSK signal in a broadband noise channel is given in (3.53). The symbol signal-to-jamming noise ratio in (3.53) can be written as

$$
\begin{aligned}
\rho &= \frac{(k_F+k_P)\beta_{ss}/R_b}{J/S} \\
&= \frac{k_P(\beta_{ss}/R_b)(k_F+k_P)/k_P}{J/S} \\
&= \frac{k_P PG_P}{J/S} \cdot \frac{k_F+k_P}{k_P} \qquad (5.13)
\end{aligned}
$$

where PG_P denotes the processing gain of the conventional FH/M_P-ary DPSK system. One of the advantages of FH/JFPM over the conventional FH system can be observed from (5.13), where the processing gain of the combined FH/M_P-ary DPSK may be defined as

$$PG_{DPSK} = PG_P I_P \qquad (5.14)$$

where I_P is given in (3.57). According to (5.13) and (5.14), the processing gain of the combined FH/M_P-ary DPSK signals have an improvement over the conventional FH/M_P-ary DPSK signals by a factor of I_P.

The symbol error probability for FH/JFPM signals in broadband noise jamming is given in (3.45). The total bit error probability for a JFPM signal set is given in (3.61) and it is evaluated numerically for different JFPM formats and the results are given in Section (3.4.3). From these results it can be observed that the FH/JFPM system is less sensitive to broad band jamming than the conventional frequency hopped systems.

5.3.2 Partial-Band Jamming

In the presence of partial-band noise jamming, the jammer concentrates the available power J over a fraction γ of the total spread spectrum bandwidth β_{ss}, where $0 < \gamma \leq 1$. The partial-band jamming model is depicted in Fig. 5.3.

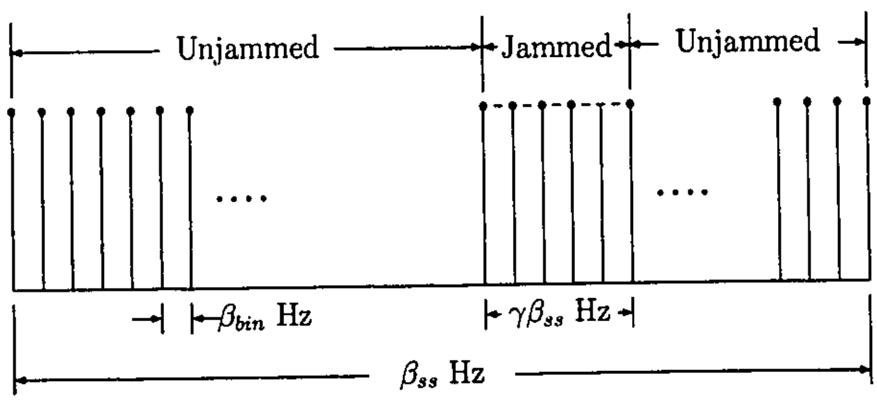

Figure 5.3 : Partial-band jamming model.

The power spectral density of the jamming signal in this jammed fraction of bandwidth is $n_j = J/\gamma\beta_{ss} = N_j/\gamma$ where N_j was defined in (5.8). The remaining $(1 - \gamma)$ fraction of the band is not jammed. Therefore, if the signal is randomly hopped, then on average the probability that the carrier band is jammed equals γ, and during this fraction of time the noise density is the sum of the jamming noise density n_j and the thermal noise density N_0. For the fraction $(1-\gamma)$ when the signal is not jammed, only thermal noise is present. Using $P_e(x)$ to denote the symbol error probability as a function of x, then the probability of symbol error as a function of energy per bit to jamming noise density ratio can be expressed as

$$P_e\left(\frac{E_b}{N_j}\right) = \gamma P_e\left(\frac{E_b}{n_j+N_0}\right) + (1-\gamma)P_e\left(\frac{E_b}{N_0}\right). \tag{5.15}$$

For a large value of E_b/N_0 the last term in (5.15) can be ignored and the equation can be rewritten as

$$\begin{aligned} P_e\left(\frac{E_b}{N_j}\right) &\simeq \gamma P_e\left(\frac{E_b}{n_j}\right) \\ &= \gamma P_e\left(\frac{\gamma E_b}{N_j}\right) \end{aligned} \tag{5.16}$$

where

$$\frac{E_b}{n_j} = \frac{S/R_b}{J/\gamma\beta_{ss}} = \gamma\frac{E_b}{N_j} = \gamma\rho_b. \tag{5.17}$$

From (3.61), (5.16) and (5.17) we can write the probability of bit error as

$$P_b(\rho_b) = \frac{E_b/n_j}{\rho_b}\left\{P_{b1}\left(\frac{E_b}{n_j}\right) + P_{b2}\left(\frac{E_b}{n_j}\right)\right\} \tag{5.18}$$

As stated in [20], for any value of E_b/N_j and at a given M, there is an optimum value of γ from the jammer's strategy that maximizes the probability of bit error. This is the worst case value of γ and is denoted as γ_{wc}. The maximum value of $P_b(\rho_b)$ can be found by differentiating $P_b(\rho_b)$ with respect to E_b/n_j and equating the result to zero. This yields

$$\frac{\partial(E_b/n_j)}{(E_b/n_j)} = -\frac{\partial\left\{P_{b1}\left(\frac{E_b}{n_j}\right) + P_{b2}\left(\frac{E_b}{n_j}\right)\right\}}{\left\{P_{b1}\left(\frac{E_b}{n_j}\right) + P_{b2}\left(\frac{E_b}{n_j}\right)\right\}}. \tag{5.19}$$

The solution of the above differential equation can be expressed in the form of [20]

$$\rho_{b_0} = \frac{\xi_b}{P_{b1}(\rho_{b_0}) + P_{b2}(\rho_{b_0})} \tag{5.20}$$

where the value of E_b/n_j that maximizes (5.18) is denoted as ρ_{b_0} and ξ_b is a constant which depends on the number of levels M_F and M_P. Substituting ρ_{b_0} from (5.20) into (5.18), the probability of bit error for partial or broadband jamming (in partial-band jamming $\gamma < 1$ or $\rho_b > \rho_{b_0}$, and in broadband jamming $\gamma = 1$ or $\rho_b \leq \rho_{b_0}$) is obtained as

$$P_b(\rho_b) = \begin{cases} \frac{\xi_b}{\rho_b} & \rho_b > \rho_{b_0} \\ P_{b1}(\rho_b) + P_{b2}(\rho_b) & \rho_b \leq \rho_{b_0} \end{cases} \tag{5.21}$$

By writing (3.61) in the form of (5.18) and differentiating $P_b(\rho_b)$ with respect to E_b/n_j, the resulting differential equation does not seem to have an analytical solution. However, ρ_{b_0} can be solved numerically. An easy way to find the optimal value of ρ_{b_0} that maximizes the probability of error numerically is by finding the maximum value of $\rho_b P_b(\rho_b)$ which is equal to the parameter ξ_b in (5.20). The value of ρ_b at this point is denoted as ρ_{b_0}. Then, in the worst case jamming, from (5.17) the value of γ_{wc} is given as

$$\gamma_{wc} = \frac{\rho_{b_0}}{\rho_b}. \tag{5.22}$$

The value of ξ_b and ρ_{b0} are evaluated numerically for different JFPM formats and tabulated in Table 5.1. A comparison of ξ_b and ρ_{b0} of FH/JFPM, FH/M-ary FSK and FH/M-ary DPSK are also given in Table 5.1.

In the worst case partial-band noise jamming, the bit error rate performance as a function of ρ_b for FH/JFPM has been calculated by using (5.21) and the values of ξ_b given in Table 5.1. The results are plotted in Fig. 5.4, Fig. 5.5 and Fig. 5.6 for

Table 5.1 : Parameters of bit error performance for FH/M-ary JFPM, FH/M-ary FSK and FH/M-ary DPSK signals in worst case partial-band noise jamming (ρ_{b0} in dB, the values of ξ_b for the conventional FH/M-ary FSK and FH/M-ary DPSK are given in [18] and [20])

M	M_FF/2P		M_FF/4P		M_FF/8P		M-FSK		M-DPSK	
$M_F \times M_P$	ξ_b	ρ_{b0}	ξ_b	ρ_{b0}	ξ_b	ρ_{b0}	ξ_b	ρ_{b0}	ξ_b	ρ_{b0}
2	–	–	–	–	–	–	0.3679	3.01	0.1839	0.00
4	0.1669	-0.54	–	–	–	–	0.2329	0.76	0.2118	0.95
8	0.1512	-1.22	0.1402	-1.01	–	–	0.1954	-0.33	0.4269	4.88
16	0.1454	-1.68	0.1305	-1.86	0.1515	1.17	0.1812	-0.59	1.1579	9.64
32	0.1447	-1.89	0.1275	-2.33	0.1279	-1.12	0.1759	-1.41	3.5586	14.68
64	–	–	0.1282	-2.62	0.1223	-2.11	–	–	–	–
128	–	–	–	–	0.1220	-2.61	–	–	–	–

combination of M_FF/2P, M_FF/4P and M_FF/8P respectively when $M_F = 2, 4, 8, 16$. We have again included the conventional M-ary FSK and M-ary DPSK curves for comparison.

A careful observation of these graphs reveals that when $M_P = 2, 4, 8$, the bit error probability appears almost independent of M_F. This is because the improvement factor I_F of the FSK-part of the joint receiver starts to decrease when the alphabet size M_F increases while M_P remains fixed. These results also indicate that the JFPM formats M_FF/2P, M_FF/4P and M_FF/8P are less sensitive to worst case partial-band noise jamming than the conventional FH/M-ary FSK and FH/M-ary DPSK systems. In Figs. 3.10-3.12 it was observed that in broadband noise jamming, increasing M_P beyond 4 resulted in performance degradation. However, a comparison of Figs. 5.4-5.6 indicates that by increasing M_P or M_F the FH/JFPM system performs better than the conventional FH systems. The reason for this behavior is that, the bit error rate of JFPM system is limited to either FSK-part or DPSK-part (whichever one can provide the highest bit error rate). Also, worst case partial-band jamming converts

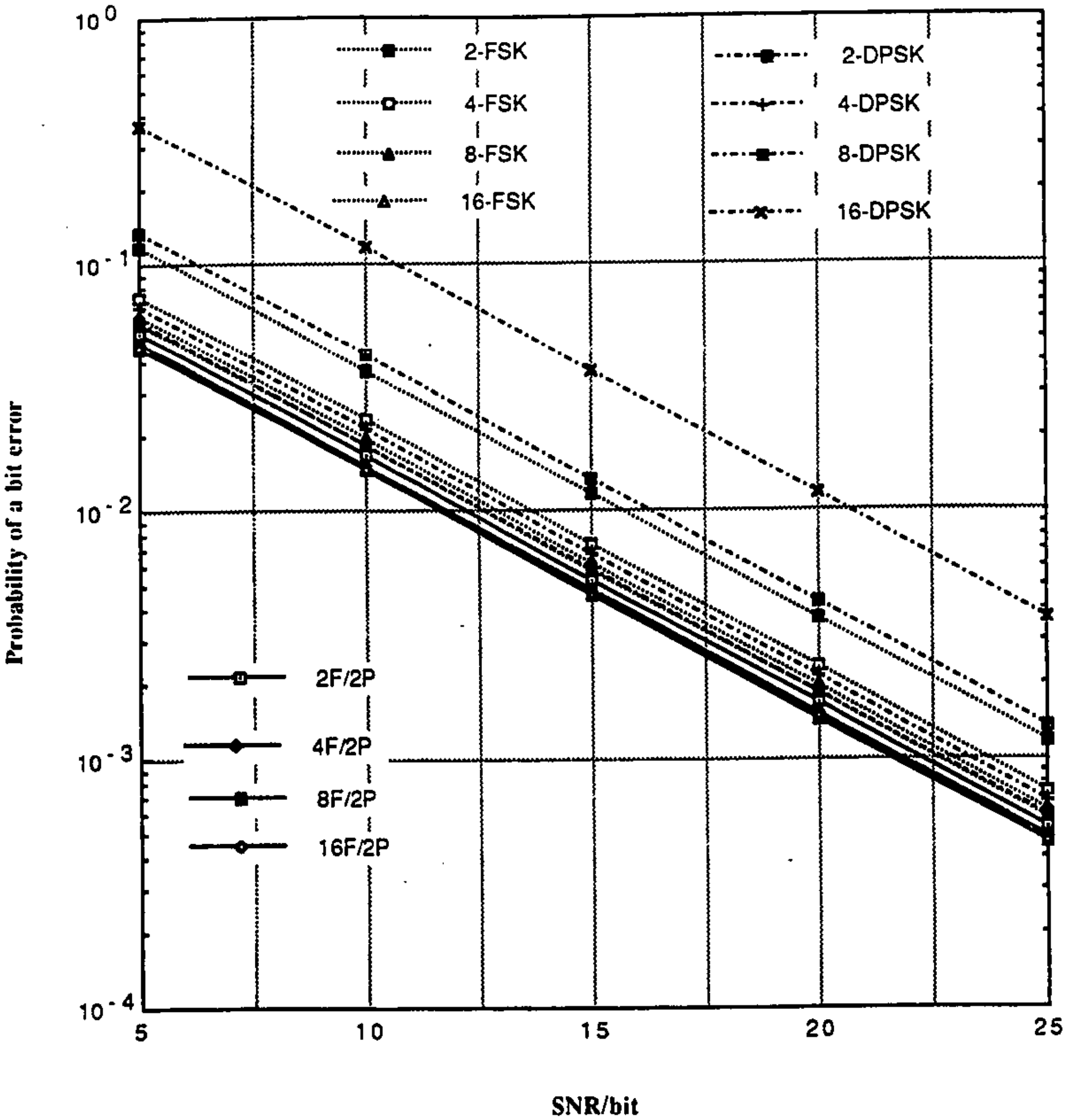

Figure 5.4 : Bit error probability performance for FH/JFPM in worst case partial band noise jamming with a combination $M_F F/2P$ when $M_F = 2, 4, 8, 16$.

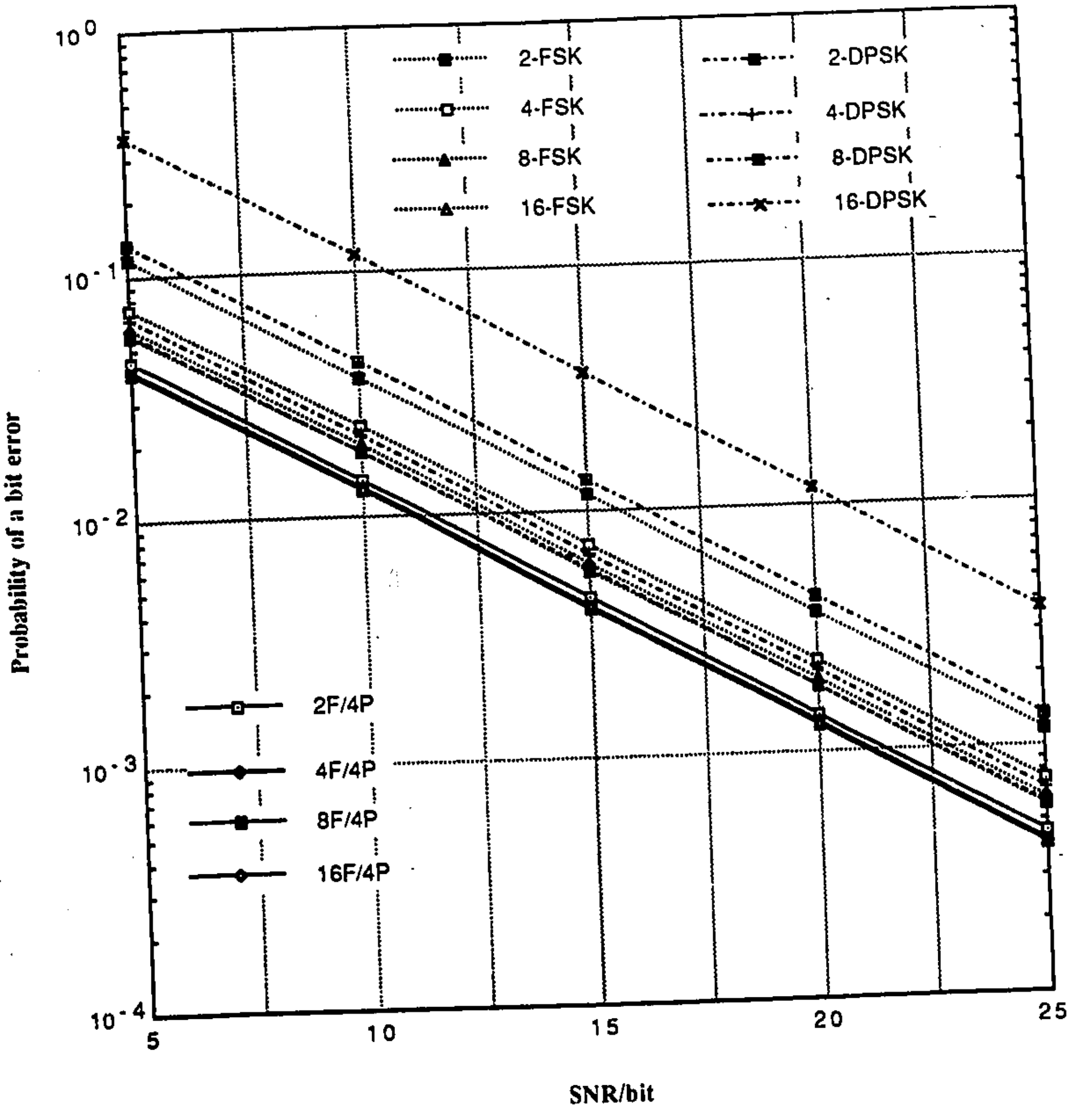

Figure 5.5 : Bit error probability performance for FH/JFPM in worst case partial band noise jamming with a combination $M_F F/4P$ when $M_F = 2, 4, 8, 16$.

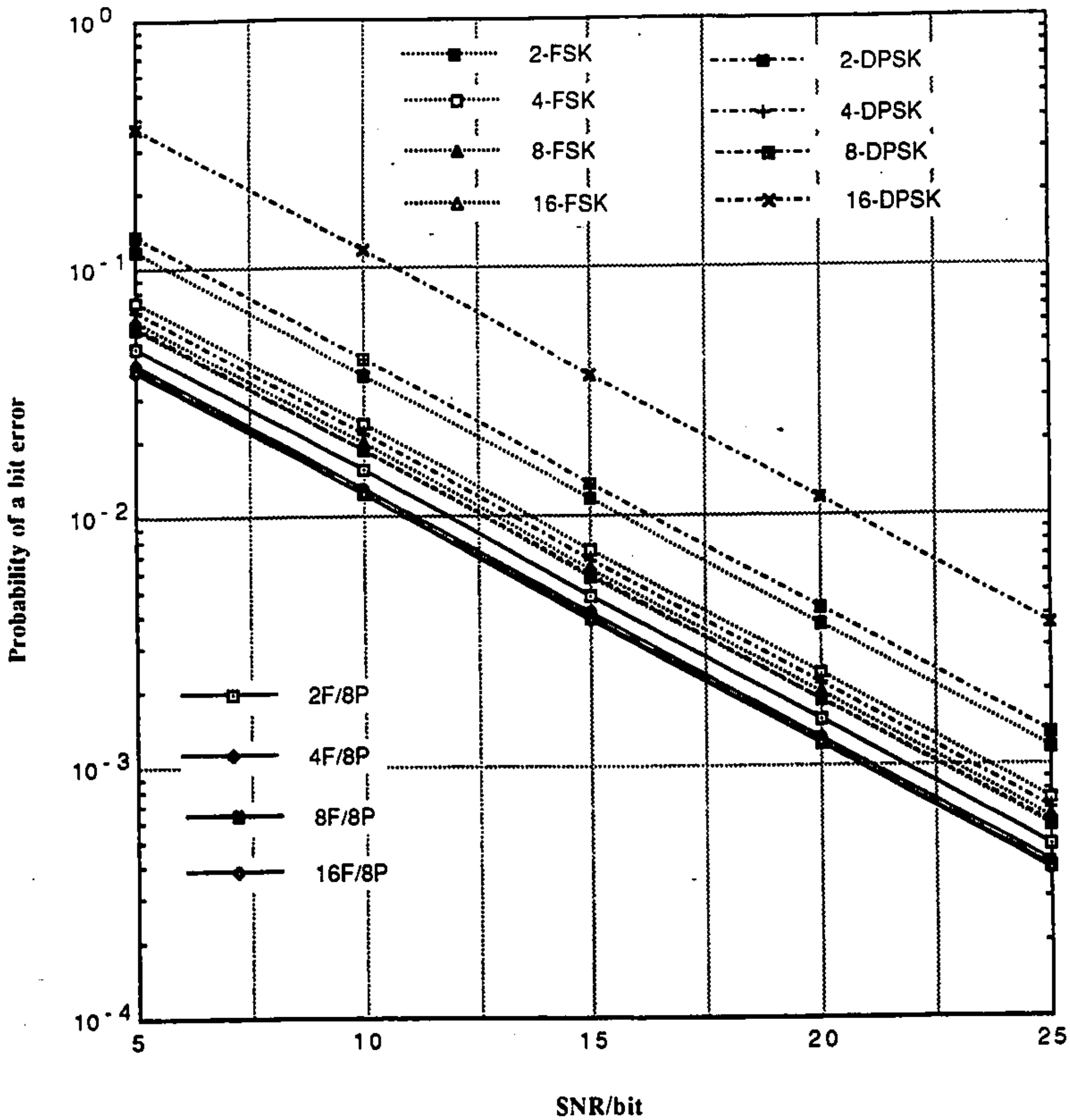

Figure 5.6 : Bit error probability performance for FH/JFPM in worst case partial band noise jamming with a combination $M_F F/8P$ when $M_F = 2, 4, 8, 16$.

the relationship between the bit error rate and the signal-to-jamming noise ratio from exponential to inverse linear dependence. Therefore, this behavior can occur.

The asymptotic gain performance of FH/M-ary JFPM for worst case partial-band noise jamming over the conventional FH/M-ary FSK, $\Delta(\rho_b)_{FSK}$ (additional ρ_b in dB needed for FH/M-ary FSK system to achieve the same BER) and FH/M-ary DPSK, $\Delta(\rho_b)_{DPSK}$ (additional ρ_b in dB needed for FH/M-ary DPSK system to achieve the same BER) is tabulated for different FH/JFPM formats as shown in Table 5.2. Where the asymptotic gain, $\Delta(\rho_b)_{FSK}$ in dB is defined as

$$\Delta(\rho_b)_{FSK} = 10\log_{10}\frac{\xi_{b,FSK}}{\xi_{b,JFPM}} \tag{5.23}$$

where $\xi_{b,JFPM}$ and $\xi_{b,FSK}$ are the values of ξ_b for FH/M-ary JFPM and the conventional FH/M-ary FSK in worst case partial-band noise jamming (see Table 5.1). The asymptotic gain, $\Delta(\rho_b)_{DPSK}$ in dB is defined as

$$\Delta(\rho_b)_{DPSK} = 10\log_{10}\frac{\xi_{b,DPSK}}{\xi_{b,JFPM}} \tag{5.24}$$

where $\xi_{b,DPSK}$ is the value of ξ_b of the conventional FH/M-ary DPSK in the worst case partial-band noise jamming and is given in [18].

Table 5.2 : Asymptotic gain performance of FH/M-ary JFPM for worst case partial-band noise jamming over the conventional FH/M-ary FSK and FH/M-ary DPSK.

M	$\Delta(\rho_b)_{FSK}$ dB			$\Delta(\rho_b)_{DPSK}$ dB		
$M_F \times M_P$	M_FF/2P	M_FF/4P	M_FF/8P	M_FF/2P	M_FF/4P	M_FF/8P
4	1.447	–	–	1.035	–	–
8	1.114	1.442	–	4.508	4.836	–
16	0.956	1.426	0.778	9.011	9.481	8.833
32	0.848	1.398	1.384	13.908	14.458	14.444

Comparing the result in Table 5.2, we observe that FH/M-ary JFPM is less sensitive to worst case partial-band noise jamming than FH/M-ary FSK and FH/M-ary DPSK systems.

5.4 The FFH/JFPM System

The fast frequency hopping technique is used to improve reliability in the reception of signals that are subject to fading or jamming [55]-[60]. The purpose of this section is to present the design and performance analysis of FFH/JFPM spread spectrum communication system, employing in the FSK part noncoherent demodulation and in the DPSK part differential detection. The system described here assumes that coherent frequency synthesizer can be realized [32, 33] and [68]-[72]. In this section the performance analysis FFH/JFPM system over Rayleigh fading channels is obtained.

5.4.1 The FFH/JFPM System Model

The mechanism of FFH is accomplished by making L copies of the information symbol and transmitting these copies over L hops. It is assumed that the time duration of each of these copies is equal to the hop duration T_h and the energy content of each of these copies is one Lth of the energy of one data symbol. In one symbol duration the transmitted waveform $s_t(t)$ consists of a series of tones at frequencies $f_{h_l} + f_m$, each of duration T_h, and with a phase $\theta^{(k)}$. Thus $s_t(t)$ may be expressed as

$$s_t(t) = \sum_{k=1}^{L} s_{mn}^{(l)}(t - kT_h) \quad \text{for } l = 1, 2, ...q. \tag{5.25}$$

where $s_{mn}^{(l)}(t)$ is given in (5.6). In each hop the parameter l changes its value according to the hopping pattern. Hence the signal is subject to frequency diversity.

A typical frequency hopping receiver for FFH/JFPM is shown in Fig. 5.7. The received signal is mixed with the locally generated frequency hop signal (assume that the PN code generators in the transmitter and receiver are in synchronized). The output of the mixer is then a series of signals each of frequency f_m and phase $\theta^{(k)}$, and the duration of each of these signals is equal to the hop duration. Because of

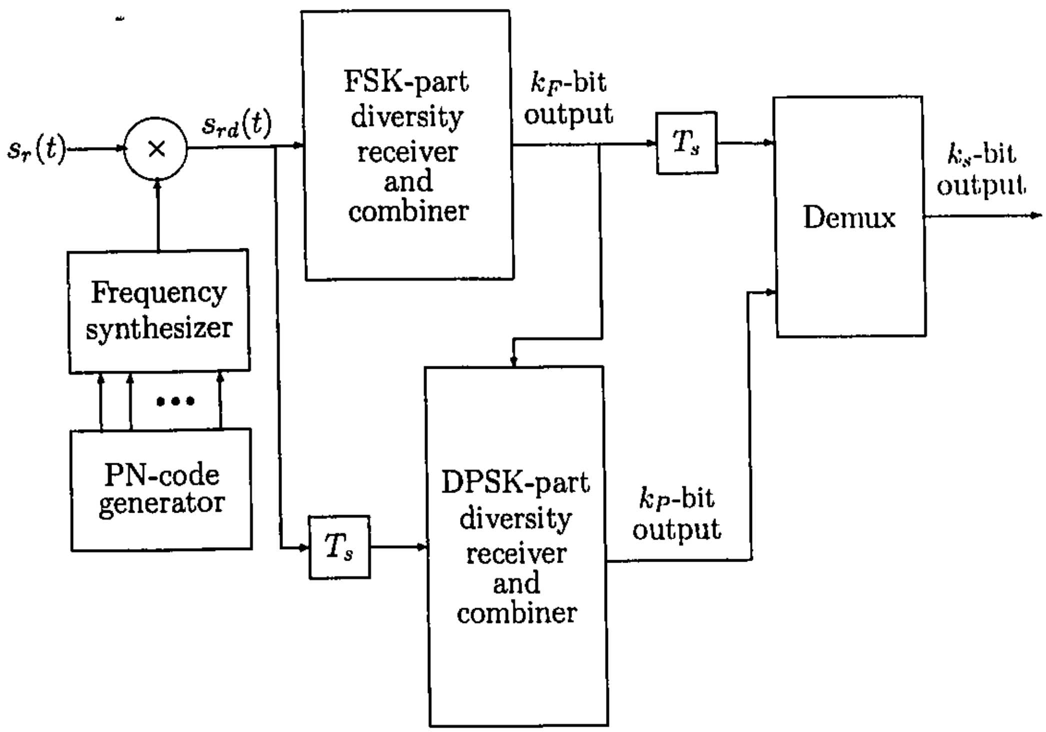

Figure 5.7 : Block diagram of a diversity receiver for an FFH/JFPM system.

the special form of JFPM signals, a two stage decision process is used to establish which signal was received. In the first stage, the frequency of the received signal is determined. The second stage, used to determine the signal phase. As illustrated in Fig. 5.7 the frequency of the received signal can be determined without any phase information, but the estimate of the signal phase requires a knowledge of the transmitted frequency. For this purpose, the inputs to the DPSK-part are the one-symbol delayed signal and the estimate of the frequency provided by the FSK-part. This frequency estimate can be obtained from a frequency synthesizer driven by the output of the FSK-detector. The one symbol delay in the DPSK-part is later compensated in demultiplexing (bit combining) by introducing a one-symbol delay following the FSK detector.

A possible implementation of the FSK part and DPSK part diversity receiver and combiner are shown in Fig. 5.8 and 5.9. For the FSK-part as depicted in Fig. 5.8, the dehopped signal $s_{rd}(t)$ is processed by the square-law combining the M_F-ary FSK receiver. The receiver consists of M_F branches; each branch is tuned to one of the baseband frequencies, say f_i for $i = 1, 2, ..., M_F$. The correlators outputs are sampled every hop duration T_h and followed by the square-law detector. The sampled values v_{ij} for $i = 1, 2, ..., L$ and $j = 1, 2, ..., M_F$ are linearly combined for each branch to form the variables u_j for $j = 1, 2, ..., M_F$. These variables are then compared and the decision on the transmitted tone is made corresponding to the largest one.

For the DPSK part, a possible implementation of the diversity receiver and combiner is shown in Fig. 5.9. This receiver has two branches: the first one correlates the dehopped signal $s_{rd}(t)$ with $\sin(2\pi f_i t)$ and the other correlates $s_{rd}(t)$ with $\cos(2\pi f_i t)$; the frequency f_i is the frequency that is estimated by the FSK part in the same symbol interval (note that the input signal to the DPSK part is the delayed version of

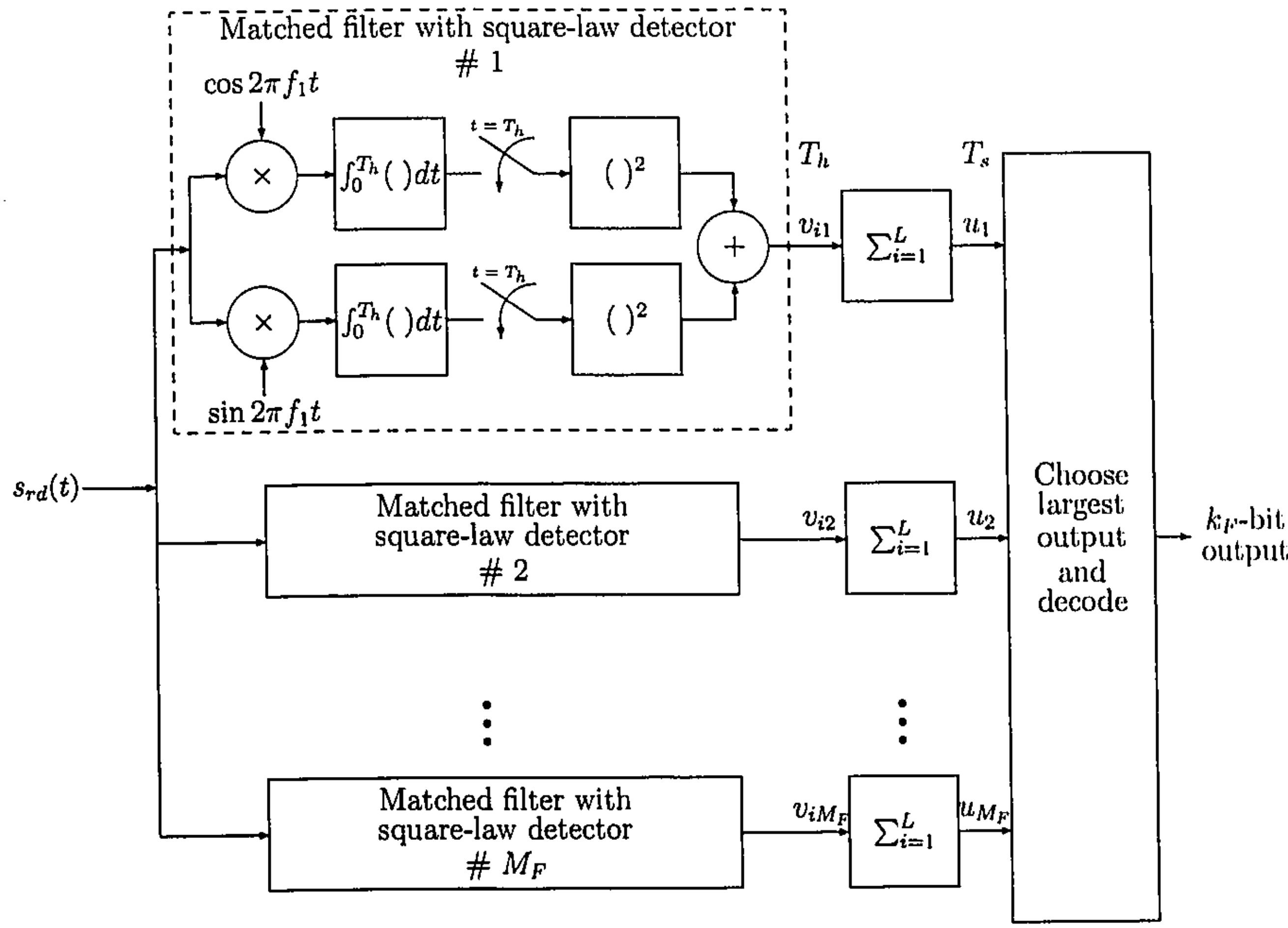

Figure 5.8 : Block diagram of a noncoherent FSK-part diversity receiver and combiner.

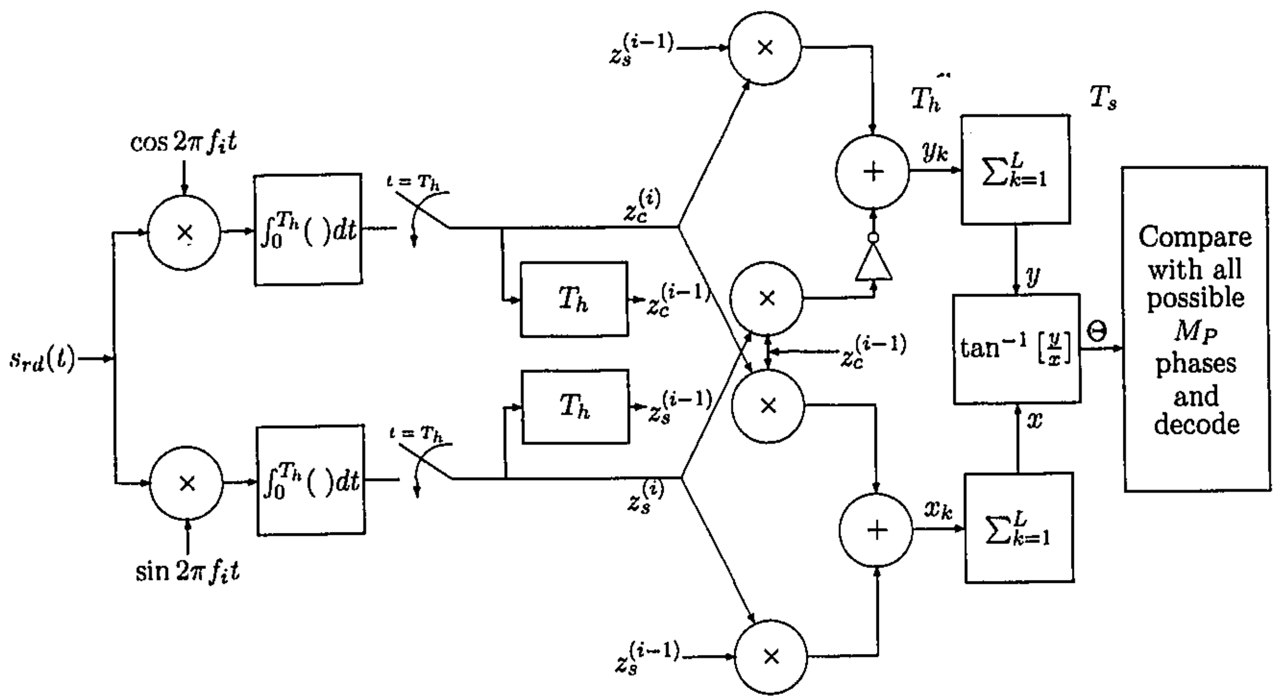

Figure 5.9 : Block diagram of a DFSK-part diversity receiver and combiner.

the input signal to the FSK part). The correlators outputs are then sampled every hop duration T_h. The sampled values $z_c^{(i)}$ and $z_s^{(i)}$ for $i = 1, 2, ..., L$ are then used with the delayed samples $z_c^{(i-1)}$ and $z_s^{(i-1)}$ to form the statistics x_i and y_i. These statistics are then combined to provide the decision samples x and y. The decision samples x and y are passed through a circuit that produces the inverse tangent of y/x. The output of this circuit, denoted as Θ, is the phase estimate of the incoming signal. This estimate of the phase is compared with all possible M_P phases and the decision is made based on the phase that provides the smallest difference.

5.4.2 Performance Analysis of FFH/JFPM

We now turn our attention to the analysis of the theoretical performance of the FFH/JFPM system over Rayleigh fading channels and random noise. We have assumed that the minimum frequency spacing between frequency hop slots is larger than the channel coherence bandwidth, so that each dehopped signal fades independently [46] and [59]-[61]. We also assume that for each hop the channel is modeled as a multipath Rayleigh-fading nonfrequency selective channel, and the parameters associated with the channel do not vary significantly over two consecutive hop durations. Hence, the signal bandwidth is assumed to be much smaller than the coherence bandwidth of the channel and the coherence time of the channel is much greater than the hop duration [46, 59] and [60], which means that the requiring hop rate is large compared to the channel Doppler spread.

The complex lowpass equivalent impulse response of the channel described above is given by [46]

$$h(\tau) = \sum_k \alpha_k \delta\left(\tau - \tau_k\right) e^{-j\phi_k} \tag{5.26}$$

where α_k, τ_k and ϕ_k are the path gain, propagation delay and phase of the k-th path, respectively. Under our assumption, the dehopped signal amplitude can be considered as a Rayleigh random variable.

The equivalent low-pass representation of the dehopped signal in the k-th symbol interval may thus be written in the form

$$\beta_{rd}(t) = \sum_{l=1}^{L} \alpha_l e^{-j\phi_l} \beta_{kmn}^{(l)}(t - lT_h) + \nu_l(t) \tag{5.27}$$

where $\alpha_l e^{-j\phi_l}$ is the channel parameters during the l-th hop, $\beta_{kmn}^{(l)}(t)$ represents the mn-th signal transmitted during the k-th symbol interval in the l-th hop, and $\nu_l(t)$ is a zero mean complex-valued white Gaussian noise process with power spectral density N_0.

Now let us evaluate the performance of FFH/JFPM system for equally likely, and equal energy signals. If the information signal $s_{mn}(t)$ is hopped in frequency, a correct decision is made in favour of the signal corresponding to

$$\max_{i=1,\dots,M_F} [u_i] \tag{5.28}$$

(see Fig. 5.8) and the measured phase difference satisfies the following equation

$$\min_{k=1,\dots,M_P} [|\psi| = |\Theta - \theta_k|] \tag{5.29}$$

(see Fig. 5.9) where the value of u_i for $i = 1, 2, \dots, M_F$ at which (5.28) is satisfied should be equal to u_m, and the value of θ_k for $k = 1, 2, \dots, M_P$ at which (5.29) is satisfied is equal to θ_n.

Now the probability of a correct decision for the receiving system is equal to the probability that $u_m = \max[u_i]$ for $i = 1, 2, \dots, M_F$ times the probability that the absolute value of the measured phase difference ψ is less than π/M_P given that $u_m = \max[u_i]$ for $i = 1, 2, \dots, M_F$. That is

$$P_c = \text{Prob}\left(u_m = \max_{i=1,\dots,M_F} [u_i]\right) \text{Prob}\left(|\psi| < \pi/M_P \middle| u_m = \max_{i=1,\dots,M_F} [u_i]\right). \tag{5.30}$$

In order to evaluate the probability of a correct decision, it is mathematically convenient to evaluate the probability of the two terms given in (5.30). Let us derive first the probability of the first term given in (5.30), i.e.,

$$\text{Prob}\left(u_m = \max_{i=1,\dots,M_F}[u_i]\right) \tag{5.31}$$

This is equivalently equal to the probability that the receiver makes a correct decision on the frequency of the received signal. Our analysis of this event requires the statistics of the decision samples u_i for $i = 1, 2, ..., M_F$ where u_i is given by

$$u_i = \sum_{j=1}^{L} v_{ij} \quad \text{for} \quad i = 1, 2, ..., M_F. \tag{5.32}$$

Assume that the information signal $s_{mn}(t)$ was transmitted. The probability density function of the normalized sampled output v_{ij} is given by [62]

$$p_{v_{ij}}(v|s_{mn}) = \begin{cases} \frac{1}{1+\bar{\rho}_h} e^{-v/(1+\bar{\rho}_h)} & i = m,\ v \geq 0 \\ \\ e^{-v} & i \neq m,\ v \geq 0 \end{cases} \tag{5.33}$$

where $\bar{\rho}_h$ represents the average signal-to-noise ratio in the L-hop symbol and it can be written as

$$\begin{aligned} \bar{\rho}_h &= \frac{E_h}{N_0}\mathcal{E}\left\{\alpha_k^2\right\} \\ &= \frac{E_b}{N_0}\frac{k_F + k_P}{L}\mathcal{E}\left\{\alpha_k^2\right\} = \bar{\rho}_b\frac{k_F + k_P}{L} \end{aligned} \tag{5.34}$$

where E_h denotes the hop energy and $\bar{\rho}_b$ is the average signal-to-noise ratio per bit. It is assumed that the fading on the L hops is statistically independent, then the output samples v_{ij} for $i = 1, 2, ..., M_F$ are statistically independent.

Let us now evaluate the pdf of the decision samples u_i. This may be accomplished via the characteristic function. The characteristic function of v_{ij} is easily determined and its given by [65]

$$\Gamma_{v_{ij}}(j\omega) = \begin{cases} \frac{1}{1-j\omega(\bar{\rho}_h+1)} & i = m \\ \\ \frac{1}{1-j\omega} & i \neq m \end{cases} \tag{5.35}$$

By using (5.32) and (5.35) the characteristic function of u_i for $i = 1, 2, ..., M_F$ is easily shown to be [65]

$$\Gamma_{u_i}(j\omega) = \begin{cases} \left(\frac{1}{1-j\omega(\bar{\rho}_h+1)}\right)^L & i = m \\ \\ \left(\frac{1}{1-j\omega}\right)^L & i \neq m \end{cases} \tag{5.36}$$

Now the pdf of u_i (inverse transform of $\Gamma_{u_i}(j\omega)$) becomes

$$p_{u_i}(v|s_{mn}) = \begin{cases} \frac{v^{L-1}}{(1+\bar{\rho}_h)^L(L-1)!}e^{-v/(1+\bar{\rho}_h)} & i = m,\ v \geq 0, \\ \\ \frac{v^{L-1}}{(L-1)!}e^{-v} & i \neq m,\ v \geq 0. \end{cases} \tag{5.37}$$

Having obtained the pdf of u_i, it is well known that the probability of the event given in (5.31) is given by

$$\text{Prob}\left(u_m = \max_{i=1,\ldots,M_F}[u_i]\right) = \int_0^\infty p_{u_m}(v|s_{mn})\left[\int_0^v p_{u_i}(v|s_{mn})\right]^{M_F-1} dv \ \text{ for } i \neq m. \tag{5.38}$$

The integral in the brackets can be evaluated to yield [63]

$$\text{Prob}\left(u_m = \max_{i=1,\ldots,M_F}[u_i]\right) = \int_0^\infty \frac{v^{L-1}e^{-v/(1+\bar{\rho}_h)}}{(1+\bar{\rho}_h)^L(L-1)!}\left[1 - e^{-v}\sum_{k=0}^{L-1}\frac{v^{L-k-1}}{(L-k-1)!}\right]^{M_F-1} dv \tag{5.39}$$

By expanding the integral in (5.39) and collecting terms [62], (5.39) reduces to

$$\text{Prob}\left(u_m = \max_{i=1,\ldots,M_F}[u_i]\right) = \sum_{k=0}^{M_F-1}\frac{(-1)^k}{(L-1)!}\binom{M_F-1}{k}\sum_{n=0}^{k(L-1)}\sigma_{n,k}\frac{(\bar{\rho}_h+1)^n(L+n-1)!}{(k\bar{\rho}_h+k+1)^{L+n}} \tag{5.40}$$

The set of the coefficients $\sigma_{n,k}$ is given in the following equation

$$\sigma_{n,k} = \sum_{m=n-(L-1)}^{n}\sigma_{n,k-1}\frac{1}{(n-m)!}Q(m,k,L) \tag{5.41}$$

where $Q(m, k, L)$ is given by

$$Q(m,k,L) = \begin{cases} 1 & 0 \leq m \leq (k-1)(L-1). \\ 0 & \text{otherwise} \end{cases} \tag{5.42}$$

where

$$\begin{aligned} \sigma_{0,0} &= 1 & \sigma_{0,k} = 1 \\ \sigma_{1,k} &= k & \sigma_{n,1} = \frac{1}{n!}. \end{aligned}$$

Now let us evaluate the probability of the second term given in (5.30), i.e.,

$$\text{Prob}\left(|\psi| < \pi/M_P \,\middle|\, u_m = \max_{i=1,\ldots,M_F} [u_i]\right) = \int_{-\pi/M_P}^{\pi/M_P} p_\psi(\psi) d\psi. \tag{5.43}$$

Our analysis requires the statistics of the measured phase difference ψ. Without loss of generality, if we assume that the transmitted signal phase $\theta_n = 0$, then the measured phase difference ψ may be written as

$$\psi = \arctan\left[\frac{y}{x}\right] \tag{5.44}$$

The decision samples x and y are given by

$$x = \sum_{i=1}^{L} x_i \tag{5.45}$$

$$y = \sum_{i=1}^{L} y_i. \tag{5.46}$$

According to Fig. 5.9, the statistics x_i and y_i are given by

$$x_i = z_c^{(i)} z_c^{(i-1)} + z_s^{(i)} z_s^{(i-1)} \tag{5.47}$$

$$y_i = z_c^{(i)} z_s^{(i-1)} - z_s^{(i)} z_c^{(i-1)}. \tag{5.48}$$

The pdf of ψ can be computed based on the characteristic function of the joint probability distribution function of the random variables x and y. The pdf of ψ is obtained by [64] and it was shown that $p_\psi(\psi)$ is an even function, so that the above integral in (5.43) can be evaluated in terms of an auxiliary function $G(\psi)$:

$$\mathrm{Prob}(\psi_{min} \le \psi \le \psi_{max}) = G(\psi_{max}) - G(\psi_{min}) \quad \text{for } 0 \le \psi \le \pi \tag{5.49}$$

where $G(\psi)$ is given by

$$G(\psi) = \frac{(-1)^{L-1}(1-\mu^2)^L}{2\pi(L-1)!}\frac{\partial^{L-1}}{\partial r^{L-1}}\left(\frac{1}{r-\mu^2}\left[\frac{\mu\sqrt{1-((r/\mu^2)-1)\Psi^2}}{r^{1/2}}\cot^{-1}(\Psi)\right.\right.$$
$$\left.\left.\left. - \cot^{-1}\frac{\Psi r^{1/2}/\mu}{\sqrt{1-((r/\mu^2)-1)\Psi^2}}\right]\right)\right|_{r=1} \tag{5.50}$$

where μ is equal to

$$\mu = \frac{\bar{\rho}_h}{1+\bar{\rho}_h} \tag{5.51}$$

and Ψ is given by

$$\Psi = \frac{\mu\cos(\psi)}{\sqrt{r-\mu^2\cos(\psi)}}. \tag{5.52}$$

By using (5.49) and (5.50), and due to the fact that $p_\psi(\psi)$ is an even function and $G(0)=0$, the probability given in (5.43) can be expressed as

$$\mathrm{Prob}(-\pi/M \le \psi \le \pi/M) = 2G(\pi/M_P) \tag{5.53}$$

where $G(\pi/M_P)$ is given by

$$\begin{aligned} G(\pi/M_P) &= \frac{1}{2} - \frac{(-1)^{L-1}(1-\mu^2)^L}{2\pi(L-1)!}\left\{\frac{\partial^{L-1}}{\partial r^{L-1}}\left[\frac{1}{r-\mu^2}\left(\frac{\pi}{M_P}(M_P-1)\right.\right.\right. \\ &- \left.\left.\left.\left.\frac{\mu\sin(\pi/M_P)}{\sqrt{r-\mu^2\cos^2(\pi/M_P)}}\cot^{-1}\left[\frac{-\mu\cos(\pi/M_P)}{\sqrt{r-\mu^2\cos^2(\pi/M_P)}}\right]\right)\right]\right\}\right|_{r=1} \end{aligned} \tag{5.54}$$

Now the probability of a correct decision for the FFH/JFPM system can be obtained by substituting (5.40) and (5.53) into (5.30)

$$P_c = \frac{1}{(L-1)!}\sum_{k=0}^{M_F-1}(-1)^k\binom{M_F-1}{k}\sum_{n=0}^{k(L-1)}\sigma_{n,k}\frac{(\bar{\rho}_h+1)^n(L+n-1)!}{(k\bar{\rho}_h+k+1)^{L+n}}$$

$$
\begin{aligned}
&\times \left\{1 - \frac{(-1)^{L-1}(1-\mu^2)^L}{\pi\,(L-1)!}\left\{\frac{\partial^{L-1}}{\partial r^{L-1}}\left[\frac{1}{r-\mu^2}\left(\frac{\pi}{M_P}(M_P-1)\right.\right.\right.\right. \\
&- \left.\left.\left.\left.\frac{\mu\sin(\pi/M_P)}{\sqrt{r-\mu^2\cos^2(\pi/M_P)}}\cot^{-1}\left[\frac{-\mu\cos(\pi/M_P)}{\sqrt{r-\mu^2\cos^2(\pi/M_P)}}\right]\right)\right]\right\}_{r=1}\right\} \qquad (5.55)
\end{aligned}
$$

and the probability of a symbol error which is $P_e(M) = 1 - P_c$, may be expressed as

$$
\begin{aligned}
P_e(M) &= 1 - \frac{1}{(L-1)!}\sum_{k=0}^{M_F-1}(-1)^k\binom{M_F-1}{k}\sum_{n=0}^{k(L-1)}\sigma_{n,k}\frac{(\bar{\rho}_h+1)^n(L+n-1)!}{(k\bar{\rho}_h+k+1)^{L+n}} \\
&\times \left\{1 - \frac{(-1)^{L-1}(1-\mu^2)^L}{\pi\,(L-1)!}\left\{\frac{\partial^{L-1}}{\partial r^{L-1}}\left[\frac{1}{r-\mu^2}\left(\frac{\pi}{M_P}(M_P-1)\right.\right.\right.\right. \\
&- \left.\left.\left.\left.\frac{\mu\sin(\pi/M_P)}{\sqrt{r-\mu^2\cos^2(\pi/M_P)}}\cot^{-1}\left[\frac{-\mu\cos(\pi/M_P)}{\sqrt{r-\mu^2\cos^2(\pi/M_P)}}\right]\right)\right]\right\}_{r=1}\right\}. \qquad (5.56)
\end{aligned}
$$

In the special case where $M = 4$ (i.e., $M_F = 2$ and $M_P = 2$) the expression of the probability of error given in (5.56) can be simplified to

$$
P_e(4) = 1 - \frac{1}{4}\left[1+\mu_F\sum_{k=0}^{L-1}\binom{2k}{k}\left(\frac{1-\mu_F^2}{4}\right)^k\right]\left[1+\mu_P\sum_{k=0}^{L-1}\binom{2k}{k}\left(\frac{1-\mu_P^2}{4}\right)^k\right] \qquad (5.57)
$$

where μ_F and μ_P are defined as

$$
\mu_F = \frac{\bar{\rho}_h}{2+\bar{\rho}_h} \qquad \text{and} \qquad \mu_P = \frac{\bar{\rho}_h}{1+\bar{\rho}_h}. \qquad (5.58)
$$

The probability of error for M-ary symbols $P_e(M)$ can be converted to a bit error probability for the equivalent $(k_F + k_P)$-bit groups by using the same analysis given in Section 3.4.2. Based upon the decision rule of JFPM signals, the probability of bit error due to an error in the first stage is equal to

$$
P_{b1} = \frac{k_s M - k_P M_P}{2k_s(M - M_P)}\left\{1 - \text{Prob}\left(u_m = \max_{i=1,\ldots,M_F}[u_i]\right)\right\} \qquad (5.59)
$$

and the probability of bit error due to an error in the second stage can be expressed as

$$
P_{b2} = \frac{1}{k_s}\left(P_e(M) - \left\{1 - \text{Prob}\left(u_m = \max_{i=1,\ldots,M_F}[u_i]\right)\right\}\right). \qquad (5.60)
$$

Using (5.59) and (5.60), the total bit error probability for the JFPM signal set is given by

$$
\begin{aligned}
P_b(M) &= \frac{k_s M - k_P M_P}{2k_s(M - M_P)} \sum_{k=1}^{M_F-1} \frac{(-1)^{k+1}}{(L-1)!} \binom{M_F - 1}{k} \sum_{n=0}^{k(L-1)} \sigma_{n,k} \frac{(\bar{\rho}_h + 1)^n (L+n-1)!}{(k\bar{\rho}_h + k + 1)^{L+n}} \\
&+ \frac{1}{k_s(L-1)!} \sum_{k=0}^{M_F-1} (-1)^k \binom{M_F - 1}{k} \sum_{n=0}^{k(L-1)} \sigma_{n,k} \frac{(\bar{\rho}_h + 1)^n (L+n-1)!}{(k\bar{\rho}_h + k + 1)^{L+n}} \\
&\times \left\{ \frac{(-1)^{L-1} (1-\mu^2)^L}{\pi (L-1)!} \left\{ \frac{\partial^{L-1}}{\partial r^{L-1}} \left[\frac{1}{r - \mu^2} \left(\frac{\pi}{M_P}(M_P - 1) \right.\right.\right.\right. \\
&- \left.\left.\left.\left. \frac{\mu \sin(\pi/M_P)}{\sqrt{r - \mu^2 \cos^2(\pi/M_P)}} \cot^{-1} \left[\frac{-\mu \cos(\pi/M_P)}{\sqrt{r - \mu^2 \cos^2(\pi/M_P)}} \right] \right) \right] \right\}_{r=1} \right\}. \qquad (5.61)
\end{aligned}
$$

The probability of a bit error as a function of $\bar{\rho}_b$ has been calculated numerically for FFH/JFPM system with 2F/2P and 2F/4P when the diversity level $L = 2, 3, 4, 5$. These data are compared with the conventional frequency hopped 2FSK and 4FSK systems and the results have been plotted in Figs. 5.10-5.13. From these figures It is shown that for a given bit error rate and as the diversity level is increased, significant performance gain is achieved.

Fig. 5.10 gives a comparison of FFH/JFPM system with 2F/2P and the conventional FFH/2FSK system when the diversity level $L = 2, 3, 4, 5$. we can see that the FFH/JFPM with 2F/2P has a gain of more than 3 dB in $\bar{\rho}_b$ compared with the conventional FFH/2FSK system when the two systems have the same diversity level. Fig. 5.11 shows the difference in performance between JFPM with 2F/2P and the conventional 4FSK system for different diversity level $L = 2, 3, 4, 5$. It is shown that the combination 2F/2P FFH/JFPM has a gain of approximately 1.1 dB in $\bar{\rho}_b$ compared with the conventional FFH/4FSK system for the same diversity level. More performance gain can be achieved by using more complex configurations of JFPM. For example, using a 2F/4P combination provides more than 4.5 dB improvement over the conventional FH/2FSK system when the two systems have the same number of diversity levels. This improvement appears clearly in Fig. 5.12. Fig. 5.13 shows the difference in performance between JFPM with 2F/4P and the conventional 4FSK system for different diversity level $L = 2, 3, 4, 5$. It is shown that the combination 2F/4P FFH/JFPM has a gain of 1.9 dB in $\bar{\rho}_b$ compared with the conventional FFH/4FSK system when the two systems have the same diversity level.

Let us observe the bit error rate performance of the conventional FFH/FSK system and FFH/JFPM system as a function of the number of diversity level L. Fig. 5.14 illustrates the characteristics of the probability of bit error for the conventional FFH/2FSK system and FFH/JFPM system with 2F/2P as a function of the number of diversity level L when the signal-to-noise ratio per bit $\bar{\rho}_b$ remains fixed. The results given in Fig. 5.14 indicate that there is an optimum value of the diversity order L for each $\bar{\rho}_b$, which means that, for any value of the signal-to-noise ratio per bit there is a value of the diversity level L that minimizes the probability of bit error. A careful observation of these curves reveals that the minimum probability of a bit error for FFH/JFPM is obtained when the number of diversity level is twice that of the conventional FFH/2FSK system.

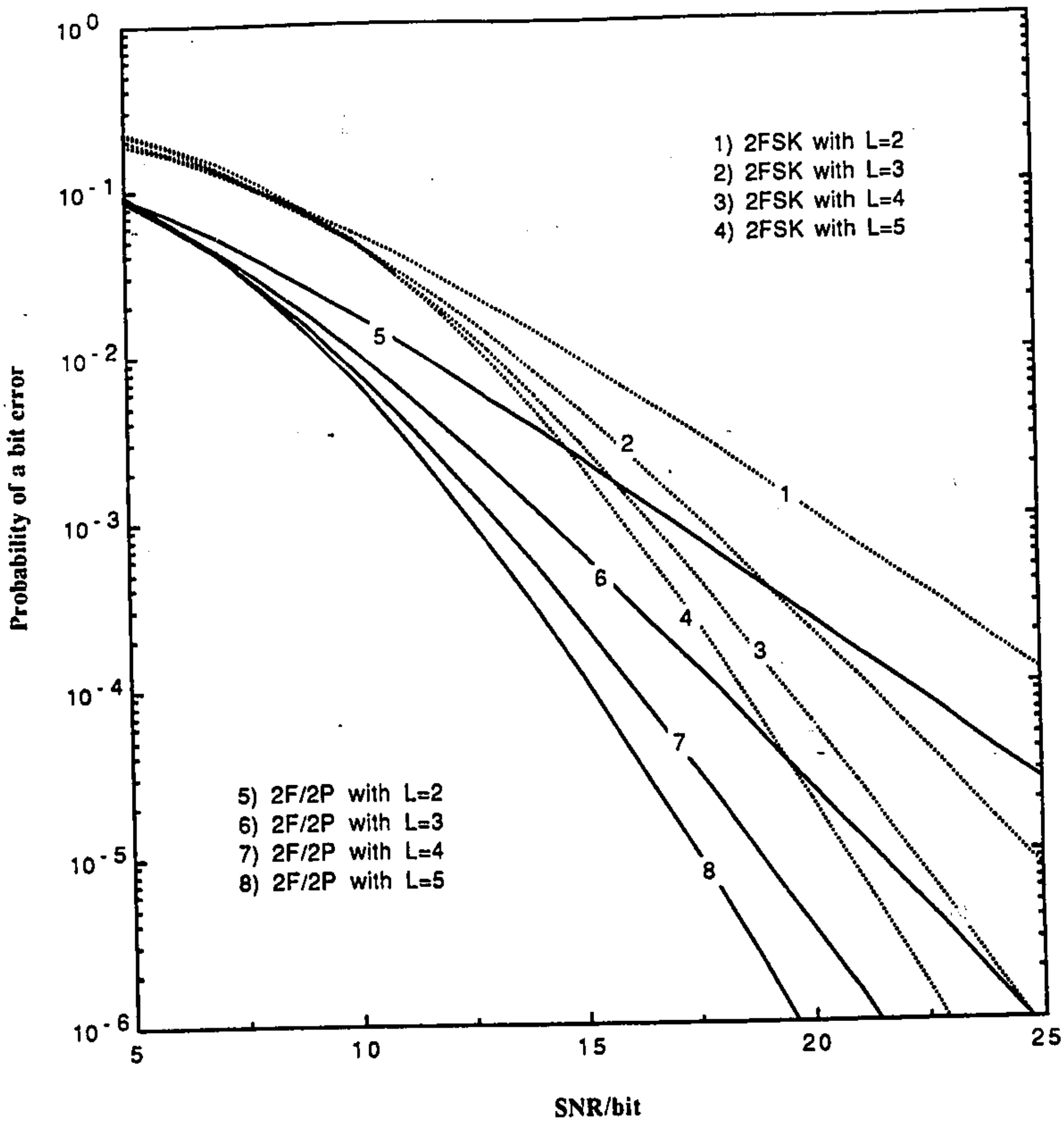

Figure 5.10 : Bit error probability performance for FFH/JFPM with a combination 2F/2P and the conventional FFH/2FSK system in Rayleigh fading channels for different diversity levels when $L = 2, 3, 4, 5$.

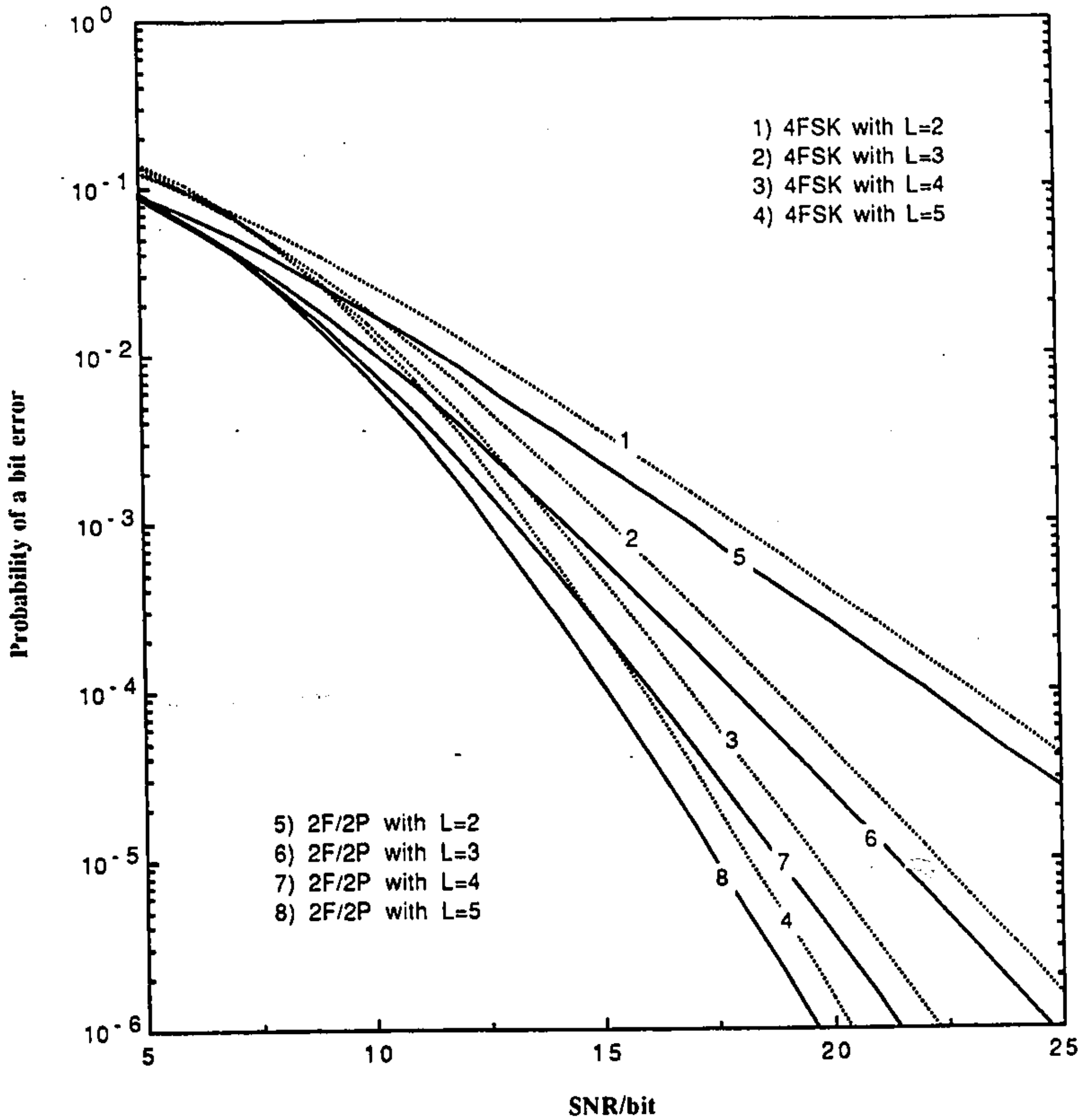

Figure 5.11 : Bit error probability performance for FFH/JFPM with a combination 2F/2P and the conventional FFH/4FSK system in Rayleigh fading channels for different diversity levels when $L = 2, 3, 4, 5$.

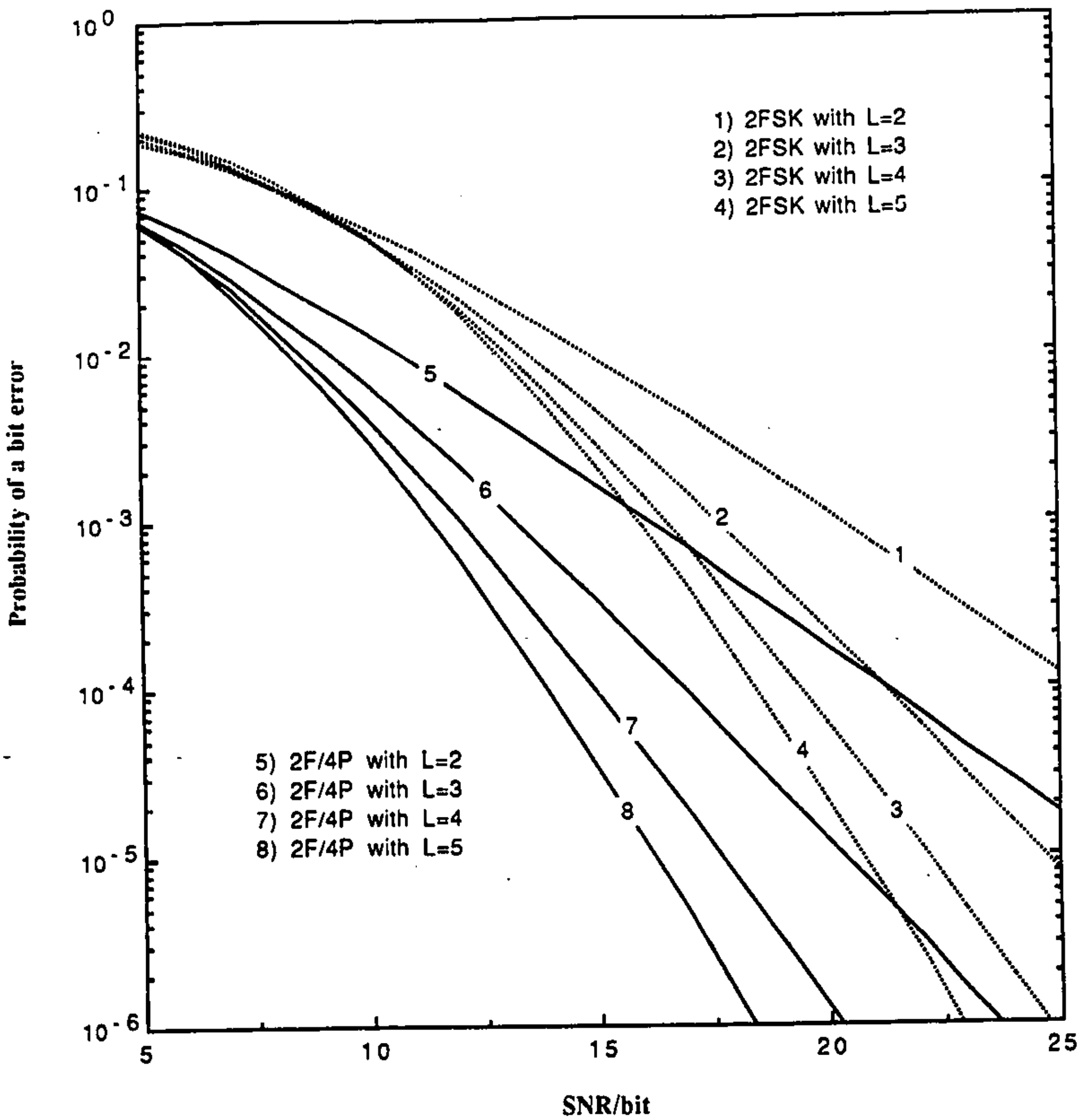

Figure 5.12 : Bit error probability performance for FFH/JFPM with a combination 2F/4P and the conventional FFH/2FSK system in Rayleigh fading channels for different diversity levels when $L = 2, 3, 4, 5$.

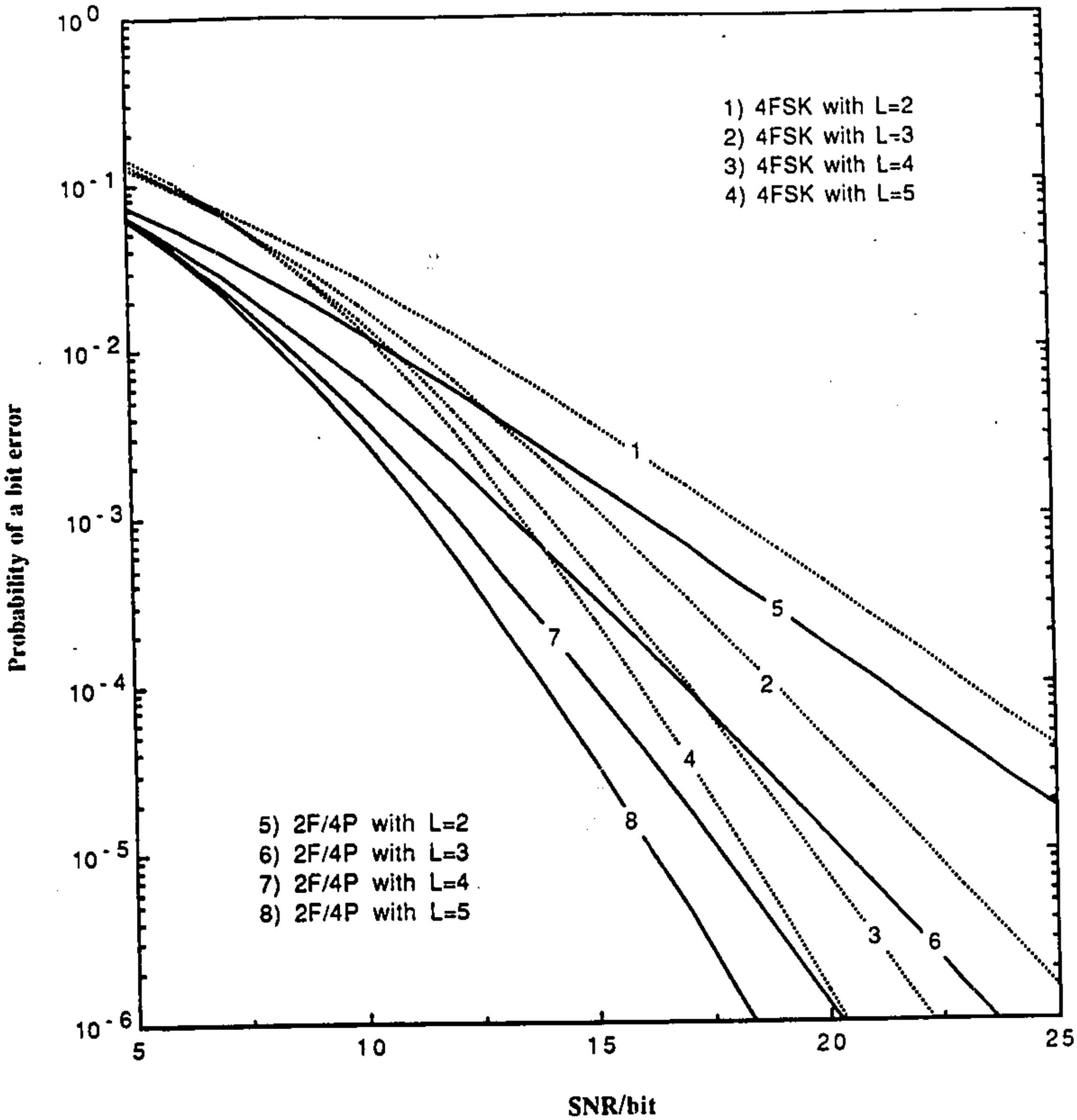

Figure 5.13 : Bit error probability performance for FFH/JFPM with a combination 2F/4P and the conventional FFH/4FSK system in Rayleigh fading channels for different diversity levels when $L = 2, 3, 4, 5$.

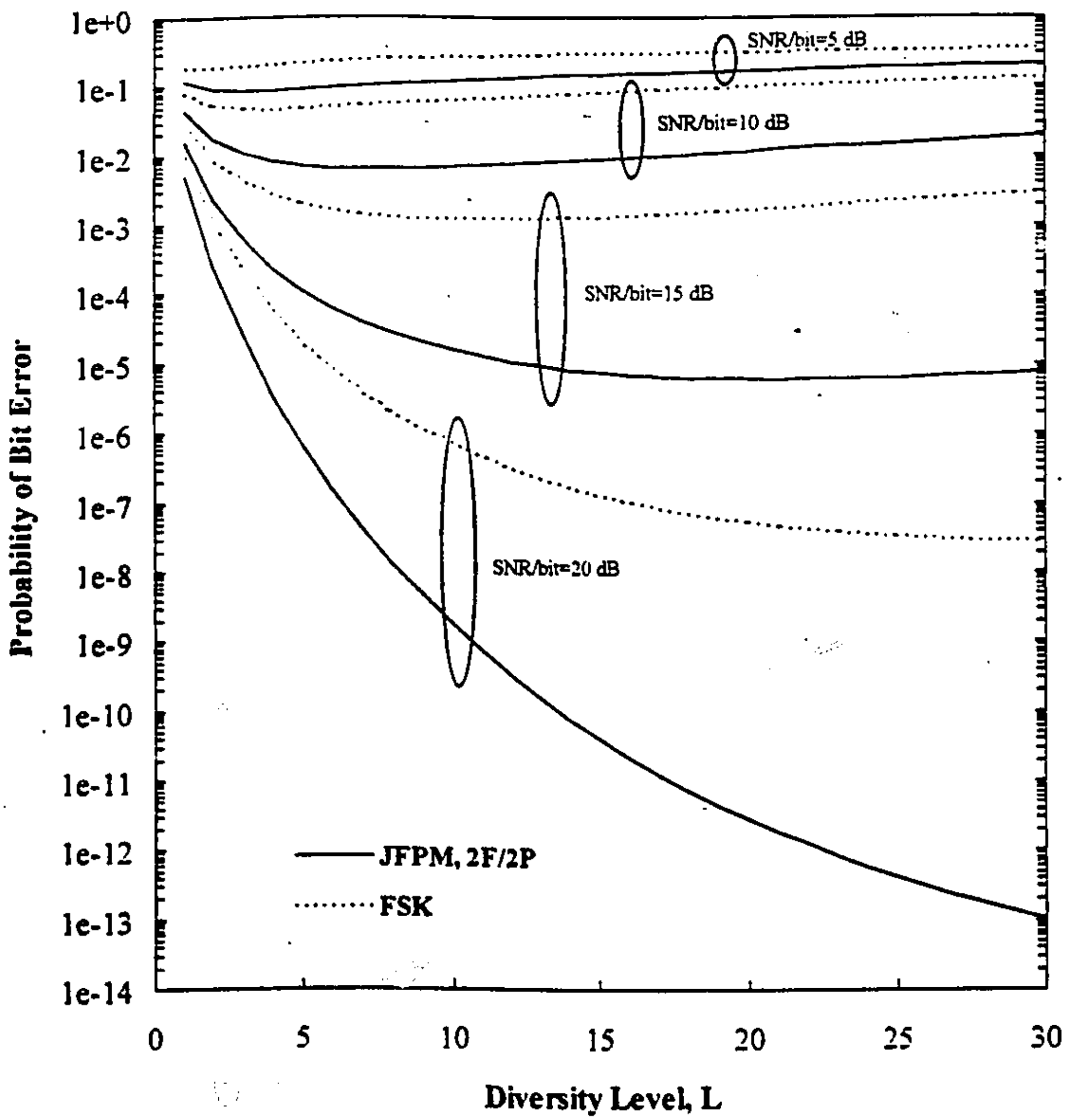

Figure 5.14 : Performance of FFH/JFPM with a combination 2F/2P and the conventional FFH/2FSK system in Rayleigh fading channels as a function of diversity levels.

5.5 Conclusions

A frequency hopped spread spectrum system referred to as FH/JFPM has been introduced. The descriptions for both SFH/JFPM and FFH/JFPM systems were given, and the performance of SFH/JFPM system in the presence of broadband noise and partial-band jamming environments analyzed. The error probability expression has been derived and the optimal jamming strategy has been evaluated. The results show that the SFH/JFPM is a power efficient frequency hopped spread spectrum system. It was found that FH/JFPM with combinations of M_FF/2P, M_FF/4P and M_FF/8P is less sensitive to partial-band noise jamming than conventional FH/M-ary FSK and FH/M-ary DPSK systems. In broadband noise jamming, SFH/JFPM with a combination M_FF/2P was found to be the most power efficient system compared to the conventional frequency hopped systems. The design and performance analysis of the FFH/JFPM system has been presented. The performance of this system in Rayleigh fading channels was analyzed and an expression was obtained for the probability of a bit error. It was shown that for a given bit error rate and as the diversity level is increased, significant performance gain is achieved compared with a single diversity level system. Significant performance gain is also achieved compared with the conventional FH systems for a given bit error rate and for the same number of diversity levels. Finally, it was shown that, for a given channel bandwidth and at a fixed data rate, the processing gain of the two parts of the FH/JFPM system is improved.

Chapter 6

The Performance of Slow Frequency Hopped/Multi-Phase Signaling in the Presence of Multitone Jamming Interference

6.1 Introduction

In Chapter 5, we have studied the performance of JFPM in the presence of broadband jamming and partial-band jamming. As we were reviewing the literature for jamming, we realized that the performance of coherent FH/M-ary PSK for $M > 4$ in multitone jamming has not been reported. Furthermore the analysis of FH/DPSK given in the literature applies to only some special cases, and a more general treatment is desirable. Since determining the performance of PSK part is the first step in determining the performance of JFPM, we have tackled this problem. Based on the analysis given in this chapter, work on JFPM can be done but this will not be attempted in this thesis.

This chapter is divided into two parts; in the first part we study the performance of coherent FH/M-ary PSK signals in multitone jamming, in the second part we study the performance of FH/M-ary DPSK signals in multitone jamming.

A coherent frequency hopped spread spectrum system was proposed in [66, 67] as a possible way to combat interference introduced by a jammer in a digital radio system. In that early work, Simon and Polydoros [66] examined the performance of quadrature modulations in the presence of jamming. The analysis given in [66] was based on the assumption that either a coherent frequency synthesizer can be realized or the phase continuity from one hop to another can be maintained by other means. Recently, considerable attention has been devoted to study the performance of several coherent frequency hopped systems in the presence of jamming [68]-[73]. The assumption of coherent frequency synthesizer in which the phase of the signal can be tracked from the dehopped signal is used in [68]-[70]. In [69, 70] the performance of binary signals in partial-band noise jamming and partial-band multitone jamming was obtained and the effect of nonideal channel phase response was studied. Coherent systems are sensitive to phase distortions [71, 72], and a design and analysis of a coherent frequency hopped system employing both channel equalization and joint phase/time tracking loop is presented in [73].

In the previous works, the performance evaluation of coherent frequency hopped PSK in the presence of multitone jamming has been limited to BPSK and QPSK systems. The performance of coherent frequency hopped M-ary PSK system for $M > 4$ has not been reported in the literature because such systems have been considered as impractical. However, with the technological advances of the last two decades and with the newly proposed techniques for phase tracking (e.g. [74]), coherent detection may now be feasible.

In a coherent M-ary PSK receiver, the phase of the incoming signal is determined and compared to all M phases, and the symbol corresponding to the smallest difference is chosen as the estimate of the transmitted symbol. In this work, we assume that a coherent frequency synthesizer can track the phase of the received dehopped signal. A general probability of error analysis requires the probability density function (pdf) of the received signal phase. The main contribution of this chapter is to derive the expression for the probability density function of the received signal phase in the presence of multitone jamming. Then using this pdf, the probability of error expressions are obtained for any M-ary PSK signal. For QPSK (i.e., $M = 4$) our probability of error expressions are identical to the ones given in [18, Vol. II, Ch. 3] which were obtained using a different approach.

Since differentially coherent detection of M-ary DPSK signals employs two symbols in a symbol decision interval, each of the data symbols may or may not have been subjected to the jamming interference in a multitone jamming strategy situation. In the general literature, the authors in [20, 21] and [23, 24] considered the performance of the FH/DPSK system in a multitone jamming environment. Their analysis is applicable to the case where an entire hop is either jammed or not (i.e., no partially jammed hops). They assumed that the jamming tone over a jammed hop is continuous, i.e., the amplitude and initial phase are constant over a particular hop. Based on the analysis given in the first part of this chapter, we provide a theoretical basis for the analysis of FH/M-ary DPSK system in the presence of multitone jamming. In our analysis we assume that the jamming signal in two consecutive DPSK symbols may have are different phases, i.e., the jamming rate can be equal to the symbol rate.

The organization of the chapter is as follows. In Section 6.2, the parameters of a FH system are defined. In Section 6.3, first a brief description of FH/M-ary PSK signals is given. Then the probability density function of the received signal phase is derived and the probability of symbol and bit error expressions are obtained. Also, the performance of the system under worst case jamming is analyzed. Based on the analysis given in Section 6.3, a complete analysis of the probability of error for the FH/M-ary DPSK system in the presence of multitone jamming is given in Section 6.4. Concluding remarks are presented in Section 6.5.

6.2 FH System Model

The modulating signal hops over the entire spread spectrum bandwidth β_{ss}. The total bandwidth is equally divided into several frequency bins. If the frequency spacing between the bins is equal to the symbol rate $R_s = 1/T_s$ of an M-ary symbol, then the total number of frequency bins available can be expressed as

$$N = \frac{\beta_{ss}}{R_s} = \frac{\beta_{ss}}{R_b/\log_2 M} = \frac{\beta_{ss}\log_2 M}{R_b} \tag{6.1}$$

In the jamming model we considered, the jammer is assumed to have the knowledge of the system operation (i.e., the spreading bandwidth and the number of frequency bins in this bandwidth). The jammer does not know a priori where within the spread spectrum bandwidth to concentrate his jamming tones. An intelligent jammer attempts to split the total available jamming power J among q_t random phase tones and vary the number of jamming tones q_t to cause the highest error rate. If there is at most one jamming tone per bin, then the fraction of the bins jammed is given by

$$p = \frac{q_t}{N} \tag{6.2}$$

Therefore, on the average, the jammer hits a frequency bin in any one hop with a probability p. It is convenient to denote the ratio of the received jamming power for each tone to the signal power by

$$\eta^2 = \frac{J/q_t}{S} \tag{6.3}$$

where S denotes the signal power. Using (6.1) and (6.3), p in (6.2) can be written as

$$\begin{aligned} p &= \frac{J/(\eta^2 S)}{(\beta_{ss}\log_2 M)/R_b} = \frac{1}{(S/J)(\beta_{ss}/R_b)\eta^2\log_2 M} \\ &= \frac{1}{(E_b/N_j)\eta^2\log_2 M} = \frac{1}{\rho_b\eta^2\log_2 M} \end{aligned} \tag{6.4}$$

where $\rho_b = E_b/N_j$ denotes the ratio of signal energy per bit-to-jamming noise spectral density.

6.3 Coherent FH/M-ary PSK System

In a coherent FH/M-ary PSK system, the phase to be transmitted in the i-th signaling interval takes its value from the set of allowable phases

$$\theta_k = \frac{(2k-1)\pi}{M} \qquad k = 1, 2, ..., M \tag{6.5}$$

Thus, in the complex notation, the transmitted signal in the i-th signaling interval can be represented by

$$s^{(i)} = \sqrt{2S}e^{j\theta^{(i)}} \tag{6.6}$$

where $s^{(i)}$ denotes the transmitted signal and $\theta^{(i)}$ is the phase of this signal in the i-th signaling interval. It is assumed that the transmitted signal in any symbol interval has a constant amplitude ($\sqrt{2S}$), a constant phase and a fixed frequency.

In a multitone jamming environment, the jamming signal in the i-th signaling interval is represented in the complex form by

$$J^{(i)} = \sqrt{2I}e^{j\phi^{(i)}} \tag{6.7}$$

where both the jamming power per tone ($I = J/q_t$) and the phase are constant during one symbol interval. It is assumed that $\phi^{(i)}$ is a random phase uniformly distributed in the interval $(-\pi, \pi)$. The jamming signal in the interval $(i-1)T_s \leq t \leq iT_s$ falling into the same frequency bin as the transmitted tone is added to the transmitted signal, and the received signal is represented as

$$s_r^{(i)} = \sqrt{2S}e^{j\theta^{(i)}} + \sqrt{2I}e^{j\phi^{(i)}} \tag{6.8}$$

If the optimum receiver structure for M-ary PSK signals in the presence of a wideband noise is employed, then the receiver compares the received signal phase $(\arg(s_r^{(i)}))$ with all possible M phases and decides on the phase that provides the smallest absolute phase difference. Then the probability of symbol error for symbol intervals which are jammed $(P_{e,j})$ is given by

$$P_{e,j} = 1 - \text{Prob}\left(\left|\arg(s_r^{(i)}) - \theta^{(i)}\right| \leq \frac{\pi}{M}\right) \tag{6.9}$$

To analyze the probability of error for the M-ary PSK system, it is necessary to obtain the pdf of the random phase difference, which can be written as

$$\psi = \arg(s_r^{(i)}) - \theta^{(i)} \tag{6.10}$$

6.3.1 The Probability Density Function of ψ

To evaluate the probability density function of the random phase ψ, the derivation can be significantly simplified by first finding the pdf of $u = \arg(s_r^{(i)})$ and then establishing the pdf of ψ. To do so, let us consider the pdf of u, where u can be expressed as

$$\begin{aligned} u &= \arg\left\{s_r^{(i)}\right\} = \arg\left\{\sqrt{2S}e^{j\theta^{(i)}} + \sqrt{2I}e^{j\phi^{(i)}}\right\} \\ &= \arctan\left\{\frac{\frac{1}{\eta}\sin(\theta^{(i)}) + \sin(\phi^{(i)})}{\frac{1}{\eta}\cos(\theta^{(i)}) + \cos(\phi^{(i)})}\right\} = g\left(\phi^{(i)}\right) \quad u_{min} \leq u \leq u_{max} \end{aligned} \tag{6.11}$$

where u_{min} and u_{max} are given in Appendix A. η^2 denotes the ratio of the jamming tone power to the signal power and it is defined as

$$\eta^2 = \frac{I}{S} \tag{6.12}$$

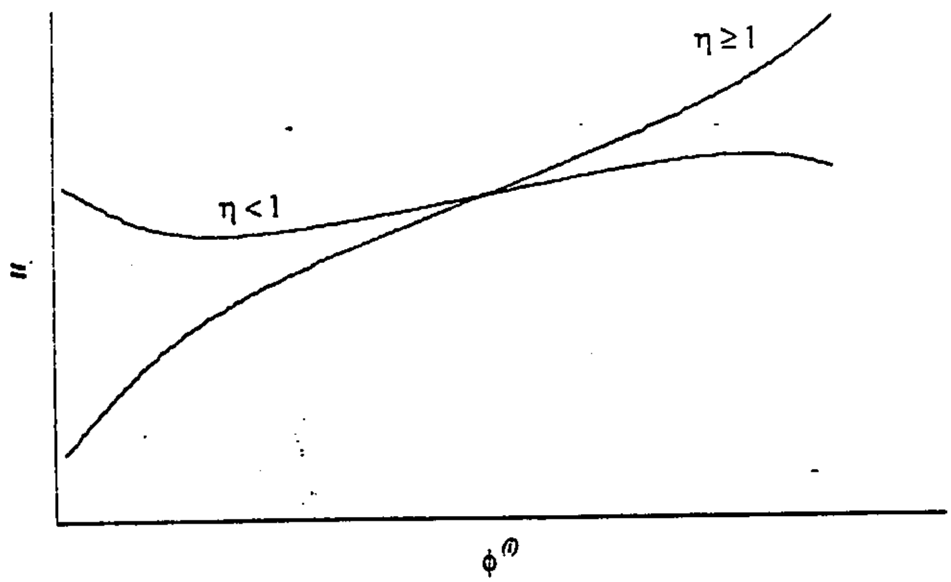

Figure 6.1 : The function $u = g\left(\phi^{(i)}\right)$ for both jamming cases.

Closely inspecting $u = g\left(\phi^{(i)}\right)$ permits us to consider the problem for two cases which are illustrated in Fig. 6.1. The first case occurs when the signal power is greater than the jamming tone power (i.e., $0 < \eta < 1$). In this case, we see that the inverse transformation of the function $u = g\left(\phi^{(i)}\right)$ is double valued (i.e., for a given value of u, there corresponds two values of $\phi^{(i)}$). The second case is observed when the jamming tone power is greater than the signal power (i.e., $\eta \geq 1$), in this case the inverse transformation of $u = g\left(\phi^{(i)}\right)$ is single valued.

To find the pdf of $\mathbf{u}$ for a specific $\phi^{(i)}$, we need to solve the equation $u = g\left(\phi^{(i)}\right)$. Note that the domain of $g\left(\phi^{(i)}\right)$ can be subdivided into a set of disjoint intervals that are exhaustive. Thus, the domain of $g\left(\phi^{(i)}\right)$ can be expressed as a union of intervals, such that $g\left(\phi^{(i)}\right)$ is monotonically increasing or monotonically decreasing in each interval. The distribution function of $\mathbf{u}$ is then, given by

$$F_u(u) = P(\mathbf{u} \leq u) = P(g(\phi^{(i)}) \leq u) \tag{6.13}$$

and the density function of $\mathbf{u}$ can be obtained from

$$p_u(u) = \frac{dF_u(u)}{du} \tag{6.14}$$

In the following, we present detailed analysis for the probability density function of the random phase ψ in both jamming cases. The final expression of $p_\psi(\psi)$ for $\eta > 0$ is also given.

Evaluation of $p_\psi(\psi)$ for $0 < \eta < 1$

From Fig. 6.2, it can be seen that the inverse transformation of $u = g\left(\phi^{(i)}\right)$ is double valued. In Appendix A, $\phi^{(i)}$ is evaluated as a function of u and the results are given by

$$\phi^{(i)} = u + \arcsin\left[\frac{1}{\eta}\sin(u - \theta^{(i)})\right] \tag{6.15}$$

when $u = g\left(\phi^{(i)}\right)$ is monotonically increasing and by

$$\phi^{(i)} = u - \pi - \arcsin\left[\frac{1}{\eta}\sin(u - \theta^{(i)})\right] \tag{6.16}$$

when $u = g\left(\phi^{(i)}\right)$ is monotonically decreasing.

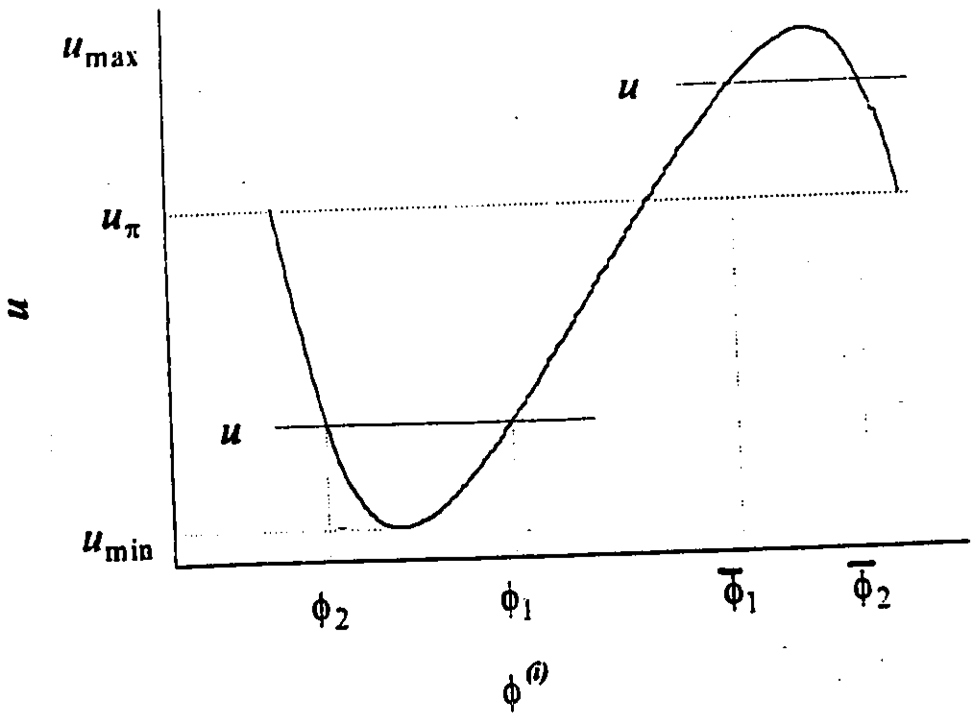

Figure 6.2 : The function $u = g\left(\varphi^{(i)}\right)$ *for* $0 < \eta < 1$.

In Appendix B, we derive bounds on the possible values of $u = g\left(\phi^{(i)}\right)$. These bounds are given by

$$\begin{aligned}\min\left\{\left[\theta^{(i)} - \arcsin(\eta)\right], \left[\theta^{(i)} + \arcsin(\eta)\right]\right\} \leq u \leq \\ \max\left\{\left[\theta^{(i)} - \arcsin(\eta)\right], \left[\theta^{(i)} + \arcsin(\eta)\right]\right\}\end{aligned} \tag{6.17}$$

Having defined the region of the random variable $\mathbf{u} = g\left(\phi^{(\mathbf{i})}\right)$, let us now express the distribution function $F_u(u)$ in terms of the distribution function $F_{\phi^{(i)}}\left(\phi^{(i)}\right)$ and the function $g\left(\phi^{(i)}\right)$. For this purpose, we must determine the distribution function $F_u(u)$ of the random variable $\mathbf{u}$. In this particular case, we handle this problem by sectioning the function $u = g\left(\phi^{(i)}\right)$ into two functions (see Fig. 6.2). The first function is bounded by $u_{min} \leq u \leq u_\pi$ and the second one is bounded by $u_\pi < u \leq u_{max}$. The limits are defined as

$$u_{min} = \min\left\{\left[\theta^{(i)} - \arcsin(\eta)\right], \left[\theta^{(i)} + \arcsin(\eta)\right]\right\} \tag{6.18}$$

and

$$u_{max} = \max\left\{\left[\theta^{(i)} - \arcsin(\eta)\right], \left[\theta^{(i)} + \arcsin(\eta)\right]\right\} \tag{6.19}$$

and

$$u_\pi = g(\pi) = \arctan\left\{\frac{\frac{1}{\eta}\sin(\theta^{(i)})}{\frac{1}{\eta}\cos(\theta^{(i)}) - 1}\right\} \tag{6.20}$$

For the first section, when $u_{min} \leq u \leq u_\pi$ we have

$$\begin{aligned} F_u(u) &= P(\mathbf{u} \leq u) = P\left(g\left(\phi^{(\mathbf{i})}\right) \leq u\right) \\ &= P\left(\phi_2 \leq \phi^{(\mathbf{i})} \leq \phi_1\right) \end{aligned} \tag{6.21}$$

where ϕ_1 and ϕ_2 are defined as

$$\phi_1 = u + \arcsin\left[\frac{1}{\eta}\sin(u - \theta^{(i)})\right] \tag{6.22}$$

and

$$\phi_2 = u - \pi - \arcsin\left[\frac{1}{\eta}\sin(u - \theta^{(i)})\right] \tag{6.23}$$

Recall that the pdf of the random variable $\phi^{(i)}$ is uniform in the interval $(-\pi, \pi)$. Then we get

$$\begin{aligned} F_u(u) &= \int_{\phi_2}^{\phi_1} p_{\phi^{(i)}} d\phi^{(i)} \\ &= \frac{1}{2\pi}\left(\pi + 2\arcsin\left[\frac{1}{\eta}\sin(u - \theta^{(i)})\right]\right) \end{aligned} \tag{6.24}$$

For the second section, when $u_\pi < u \le u_{max}$ we have

$$\begin{aligned} F_u(u) &= P(\mathbf{u} \le u) = P\left(g\left(\phi^{(i)}\right) \le u\right) \\ &= P\left(\bar{\phi}_2 \le \phi^{(i)} \le \bar{\phi}_1\right) \end{aligned} \tag{6.25}$$

where $\bar{\phi}_1 = \phi_1$ and $\bar{\phi}_2 = \phi_2$ are defined in (6.22) and (6.23). Then we get

$$\begin{aligned} F_u(u) &= 1 - \int_{\bar{\phi}_1}^{\bar{\phi}_2} p_{\phi^{(i)}} d\phi^{(i)} \\ &= 1 - \frac{1}{2\pi}\left(\pi - 2\arcsin\left[\frac{1}{\eta}\sin(u - \theta^{(i)})\right]\right) \end{aligned} \tag{6.26}$$

Now by substituting (6.24) and (6.26) into (6.14) the pdf of $\mathbf{u}$ can be expressed as

$$p_u(u) = \begin{cases} \dfrac{\cos\left(u - \theta^{(i)}\right)}{\pi\sqrt{\eta^2 - \sin^2\left(u - \theta^{(i)}\right)}} & \text{for } u_{min} \le u \le u_{max}. \\ 0 & \text{otherwise.} \end{cases} \tag{6.27}$$

where u_{min} and u_{max} are defined in (6.18) and (6.19).

Let us now obtain the probability density function of the random phase difference ψ which is functionally related to u by

$$\psi = u - \theta^{(i)} \tag{6.28}$$

the density $p_\psi(\psi)$ may be written as [65]

$$p_\psi(\psi) = p_u(\psi + \theta^{(i)}) \tag{6.29}$$

substituting $p_u(u)$ given in (6.27) into (6.29), the probability density function of ψ is given by

$$p_\psi(\psi) = \begin{cases} \frac{\cos(\psi)}{\pi\sqrt{\eta^2 - \sin^2(\psi)}} & \text{for} \quad -\arcsin(\eta) \le \psi \le \arcsin(\eta). \\ 0 & \text{otherwise.} \end{cases} \tag{6.30}$$

Evaluation of $p_\psi(\psi)$ for $\eta > 1$

We turn now to the case where the jamming power is greater than the signal power. In this case, it is observed that u is monotonically increasing with $\phi^{(i)}$ and the inverse transformation of $u = g\left(\phi^{(i)}\right)$ is single-valued. Hence, $\phi^{(i)}$ is evaluated as a function of u and the result is given by

$$\phi^{(i)} = u + \arcsin\left[\frac{1}{\eta}\sin(u - \theta^{(i)})\right] \tag{6.31}$$

Of particular interest is the region where the random variable u is not equal to zero.

The probability distribution function of the random variable u is simply expressed as

$$\begin{aligned} F_u(u) &= P(\mathbf{u} \le u) = P\left(g\left(\phi^{(\mathrm{i})}\right) \le u\right) \\ &= P\left(\phi^{(\mathrm{i})} \le u + \arcsin\left[\frac{1}{\eta}\sin(u - \theta^{(i)})\right]\right) \end{aligned} \tag{6.32}$$

Recall that $\phi^{(\mathrm{i})}$ is uniform in the interval $(-\pi, \pi)$. Then we get

$$\begin{aligned} F_u(u) &= \int_{-\pi}^{u+\arcsin\left[\frac{1}{\eta}\sin(u-\theta^{(i)})\right]} \frac{1}{2\pi} d\phi^{(i)} \\ &= \frac{1}{2\pi}\left(\pi + u + \arcsin\left[\frac{1}{\eta}\sin(u - \theta^{(i)})\right]\right) \end{aligned} \tag{6.33}$$

The probability density function of u is found by differentiating the probability distribution function, and this yields

$$p_u(u) = \begin{cases} \frac{1}{2\pi}\left(1 + \frac{\cos\left(u-\theta^{(i)}\right)}{\sqrt{\eta^2-\sin^2\left(u-\theta^{(i)}\right)}}\right) & -\pi \leq u \leq \pi. \\ 0 & \text{otherwise.} \end{cases} \tag{6.34}$$

The probability density function of the random phase ψ can be obtained by using the transformation given in (6.29) and this results in

$$p_\psi(\psi) = \begin{cases} \frac{1}{2\pi}\left(1 + \frac{\cos(\psi)}{\sqrt{\eta^2-\sin^2(\psi)}}\right) & -\pi \leq \psi \leq \pi. \\ 0 & \text{otherwise.} \end{cases} \tag{6.35}$$

Evaluation of $p_\psi(\psi)$ for $\eta = 1$

For $\eta = 1$, the expression given in (6.11) reduces to the form

$$u = \frac{1}{2}\left(\phi^{(i)} + \theta^{(i)}\right) \tag{6.36}$$

The pdf of **u** may be written in the form of

$$p_u(u) = 2p_{\phi^{(i)}}\left(2u - \theta^{(i)}\right) \tag{6.37}$$

but the random variable $\phi^{(i)}$ is uniform in the interval $(-\pi, \pi)$, then **u** is uniform in the interval $(-\pi/2 + \theta^{(i)}, \pi/2 + \theta^{(i)}$ and its pdf may be written as

$$p_u(u) = \begin{cases} \frac{1}{\pi} & -\frac{\pi}{2} + \theta^{(i)} \leq u \leq \frac{\pi}{2} + \theta^{(i)} \\ 0 & \text{otherwise.} \end{cases} \tag{6.38}$$

By using (6.29), $p_\psi(\psi)$ can be obtained as

$$p_\psi(\psi) = \begin{cases} \frac{1}{\pi} & \text{for } -\frac{\pi}{2} \leq \psi \leq \frac{\pi}{2} \\ 0 & \text{otherwise.} \end{cases} \tag{6.39}$$

This result can be obtained from (6.30) by substituting $\eta = 1$.

It is convenient to write the probability density function of the random phase ψ in one expression for any value of η. According to the equations (6.30), (6.35) and (6.39), $p_\psi(\psi)$ takes the form

$$p_\psi(\psi) = \begin{cases} \frac{1}{\pi}\left(\frac{\cos(\psi)}{\sqrt{\eta^2-\sin^2(\psi)}}\right) & -\arcsin(\eta) \le \psi \le \arcsin(\eta) \text{ and } 0 < \eta \le 1. \\ \frac{1}{2\pi}\left(1+\frac{\cos(\psi)}{\sqrt{\eta^2-\sin^2(\psi)}}\right) & -\pi \le \psi \le \pi \text{ and } \eta > 1 \\ 0 & \text{otherwise.} \end{cases} \tag{6.40}$$

6.3.2 Evaluation of the Probability of Error

From the result given in (6.40), it is obvious that $p_\psi(\psi)$ is an even function and it is independent of the transmitted phase. Hence, the average probability of symbol error for symbol intervals which are jammed can be evaluated by using (6.9). This probability may be written as

$$P_{e,j} = 1 - \int_{-\pi/M}^{\pi/M} p_\psi(\psi)d\psi \tag{6.41}$$

In order to find the performance of the system, we evaluate the probability of error for the different jamming cases discussed above.

Evaluation of the probability of error for $0 < \eta \le 1$

In this case, $p_\psi(\psi) = 0$ if $\pi/M \ge \arcsin(\eta)$, therefore, $P_{e,j} = 0$. For $\pi/M \le \arcsin(\eta)$ and by substituting $p_\psi(\psi)$ from (6.30) into (6.41) we obtain

$$P_{e,j} = 1 - \int_{-\pi/M}^{\pi/M} \frac{\cos(\psi)}{\pi\sqrt{\eta^2 - \sin^2(\psi)}}d\psi \tag{6.42}$$

A change in the variable of integration $r = \sin(\psi)$ yields

$$P_{e,j} = 1 - \int_{-\sin(\pi/M)}^{\sin(\pi/M)} \frac{1}{\pi\sqrt{\eta^2 - r^2}}dr \tag{6.43}$$

The above integral can be evaluated to give:

$$\begin{aligned} P_{e,j} &= 1 - \frac{2}{\pi}\arcsin\left[\frac{\sin(\pi/M)}{\eta}\right] \\ &= \frac{2}{\pi}\arccos\left[\frac{\sin(\pi/M)}{\eta}\right] \end{aligned} \tag{6.44}$$

Evaluation of the probability of error for $\eta > 1$

Considering now the case when $\eta > 1$, the average probability of error for symbol intervals which are jammed can be obtained by substituting $p_\psi(\psi)$ from (6.35) into (6.41). Then (6.41) becomes:

$$\begin{aligned} P_{e,j} &= 1 - \int_{-\pi/M}^{\pi/M} \frac{1}{2\pi}\left(1 + \frac{\cos(\psi)}{\sqrt{\eta^2 - \sin^2(\psi)}}\right) d\psi \\ &= 1 - \frac{1}{M} - \frac{1}{\pi}\arcsin\left[\frac{\sin(\pi/M)}{\eta}\right] \end{aligned} \tag{6.45}$$

We can also write (6.45) as

$$P_{e,j} = \frac{M-2}{2M} + \frac{1}{\pi}\arccos\left[\frac{\sin(\pi/M)}{\eta}\right] \tag{6.46}$$

Combining the results of both jamming cases as given in (6.44) and (6.46). Therefore $P_{e,j}$ may be written as

$$P_{e,j} = \begin{cases} \frac{2}{\pi}\arccos\left[\frac{\sin(\pi/M)}{\eta}\right] & \pi/M \le \arcsin(\eta), \text{ and } 0 < \eta \le 1. \\ \frac{M-2}{2M} + \frac{1}{\pi}\arccos\left[\frac{\sin(\pi/M)}{\eta}\right] & \eta > 1 \\ 0 & \text{otherwise.} \end{cases} \tag{6.47}$$

The average probability of symbol error which is $P_e(M) = pP_{e,j}$ may be expressed as

$$P_e(M) = \begin{cases} \frac{2p}{\pi}\arccos\left[\frac{\sin(\pi/M)}{\eta}\right] & \pi/M \le \arcsin(\eta), \text{ and } 0 < \eta \le 1. \\ \frac{(M-2)p}{2M} + \frac{p}{\pi}\arccos\left[\frac{\sin(\pi/M)}{\eta}\right] & \eta > 1 \\ 0 & \text{otherwise.} \end{cases} \tag{6.48}$$

It is often desirable to have the error probability expressed in terms of the received signal-to-jamming noise ratio per bit (E_b/N_j). Therefore, by using (6.4) the parameter η may be written in the form of

$$\eta = \sqrt{\frac{1}{(E_b/N_j)p\log_2 M}} \tag{6.49}$$

Substituting the expression of η into (6.48), the average probability of symbol error becomes:

$$P_e(M) = \begin{cases} 0 & p\frac{E_b}{N_J} > \frac{1}{\sin^2(\pi/M)\log_2 M} \\ \frac{2p}{\pi}\arccos\sqrt{p\frac{E_b}{N_j}\log_2 M\sin^2(\pi/M)} & \frac{1}{\log_2 M} \le p\frac{E_b}{N_J} \le \frac{1}{\sin^2(\pi/M)\log_2 M} \\ \frac{(M-2)p}{2M} + \\ \frac{p}{\pi}\arccos\sqrt{p\frac{E_b}{N_j}\log_2 M\sin^2(\pi/M)} & 0 < p\frac{E_b}{N_J} < \frac{1}{\log_2 M} \end{cases} \tag{6.50}$$

At high E_b/N_j, the relationship between symbol error probability and bit error probability if Gray coding is used is well approximated by

$$P_b = \frac{1}{\log_2 M}P_e(M) = \frac{1}{k_s}P_e(M) \tag{6.51}$$

where $k_s = \log_2 M$. Therefore,

$$P_b = \begin{cases} 0 & p\frac{E_b}{N_J} > \frac{1}{k_s\sin^2(\pi/M)} \\ \frac{2p}{\pi k_s}\arccos\sqrt{p\frac{E_b}{N_j}k_s\sin^2(\pi/M)} & \frac{1}{k_s} \le p\frac{E_b}{N_J} \le \frac{1}{k_s\sin^2(\pi/M)} \\ \frac{(M-2)p}{2Mk_s} + \frac{p}{\pi k_s}\arccos\sqrt{p\frac{E_b}{N_j}k_s\sin^2(\pi/M)} & 0 < p\frac{E_b}{N_J} < \frac{1}{k_s} \end{cases} \tag{6.52}$$

For $M = 4$, the probability of a bit error is given by:

$$P_b = \begin{cases} 0 & p\frac{E_b}{N_J} > 1 \\ \frac{p}{\pi}\arccos\sqrt{p\frac{E_b}{N_j}} & \frac{1}{2} \le p\frac{E_b}{N_J} \le 1 \\ \frac{p}{8} + \frac{p}{2\pi}\arccos\sqrt{p\frac{E_b}{N_j}} & 0 < p\frac{E_b}{N_J} < \frac{1}{2} \end{cases} \tag{6.53}$$

this result is identical to the ones given in [18, Vol. II, Ch. 3] which were obtained using a different approach.

6.3.3 Worst Case Multitone jamming

In multitone jamming environment, the jammer is assumed to have finite power and finite number of tones. The optimum strategy for a jammer is to distribute the total jamming power into a number of tones, in a way to cause the highest error rate. Hence, from the jammer's point of view there is an optimum value of p that maximizes the probability of error, this value of p is called the worst case value and is denoted as p_{wc}.

let us assume that, the worst case value of p occurs in the case where the jamming tone power does not exceed the signal power ($\eta < 1$). Worst case value of p can be found by differentiating P_b with respect to p and equating the result to zero. That is,

$$\frac{\partial}{\partial p}\left[\frac{2p}{\pi k_s}\arccos\sqrt{p\frac{E_b}{N_j}k_s\sin^2(\pi/M)}\right] = 0 \tag{6.54}$$

This yields

$$\arccos\sqrt{p\frac{E_b}{N_j}k_s\sin^2(\pi/M)} = \frac{1}{2}\sqrt{\frac{p\frac{E_b}{N_j}k_s\sin^2(\pi/M)}{1-p\frac{E_b}{N_j}k_s\sin^2(\pi/M)}} \tag{6.55}$$

The solution of the above equation has been found numerically and the result is

$$p\frac{E_b}{N_j}k_s\sin^2(\pi/M) = 0.6306 \tag{6.56}$$

Now, p_{wc} may be written as

$$p_{wc} = \begin{cases} \frac{0.6306/\left(k_s\sin^2(\pi/M)\right)}{E_b/N_j} & \frac{E_b}{N_J} > \frac{0.6306}{k_s\sin^2(\pi/M)} \\ 1 & \frac{E_b}{N_J} \le \frac{0.6306}{k_s\sin^2(\pi/M)} \end{cases} \tag{6.57}$$

Thus, the average bit error probability performance in the presence of the worst case multitone jamming can be obtained by substituting (6.57) into (6.52). Therefore,

$$P_{b_{max}} = \begin{cases} \frac{0.2623}{k_s^2 \sin^2(\pi/M) E_b/N_j} & \frac{E_b}{N_J} > \frac{0.6306}{k_s \sin^2(\pi/M)} \\ \frac{2}{\pi k_s} \arccos\sqrt{\frac{E_b}{N_j} k_s \sin^2(\pi/M)} & \frac{1}{k_s} \leq \frac{E_b}{N_J} \leq \frac{0.6306}{k_s \sin^2(\pi/M)} \\ \frac{M-2}{2Mk_s} + \frac{1}{\pi k_s} \arccos\sqrt{\frac{E_b}{N_j} k_s \sin^2(\pi/M)} & 0 < \frac{E_b}{N_J} < \frac{1}{k_s} \end{cases} \tag{6.58}$$

For $M = 4$, the probability of a bit error corresponding to the worst case jammer is given by:

$$P_{b_{max}} = \begin{cases} \frac{0.1311}{E_b/N_j} & \frac{E_b}{N_J} > 0.6306 \\ \frac{1}{\pi} \arccos\sqrt{\frac{E_b}{N_j}} & \frac{1}{2} \leq \frac{E_b}{N_J} \leq 0.6306 \\ \frac{1}{8} + \frac{1}{2\pi} \arccos\sqrt{\frac{E_b}{N_j}} & 0 < \frac{E_b}{N_J} < \frac{1}{2}. \end{cases} \tag{6.59}$$

which is identical to the result obtained by [18, Vol. II, Ch. 3] by using a different approach. Bit error rate performance as a function of E_b/N_j for FH/M-ary PSK system, in the worst case multitone jamming, has been calculated by using (6.58), and the results are plotted in Fig. 6.3 when $M = 2, 4, 8, 16, 32, 64$.

6.4 The FH/M-ary DPSK System

In M-ary DPSK system, the phase to be transmitted in the i-th signaling interval takes its value from the set of allowable phases given in (6.5). This phase is then added to the total accumulated phase in the $(i-1)$-th signaling interval and is transmitted through the channel by using M-ary PSK modulator [21].

Thus, in a complex form, the transmitted signal in the i-th signaling interval can be represented by

$$s^{(i)} = \sqrt{2S} e^{j(\theta^{(i)} + \theta_T^{(i-1)})} \tag{6.60}$$

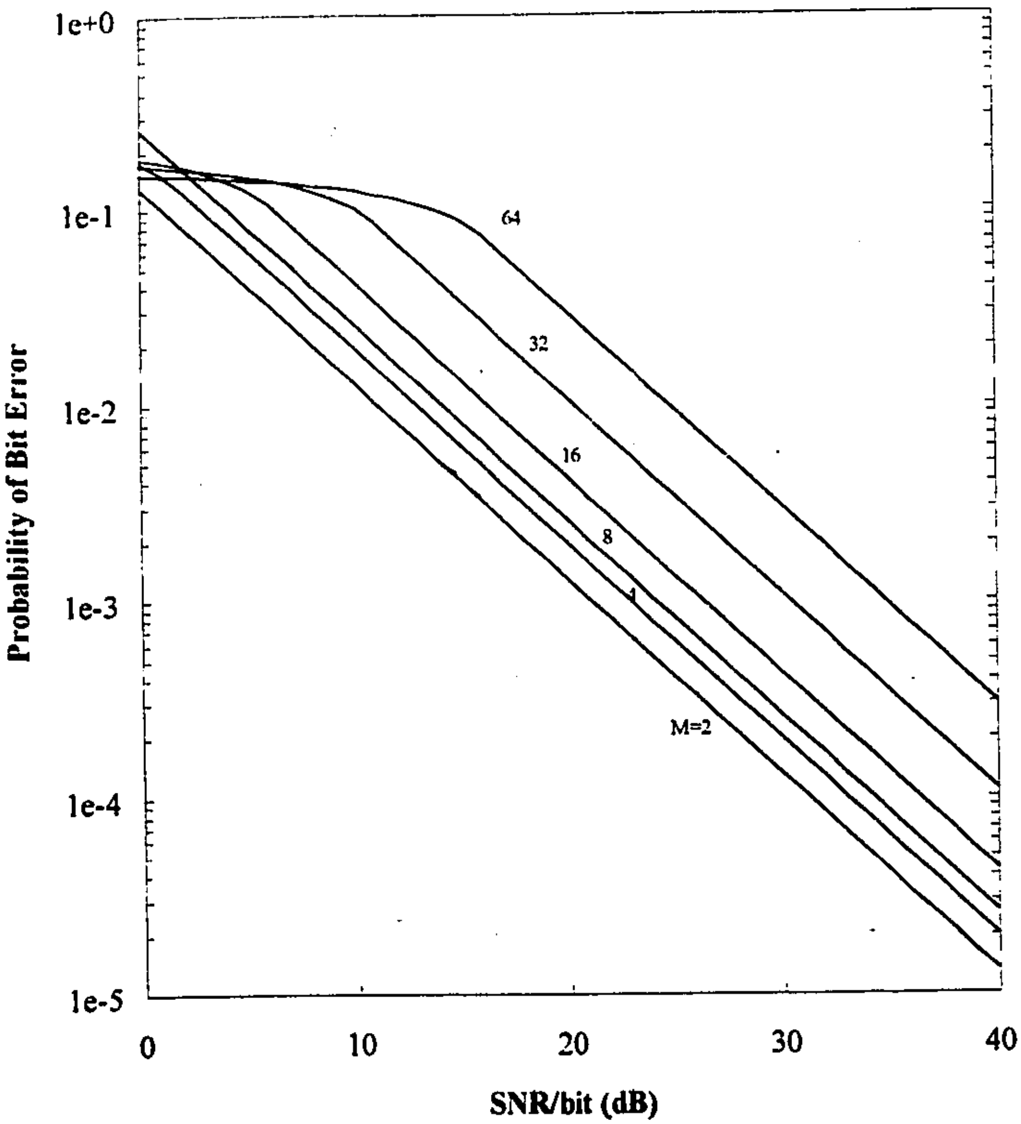

Figure 6.3 : Bit error probability performance for FH/M-ary PSK in worst case multitone jamming when $M = 2, 4, 8, 16, 32, 64$.

where

- $s^{(i)}$ is the transmitted signal in the i-th signaling interval.

- $\theta^{(i)}$ is the differential phase to be transmitted in the i-th signaling interval.

- $\theta_T^{(i-1)}$ is the total accumulated phase in the $(i-1)$-th signaling interval.

It is assumed that, the transmitted signal in any symbol interval has a constant amplitude, a constant phase and a fixed frequency.

In multitone jamming environments, the jamming signal in the i-th signaling interval is represented in the complex form by

$$J^{(i)} = \sqrt{2I}e^{j\phi^{(i)}} \tag{6.61}$$

where both the jamming power and the phase are constant during one symbol interval. It is assumed that $\phi^{(i)}$ is a random phase uniformly distributed in the interval $(-\pi, \pi)$.

Therefore, the received signal in the i-th signaling interval may be represented in the complex form by

$$s_r^{(i)} = \sqrt{2S}e^{j(\theta^{(i)}+\theta_T^{(i-1)})} + \kappa_1 J^{(i)} \tag{6.62}$$

where $\kappa_1 = 1$ or 0 whether or not the jamming signal is present in the frequency bin of interest.

In the $(i-1)$-th signaling interval the transmitted signal takes the form of

$$s^{(i-1)} = \sqrt{2S}e^{j\theta_T^{(i-1)}} \tag{6.63}$$

and the jamming signal may be represented as

$$J^{(i-1)} = \sqrt{2I}e^{j\phi^{(i-1)}} \tag{6.64}$$

Then the complex form of the received signal in the $(i-1)$-th signaling interval is given by:

$$s_r^{(i-1)} = \sqrt{2S}e^{j\theta_T^{(i-1)}} + \kappa_2 J^{(i-1)} \tag{6.65}$$

where $\kappa_2 = 1$ or 0 whether or not the jamming signal is present.

In multitone jamming strategy, either $J^{(i)}$ in (6.61) or $J^{(i-1)}$ in (6.64) or both of them may present (depending upon whether $s^{(i)}$ or $s^{(i-1)}$ or both of them were unjammed or jammed).

Let us define the joint event (κ_1, κ_2) where $\kappa_n = 1$ or 0 and $n = 1, 2$. The event κ_1 and κ_2 may be defined as:

- The event $\kappa_1 = 0$ denotes the case where the jammer does not hit the i-th signaling interval, whereas $\kappa_1 = 1$ denotes the presence of jamming tone in the i-th signaling interval.

- The event $\kappa_2 = 0$ denotes the case where the jammer does not hit the $(i-1)$-th signaling interval, whereas $\kappa_2 = 1$ denotes the presence of jamming tone in the $(i-1)$-th signaling interval.

If an optimum receiver structure is employed for M-ary DPSK signals in the presence of wideband noise, then the optimum decision of this receiver is made by comparing the phase difference $(\arg(s_r^{(i)}) - \arg(s_r^{(i-1)}))$ with all possible M phases and the decision is made based on the phase that provides the smallest difference, that is;

$$\min_{k=1,2,\ldots,M} \left\{ \left| \left(\arg(s_r^{(i)}) - \arg(s_r^{(i-1)})\right) - \theta_k \right| > \frac{\pi}{M} \right\} \tag{6.66}$$

Assuming $\theta^{(i)}$ is the transmitted phase in the i-th signaling interval, then a symbol error in FH/M-ary DPSK system occurs with a probability $\mathcal{P}_{\theta^{(i)}}$, where

$$\mathcal{P}_{\theta^{(i)}} = \Gamma(1,1) P\left(\left| \left(\arg(s_r^{(i)}) - \arg(s_r^{(i-1)})\right) - \theta^{(i)} \right| > \frac{\pi}{M} \middle| (1,1) \right)$$

$$
\begin{aligned}
&+\ \Gamma(1,0)P\left(\left|\left(\arg(s_r^{(i)})-\arg(s_r^{(i-1)})\right)-\theta^{(i)}\right|>\frac{\pi}{M}\,\middle|\,(1,0)\right)\\
&+\ \Gamma(0,1)P\left(\left|\left(\arg(s_r^{(i)})-\arg(s_r^{(i-1)})\right)-\theta^{(i)}\right|>\frac{\pi}{M}\,\middle|\,(0,1)\right)\\
&+\ \Gamma(0,0)P\left(\left|\left(\arg(s_r^{(i)})-\arg(s_r^{(i-1)})\right)-\theta^{(i)}\right|>\frac{\pi}{M}\,\middle|\,(0,0)\right) \qquad (6.67)
\end{aligned}
$$

where

$$\Gamma(\kappa_1,\kappa_2) = \text{probability of the joint event} \quad (\kappa_1,\kappa_2)$$

It may easily be shown that:

$$
\begin{aligned}
\Gamma(1,1) &= p^2\\
\Gamma(1,0) &= \Gamma(0,1) = p(1-p)\\
\Gamma(0,0) &= (1-p)^2
\end{aligned}
$$

Let us look briefly at the probability of the conditional events given in (6.67). On the basis of our definition to the jamming strategy, the jammer may hit only one of the two consecutive symbols, these events are similar and produce the same probability. This assumption is based on the fact that the jamming tones are independent. Then we have:

$$
\begin{aligned}
&P\left(\left|\left(\arg(s_r^{(i)})-\arg(s_r^{(i-1)})\right)-\theta^{(i)}\right|>\frac{\pi}{M}\,\middle|\,(1,0)\right)=\\
&\quad P\left(\left|\left(\arg(s_r^{(i)})-\arg(s_r^{(i-1)})\right)-\theta^{(i)}\right|>\frac{\pi}{M}\,\middle|\,(0,1)\right)
\end{aligned}
$$

Since jamming is considered as the only disturbance, the last term in (6.67) represents the probability of the impossible event, the event which cannot occur, then we have:

$$P\left(\left|\left(\arg(s_r^{(i)})-\arg(s_r^{(i-1)})\right)-\theta^{(i)}\right|>\frac{\pi}{M}\,\middle|\,(0,0)\right)=0$$

Now, (6.67) may be written in the form of

$$
\begin{aligned}
\mathcal{P}_{\theta^{(i)}} &= \Gamma(1,1)P\left(\left|\left(\arg(s_r^{(i)})-\arg(s_r^{(i-1)})\right)-\theta^{(i)}\right|>\frac{\pi}{M}\,\middle|\,(1,1)\right)\\
&+\ 2\Gamma(1,0)P\left(\left|\left(\arg(s_r^{(i)})-\arg(s_r^{(i-1)})\right)-\theta^{(i)}\right|>\frac{\pi}{M}\,\middle|\,(1,0)\right) \qquad (6.68)
\end{aligned}
$$

If $\theta^{(i)} = \theta_n$, then the probability of the conditional events given in (6.68) may be written as

$$\begin{aligned} \mathcal{P}_{\theta_n} &= \Gamma(1,1)P\left(\left|\left(\arg(s_r^{(i)}) - \arg(s_r^{(i-1)})\right) - \theta_n\right| > \frac{\pi}{M}\middle|(1,1)\right) \\ &+ 2\Gamma(1,0)P\left(\left|\left(\arg(s_r^{(i)}) - \arg(s_r^{(i-1)})\right) - \theta_n\right| > \frac{\pi}{M}\middle|(1,0)\right) \end{aligned} \tag{6.69}$$

then the average symbol error probability can be written in the form of:

$$P_e = \frac{1}{M}\sum_n \mathcal{P}_{\theta_n} \quad n = 1, 2...., M \tag{6.70}$$

As shown in (6.69), there are two specific cases of interest to obtain the error rate for the system under consideration. Those are:

- Case 1: In this case, the jammer hits two consecutive symbols (i.e, the jammer hits in the signaling intervals i and $(i-1)$).
- Case 2: In this case, the jammer hits only one of the two consecutive symbols (i.e, the jammer hits either in the signaling intervals i or $(i-1)$).

According to the above cases, the average probability of symbol error as given in (6.70) may be written as

$$P_e = P_{e1} + P_{e2} \tag{6.71}$$

where P_{e1} is the probability of the event where the jammer hits two consecutive symbols as discussed in case 1 and it can be written as:

$$P_{e1} = \frac{\Gamma(1,1)}{M}\sum_n P\left(\left|\left(\arg(s_r^{(i)}) - \arg(s_r^{(i-1)})\right) - \theta_n\right| > \frac{\pi}{M}\middle|(1,1)\right) \quad n = 1, 2...., M \tag{6.72}$$

and P_{e2} is the probability of the event where the jammer hits one of the two consecutive symbols as discussed in case 2 and it can be written as:

$$P_{e2} = \frac{2\Gamma(1,0)}{M} \sum_{n} P\left(\left| \left(\arg(s_r^{(i)}) - \arg(s_r^{(i-1)}) \right) - \theta_n \right| > \frac{\pi}{M} \middle| (1,0) \right) \quad n = 1, 2 ...., M \quad (6.73)$$

In the following, we present an analysis for the evaluation P_{e1} and P_{e2}. The final expression is also given for the average probability of symbol error.

6.4.1 Evaluation of P_{e1}

To evaluate the probability of error P_{e1} as given in (6.72), it is necessary to obtain the probability of the event described by case 1, which can be written as

$$P_{e1,n} = P\left(\left| \left(\arg(s_r^{(i)}) - \arg(s_r^{(i-1)}) \right) - \theta^{(i)} \right| > \frac{\pi}{M} \middle| (1,1) \right) \quad (6.74)$$

Therefore, it is necessary to obtain first the probability density function of the phase difference ψ where ψ is defined as

$$\psi = \left(\arg(s_r^{(i)}) - \arg(s_r^{(i-1)}) \right) - \theta^{(i)} \quad (6.75)$$

In this case the jammer hits two consecutive symbols. Then, $s_r^{(i)}$ and $s_r^{(i-1)}$ are given by

$$s_r^{(i)} = \sqrt{2S} e^{j(\theta^{(i)} + \theta_T^{(i-1)})} + \sqrt{2I} e^{j\phi^{(i)}} \quad (6.76)$$

and

$$s_r^{(i-1)} = A e^{j\theta_T^{(i-1)}} + \sqrt{2I} e^{j\phi^{(i-1)}} \quad (6.77)$$

To find $p_\psi(\psi)$, first the probability density function of both $u = \arg(s_r^{(i)})$ and $v = \arg(s_r^{(i-1)})$ should be determined, then, we can evaluate the joint probability density function of u and v, finally by using the transformation $\psi = u - v - \theta^{(i)}$,

$p_\psi(\psi)$ can be obtained.

By analogy between (6.76), (6.77) and (6.11), it clearly appears that the pdf of both u and v can be obtained by following a procedure similar to that leading to (6.27) for $0 < \eta < 1$ and (6.34) for $\eta > 1$.

For $0 < \eta < 1$ the pdf of u and v may be written as

$$p_u(u) = \begin{cases} \frac{\cos\left(u-(\theta^{(i)}+\theta_T^{(i-1)})\right)}{\pi\sqrt{\eta^2-\sin^2\left(u-(\theta^{(i)}+\theta_T^{(i-1)})\right)}} & \text{for } u_{min} \leq u \leq u_{max}. \\ 0 & \text{otherwise.} \end{cases} \tag{6.78}$$

and

$$p_v(v) = \begin{cases} \frac{\cos\left(v-\theta_T^{(i-1)}\right)}{\pi\sqrt{\eta^2-\sin^2\left(v-\theta_T^{(i-1)}\right)}} & \text{for } v_{min} \leq u \leq v_{max}. \\ 0 & \text{otherwise.} \end{cases} \tag{6.79}$$

where u_{min}, u_{max}, v_{min}, v_{max} are defined as

$$u_{min} = \min\left\{\left[\theta^{(i)} + \theta_T^{(i-1)} - \arcsin(\eta)\right], \left[\theta^{(i)} + \theta_T^{(i-1)} + \arcsin(\eta)\right]\right\} \tag{6.80}$$

$$u_{max} = \max\left\{\left[\theta^{(i)} + \theta_T^{(i-1)} - \arcsin(\eta)\right], \left[\theta^{(i)} + \theta_T^{(i-1)} + \arcsin(\eta)\right]\right\} \tag{6.81}$$

$$v_{min} = \min\left\{\left[\theta_T^{(i-1)} - \arcsin(\eta)\right], \left[\theta_T^{(i-1)} + \arcsin(\eta)\right]\right\} \tag{6.82}$$

and

$$v_{max} = \max\left\{\left[\theta_T^{(i-1)} - \arcsin(\eta)\right], \left[\theta_T^{(i-1)} + \arcsin(\eta)\right]\right\} \tag{6.83}$$

For $\eta > 1$ the pdf of u and v can be written as

$$p_u(u) = \begin{cases} \frac{1}{2\pi}\left(1 + \frac{\cos\left(u-(\theta^{(i)}+\theta_T^{(i-1)})\right)}{\sqrt{\eta^2-\sin^2\left(u-(\theta^{(i)}+\theta_T^{(i-1)})\right)}}\right) & -\pi \leq u \leq \pi. \\ 0 & \text{otherwise.} \end{cases} \tag{6.84}$$

$$p_v(v) = \begin{cases} \frac{1}{2\pi}\left(1 + \frac{\cos\left(v-\theta_T^{(i-1)}\right)}{\sqrt{\eta^2-\sin^2\left(v-\theta_T^{(i-1)}\right)}}\right) & -\pi \leq v \leq \pi. \\ 0 & \text{otherwise.} \end{cases} \tag{6.85}$$

The random variables $\phi^{(i)}$ and $\phi^{(i-1)}$ are assumed to be statistically independent of each other, it is obvious that u and v are also independent. From this result, the joint probability density function of u and v is given by

$$p_{u,v}(u,v) = p_u(u)p_v(v) \qquad u \in R_u, v \in R_v \tag{6.86}$$

where R_u and R_v represents the regions where $p_u(u)$ and $p_v(v)$ are nonzereo as defined in (6.80)-(6.83). Now let us find the pdf of ψ as given in (6.75). The expression given in (6.75) may be written in the form

$$\psi = u - v - \theta^{(i)} \tag{6.87}$$

define a convenient random variable

$$z = v \tag{6.88}$$

then the Jacobian $J(\psi, z/u, v)$ becomes equal to one. The joint density $p_{\psi,z}(\psi, z)$ may be expressed as

$$\begin{aligned} p_{\psi,z}(\psi,z) &= p_{u,v}(\psi + z + \theta^{(i)}, z) \\ &= p_u(\psi + z + \theta^{(i)})p_v(z) \end{aligned} \tag{6.89}$$

Now the probability density function $p_\psi(\psi)$ is given by

$$p_\psi(\psi) = \int_{R_\psi} p_{\psi,Z}(\psi, z)dz \tag{6.90}$$

where R_ψ represents the regions where $p_{\psi,Z}(\psi, z)$ is nonzereo in the ψ, z-plane for the transformation given in (6.87) and (6.88).

If $\theta^{(i)} = \theta_n$, as given in (6.74), the probability of symbol error for the symbol intervals which are jammed may be written as

$$P_{e1,n} = 1 - \int_{-\pi/M}^{\pi/M} p_\psi(\psi) d\psi \tag{6.91}$$

Then the probability of error as given in (6.72) can be written as

$$P_{e1} = \frac{\Gamma(1,1)}{M} \sum_n P_{e1,n} \quad \text{for } n = 1, 2, \ldots M \tag{6.92}$$

We cannot evaluate the integral given in (6.90) in a closed form.

6.4.2 Evaluation of P_{e2}

It is well known that with differential detection the probability of symbol error for the symbol intervals which are jammed is given by

$$P_{e2,j} = 1 - \text{Prob}\left(\left|\left(\arg(s_r^{(i)}) - \arg(s_r^{(i-1)})\right) - \theta_n\right| < \frac{\pi}{M}\right|(1,0)\right) \tag{6.93}$$

Therefore, to determine the average probability of error P_{e2} as given in (6.73), it is necessary to obtain the probability density function of the phase difference ψ where ψ is defined as

$$\psi = \left(\arg(s_r^{(i)}) - \arg(s_r^{(i-1)})\right) - \theta^{(i)} \tag{6.94}$$

In the case where the jammer hits only one of the two consecutive symbols, we may assume without loss of generality, that the received signal in the i-th signaling interval is jammed and the received signal in the $(i-1)$-th signaling interval is not jammed. For this case, $s_r^{(i)}$ and $s_r^{(i-1)}$ are:

$$s_r^{(i)} = \sqrt{2S} e^{j(\theta^{(i)} + \theta_T^{(i-1)})} + \sqrt{2I} e^{j\phi_j} \tag{6.95}$$

and

$$s_r^{(i-1)} = A e^{j\theta_T^{(i-1)}} \tag{6.96}$$

Then the phase difference ψ in (6.94) takes the form

$$\psi = \arg(s_r^{(i)}) - (\theta_T^{(i-1)} + \theta^{(i)}) \tag{6.97}$$

where

$$\begin{aligned} \arg\left\{s_r^{(i)}\right\} &= \arg\left\{\sqrt{2S}e^{j(\theta^{(i)}+\theta_T^{(i-1)})} + \sqrt{2I}e^{j\phi_j}\right\} \\ &= \arctan\left\{\frac{\frac{1}{\eta}\sin(\theta^{(i)} + \theta_T^{(i-1)}) + \sin(\phi_j)}{\frac{1}{\eta}\cos(\theta^{(i)} + \theta_T^{(i-1)}) + \cos(\phi_j)}\right\} \end{aligned} \tag{6.98}$$

The probability of symbol error for the symbol intervals which are jammed may be written as

$$P_{e2,j} = 1 - \int_{-\pi/M}^{\pi/M} p_\psi(\psi)d\psi \tag{6.99}$$

By analogy between (6.97) and (6.10), it clearly appears that the pdf of ψ is the same as the one given in (6.40). Following a procedure similar to that leading to (6.47), $P_{e2,j}$ may be written as

$$P_{e2,j} = \begin{cases} \frac{2}{\pi}\arccos\left[\frac{\sin(\pi/M)}{\eta}\right] & \pi/M \le \arcsin(\eta), \text{ and } 0 < \eta \le 1. \\ \frac{M-2}{2M} + \frac{1}{\pi}\arccos\left[\frac{\sin(\pi/M)}{\eta}\right] & \eta > 1 \\ 0 & \text{otherwise.} \end{cases} \tag{6.100}$$

Therefore, the average probability of the symbol error given in (6.73) may be expressed as

$$P_{e2} = \begin{cases} \frac{4\Gamma(1,0)}{\pi}\arccos\left[\frac{\sin(\pi/M)}{\eta}\right] & \pi/M \le \arcsin(\eta), \text{ and } 0 < \eta \le 1. \\ \frac{(M-2)\Gamma(1,0)}{M} + \frac{2\Gamma(1,0)}{\pi}\arccos\left[\frac{\sin(\pi/M)}{\eta}\right] & \eta > 1 \\ 0 & \text{otherwise.} \end{cases} \tag{6.101}$$

Now the average probability of the symbol error for FH/M-ary DPSK system in presence of multitone jamming interference can be obtained by substituting P_{e1} from (6.92) and P_{e2} from (6.101) into (6.71).

6.5 Conclusions

In this chapter, by deriving the expression for the probability density function of the received signal phase in the presence of multitone jamming, we provided a theoretical basis for the analysis of coherent frequency hopped M-ary PSK and frequency hopped M-ary DPSK systems in multitone jamming environments. Bit error rate performance of coherent frequency hopped M-ary PSK system is analyzed where a simple expression for the probability of bit error is found and the performance expression in the worst case jamming is obtained. An analysis of the probability of error for the frequency hopped M-ary DPSK system in the presence of multitone jamming is obtained.

Chapter 7

Conclusions

7.1 Summary

A mathematical model of JFPM signals has been presented. We restricted our attention to the orthogonal JFPM signals. In this case, we have shown that the required minimum frequency separation between the two adjacent tones of JFPM signals is reduced compared to FSK signals that use the same number of tones. Thus, JFPM requires less bandwidth than FSK for the same bit rate.

The power spectral density of JFPM signals has been analyzed. This analysis concluded that the spectral density of JFPM with at least two phases does not contain discrete components which waste power. The spectral efficiency of JFPM signal has been studied. It can be concluded that the same bandwidth efficiency may be achieved by using different combinations of JFPM formats, and this could give the system designer a freedom of choice under some practical limitation.

The performance of JFPM signals over AWGN as well as over Rayleigh fading channels has been studied. A differential receiver structure for JFPM signals was introduced. The probability of error has been analyzed and a bit error rate expression was obtained. It has been shown that JFPM schemes, by combining FSK and PSK properties in desirable proportions, can provide a good combination of bandwidth efficiency of PSK as the number of phases increases and the power efficiency of FSK as the number of frequencies increases. Assuming statistical independence of the diversity channels, we have analyzed the diversity combining reception of JFPM and shown that significant performance improvements can be achieved compared with the conventional systems and non-diversity. The improvements of JFPM system over the conventional systems are accompanied by a slight increase in the complexity of the transmitter and the receiver.

A spread spectrum system referred to as Frequency Hopped/Joint Frequency phase Modulation (FH/JFPM) has also been presented. The system model was described for both SFH/JFPM and FFH/JFPM. Bit error rate performance for SFH/JFPM in the presence of broadband and partial-band noise jamming was analyzed, and the worst case jamming performance of this system has been evaluated. It has been shown that SFH/JFPM is less sensitive to broadband and partial-band noise jamming than the conventional frequency hopped systems. The design and analysis of the FFH/JFPM system over Rayleigh fading channels has been presented. An expression for the probability of a bit error was obtained. It was shown that for a given channel bandwidth and at a fixed data rate, the processing gain of the two parts of the FH/JFPM system was improved. Results have shown that the FH/JFPM outperforms the conventional frequency hopped systems.

The performance of coherent frequency hopped M-ary PSK system in multitone jamming environments has also been presented. Bit error rate performance of this system was analyzed and a simple expression for the probability of a bit error was obtained. The performance of this system in worst case jamming was also given. A detailed analysis for the probability density function of the received signal phase in the presence of multitone jamming has been provided, the probability density function has been derived for any arbitrary transmitted phase. Based on this analysis, the probability of error for the FH/M-ary DPSK system in the presence of multitone jamming was obtained.

7.2 Future Research

Based on the work given in this thesis, the following topics are suggested for future research:

- Coded JFPM is a feature that could be incorporated into a JFPM system. Coding is the answer to the unequal error rate performance between the two parts of the JFPM receiver and needs further study.

- The main factor affecting the shape of the signal spectrum is the complex envelope of the waveform. Narrower spectrum and higher bandwidth-efficiency of JFPM can be obtained by using waveshaping.

- The performance of FFH/JFPM in frequency selective channels and as CDMA could also be considered for future research.

Appendix A

Derivation of inverse transformation of u

In this appendix we derive the inverse transformation of the function given in (6.11)

$$\begin{aligned} u &= \arg\left\{s_r^{(i)}\right\} = \arg\left\{\sqrt{2S}e^{j(\theta^{(i)})} + \sqrt{2I}e^{j\phi^{(i)}}\right\} \\ &= \arctan\left\{\frac{\frac{1}{\eta}\sin(\theta^{(i)}) + \sin(\phi^{(i)})}{\frac{1}{\eta}\cos(\theta^{(i)}) + \cos(\phi^{(i)})}\right\} \end{aligned} \tag{A.1}$$

The formula given in (A.1) can be written in the form

$$\left[\frac{1}{\eta}\tan(u)\right]\cos(\theta^{(i)}) - \frac{1}{\eta}\sin(\theta^{(i)}) = -\tan(u)\cos(\phi^{(i)}) + \sin(\phi^{(i)}). \tag{A.2}$$

Using the trigonometric identity $A\cos(x) - B\sin(x) = R\cos(x + \alpha)$ where $R = \sqrt{A^2 + B^2}$ and $\alpha = \arctan(B/A)$, we may rewrite (A.2) as

$$R_1\cos(\theta^{(i)} + \alpha_1) = -R_2\cos(\phi^{(i)} + \alpha_2) \tag{A.3}$$

where

$$\begin{aligned} R_1 &= \frac{1}{\eta}\sqrt{\tan^2(u) + 1} \\ R_2 &= \sqrt{\tan^2(u) + 1} \\ \alpha_1 &= \arg\left(\tan(u) + j\right) = \frac{\pi}{2} - u \\ \alpha_2 &= \arg\left(\tan(u) + j\right) = \frac{\pi}{2} - u \end{aligned}$$

After inserting R_1, R_2, α_1 and α_2 into (A.3), equation (A.3) may be expressed as

$$\frac{1}{\eta}\cos\left(\theta^{(i)} - u + \frac{\pi}{2}\right) = -\cos\left(\phi^{(i)} - u + \frac{\pi}{2}\right) \tag{A.4}$$

By using the identity $\cos(x + \pi/2) = -\sin(x)$, (A.4) becomes

$$-\frac{1}{\eta}\sin(\theta^{(i)} - u) = \sin(\phi^{(i)} - u) \tag{A.5}$$

or

$$\frac{1}{\eta}\sin(\theta^{(i)} - u) = \sin(\phi^{(i)} - u + \pi) \tag{A.6}$$

Taking the arcsin( ) for both sides of (A.5), (A.6) and considering all the possibility, we find that there are two solutions

$$\phi^{(i)} = u + \arcsin\left(\frac{1}{\eta}\sin(u - \theta^{(i)})\right) \quad \mod 2\pi \tag{A.7}$$

and

$$\phi^{(i)} = u - \pi - \arcsin\left(\frac{1}{\eta}\sin(u - \theta^{(i)})\right) \quad \mod 2\pi \tag{A.8}$$

Appendix B

Derivation on the bounds of u

In this appendix we derive bounds on the possible values of u given in (6.11)

$$u = \arctan\left\{\frac{\frac{1}{\eta}\sin(\theta^{(i)}) + \sin(\phi^{(i)})}{\frac{1}{\eta}\cos(\theta^{(i)}) + \cos(\phi^{(i)})}\right\} \tag{B.1}$$

Taking the derivative of u with respect to $\phi^{(i)}$, we get

$$\begin{aligned} \frac{du}{d\phi^{(i)}} &= \frac{\eta\cos(\phi^{(i)})(\cos(\theta^{(i)}) + \eta\cos(\phi^{(i)})) + \eta\sin(\phi^{(i)})(\sin(\theta^{(i)}) + \eta\sin(\phi^{(i)}))}{(\cos(\theta^{(i)}) + \eta\cos(\phi^{(i)}))^2} \\ &\times \frac{\left(\cos(\theta^{(i)}) + \eta\cos(\phi^{(i)})\right)^2}{(\cos(\theta^{(i)}) + \eta\cos(\phi^{(i)}))^2 + (\sin(\theta^{(i)}) + \eta\sin(\phi^{(i)}))^2} \end{aligned} \tag{B.2}$$

The value of $\phi^{(i)}$ that maximizes u can be found by equating $du/d\phi^{(i)}$ to zero, by doing so we obtain

$$\eta\cos(\phi^{(i)})(\cos(\theta^{(i)}) + \eta\cos(\phi^{(i)})) + \eta\sin(\phi^{(i)})(\sin(\theta^{(i)}) + \eta\sin(\phi^{(i)})) = 0 \tag{B.3}$$

by collecting terms and using the trigonometric identity $\cos^2(x) + \sin^2(x) = 1$, we may rewrite (B.3) as

$$\cos(\phi^{(i)})\cos(\theta^{(i)}) + \sin(\phi^{(i)})\sin(\theta^{(i)}) + \eta = 0 \tag{B.4}$$

This yields

$$\cos(\phi^{(i)} - \theta^{(i)}) = -\eta \tag{B.5}$$

or

$$\cos(\theta^{(i)} - \phi^{(i)}) = -\eta \tag{B.6}$$

By using the trigonometric identity $\arccos(-x) = \pi - \arccos(x)$, we find that the bounds on u occur at

$$\phi^{(i)} = \theta^{(i)} - \pi + \arccos(\eta) \tag{B.7}$$

$$\phi^{(i)} = \theta^{(i)} + \pi - \arccos(\eta) \tag{B.8}$$

By substituting the values of $\phi^{(i)}$ from (B.7) and (B.8) into (B.1), the bounds of u are obtained and given by

$$u = \theta^{(i)} - \arcsin(\eta) \tag{B.9}$$

$$u = \theta^{(i)} + \arcsin(\eta) \tag{B.10}$$

Then u is bounded by $u_{min} \leq u \leq u_{max}$, and the limits are defined as

$$u_{min} = \min\left\{\left[\theta^{(i)} - \arcsin(\eta)\right], \left[\theta^{(i)} + \arcsin(\eta)\right]\right\} \tag{B.11}$$

and

$$u_{max} = \max\left\{\left[\theta^{(i)} - \arcsin(\eta)\right], \left[\theta^{(i)} + \arcsin(\eta)\right]\right\} \tag{B.12}$$

Bibliography

[1] B. Sklar, "Defining, designing, and evaluating digital communication systems," *IEEE Commun. Mag.*, vol. 29, pp. 92-101, Nov. 1993.

[2] B. Sklar, "A structured overview of digital communication systems–a tutorial review–part I," *IEEE Commun. Mag.*, vol. 19, pp. 4-17, Aug. 1983.

[3] J. D. Oetting, "A comparison of modulation techniques for digital radio," *IEEE Trans. Commun.*,vol. COM-27, pp. 1752-1762, 1979.

[4] J. Wozencraft and I. Jacobs, *"Principles of Communication Engineering,"* Wiley, New York, 1965.

[5] J. B. Anderson and C. W. Sundberg, "Advances in constant envelope coded modulation," *IEEE Commun. Mag.*, vol. 29, pp. 36-45, Dec. 1991.

[6] Special Issue of the *IEEE Trans. Commun.*, vol. COM-29, March 1981.

[7] I.S. Reed and R.A. Scholtz, "N-orthogonal phase-modulated codes," *IEEE Trans. Inform. Theory,* vol. IT-12, pp. 388-395, July 1966.

[8] A.J. Viterbi and J.J. Stiffler, "Performance of N-orthogonal codes," *IEEE Trans. Inform. Theory,* vol. IT-13, pp. 521-522, July 1967.

[9] W. Lindsey and M. Simon, "L-orthogonal signal transmission and detection," *IEEE Trans. Commun.*, vol. COM-20, pp. 953-960, Oct. 1972.

[10] R. Padovani and J. K. Wolf, "Coded phase/frequency modulation," *IEEE Trans. Commun.*, vol. COM-34, pp. 446-453, May 1986.

[11] A. Chalid, I. Sasase, H. Yashima and S. Mori, "Coded nonuniform phase/frequency modulation," *The Trans. of IEICE, Japan*, vol. E-72, pp. 903-911, Aug. 1989.

[12] A. De, I. Sasase and P. Kabal, "Trellis-coded phase/frequency modulation with equal usage of signal dimensions," In *Proc. IEEE Globecom.*, 1992, Nov. pp. 1769-1773.

[13] L. Kaya and B. Honary, "Phase/frequency modulation employing array codes," *IEE Elec. Letters*, vol. 29, pp. 1833-1834, Oct. 1993.

[14] S. Periyualwar and S. Fleisher, "Multiple trellis coded frequency and phase modulation," *IEEE Trans. Commun.*, vol. COM-40, pp. 1038-1046, June 1992.

[15] S. Periyualwar and S. Fleisher, "Trellis coded of quadrature frequency/phase modulated signals," *IEEE J. Select. Areas Commun.*, vol. SAC-10, pp. 1254-1263, Oct. 1992.

[16] S. M. Fleisher and S. Qu, "Multifrequency minimum shift keying," *IEEE J. Select. Areas Commun.*, vol. SAC-10, pp. 1243-1253, Oct. 1992.

[17] R. Khalona, G. Atkin and J. LoCicero, "On the performance of a hybrid frequency and phase shift keying modulation technique," *IEEE Trans. Commun.*, vol. COM-41, pp. 655-659, May 1993.

[18] M. K. Simon et al., *"Spread spectrum communications,"* vol. II. Computer Science Press, Ma., 1985.

[19] E. A. Geraniotis and M. B. Pursley, "Error probabilities for slow-frequency-hopped spread-spectrum multiple-access communication over fading channel," *IEEE Trans. Commun.*, vol. COM-30, pp. 996-1009, May 1982.

[20] S. Houston, "Modulation techniques for communication, part I; tone and noise jamming performance of spread spectrum M-ary FSK and 2,4-ary DPSK waveforms,"in *NAECON'75 Rec.",* pp. 51-58.

[21] M. Simon, "The performance of M-ary FH-DPSK in the presence of partial-band multitone jamming," *IEEE Trans. Commun.*, vol. COM-30, pp. 953-958, May 1982.

[22] J. S. Lee and L. E. Miller, "Error performance analyses of differential phase-shift-keyed/frequency-hopping spread-spectrum communication system in the partial band jamming environments," *IEEE Trans. Commun.*, vol. COM-30, pp. 943-952, May 1982.

[23] Q. Wang, T. A. Gulliver and V. K. Bhargava, "Probability distribution of DPSK in tone interference and application to SFH/DPSK," *IEEE Select. Areas Commun.*, vol. 8, pp. 895-906, June 1990.

[24] K. S. Gong, "Performance analysis of FH/DPSK in additive white Gaussian noise (AWGN) and multitone jamming," in *Proc. IEEE MILCOM,* pp. 53.4.1-53.4.7, 1988.

[25] J. K. Winters, "On differential detection of M-ary DPSK with intersymbol interference and noise correlation," *IEEE Trans. Commun.*, vol. COM-35, pp. 117-120, Jan. 1987.

[26] W. C. Lindsey, S. H. An and R. M. Vacek "Performance of M-ary FH-DPSK systems in the presence of jamming," in *Proc. IEEE MILCOM*, pp. 34.2.1-34.2.5. Nov.1988.

[27] G. R. Cooper and R. W. Nettleton, "A spread-spectrum technique for high-capacity mobile communication," *IEEE Trans. Veh. Technol.*, vol. VT-27 pp. 264-275, Nov. 1978.

[28] P. S. Henry, "Spectrum efficiency of frequency-hopped-DPSK spread-spectrum mobile radio system," *IEEE Trans. Veh. Technol.*, vol. VT-28, pp. 264-275, Nov. 1979.

[29] G. R. Cooper, R. W. Nettleton and D. P. Grybos, "Celluar land-mobile radio: why spread-spectrum ?," *IEEE Commun. Magazine.*, vol. 17, pp. 327-332, Nov. 1979.

[30] R. W. Nettleton and G. R. Cooper, "Performance of frequency hopped differentially modulated spread-spectrum receiver in a rayleigh fading channel," *IEEE Trans. Veh. Technol.*, vol. VT-30, pp. 14-29, Feb. 1981.

[31] M. Matsumoto and G. Cooper, "Performance of nonlinear FH-DPSK spread-spectrum with multiple narrow-band interfering signals," *IEEE Trans. Commun.*, vol. COM-30, pp. 937-942, May 1982.

[32] C. Lo, E. Masry and L. Milstein, "Design and analysis of a fast frequency-hopped DBPSK communication system, part I–system description and hop timing track-

ing loop analysis," *IEEE Trans. Commun.,* vol. COM-41, pp. 1552-1564, Oct. 1993.

[33] C. Lo, E. Masry and L. Milstein, "Design and analysis of a fast frequency-hopped DBPSK communication system, part II–error performance in AWGN plus partial-band noise jamming," *IEEE Trans. Commun.*, vol. COM-41, pp. 1723-1735, Nov. 1993.

[34] I. Ghareeb and A. Yongaçoḡlu, "Performance of joint frequency-phase modulation over Rayleigh fading channels," *IEE Proc. Commun.*,vol. 141, pp. 241-247, Aug. 1994.

[35] I. Ghareeb and A. Yongaçoḡlu, "Performance Evaluation of Slow-Frequency Hopped/Joint Frequency-Phase Modulation in Broadband and Partial-Band Noise Jamming," *IEICE Trans. on Commun.*, vol. E-77-B, pp. 891-899, July 1994.

[36] I. Ghareeb, "Bit Error Rate Performance and Power Spectral Density of a Non-coherent Hybrid Frequency-Phase Modulation System," *IEEE J. Select. Areas Commun.,* vol. SAC-12, Feb. 1995.

[37] I. Ghareeb and A. Yongaçoḡlu, "Performance Analysis of Frequency Hopped/Coherent MPSK in the Presence of Multitone Jamming," submitted to *IEEE Trans. on Commun,* .

[38] I. Ghareeb and A. Yongaçoḡlu, "Performance of frequency hopped/joint frequency-phase modulation in the presence of broadband and partial-band noise jamming," in *Proc. 4th International Symposium on personal indoor and mobile radio communications PIMRC'93,* Japan, pp. 662-666, Sep. 1993.

[39] I. Ghareeb and A. Yongaçoğlu, "Joint frequency-phase modulation over Rayleigh fading channels," in *Proc. International Zurich seminar,*Zurich, pp.101-112, March 1994

[40] I. Ghareeb and A. Yongaçoğlu, " Fast Frequency Hopped/Joint Frequency-Phase Modulation over Rayleigh Fading Channels," in *Proc. IEEE Milcom-94,* Oct 1994.

[41] I. Ghareeb and A. Yongaçoğlu, "Performance Analysis of Frequency Hopped/Coherent MPSK in the Presence of Multitone Jamming," in *Proc. IEEE Milcom-94,* Oct 1994.

[42] I. Ghareeb and A. Yongaçoğlu, "Joint Frequency-Phase Modulation," in *Proc. Canadian Conference on Electrical and Computer Engineering,* Canada, pp. TM2.14.1-TM2.14.4, Sept. 1992.

[43] J. Edell, "Wideband, noncoherent, frequency-hopped waveforms and their hybrids in low probability-of-intercept communications," Naval Res. Lab., Washington, DC, NRL Rep. 8025, Nov. 8, 1976.

[44] J. Gorski-Popiel, Ed., *"Frequency synthesis: techniques and applications."*New York: IEEE Press, 1975, p. 43.

[45] S. Benedetto, E. Biglieri and V. Castellani, *"Digital Transmission Theory,"* Englewood Cliffs, NJ: Prentice-Hall Publ. Co., 1987.

[46] J. G. Proakis, *"Digital Communications,"* McGraw-Hill, 1989.

[47] W. Lindsey and M. Simon, *"Telecommunication Systems Engineering,"* Englewood Cliffs, NJ: Prentice-Hill, 1973.

[48] R. F. Pawula, S.O. Rice and J.H. Roberts, "Distribution of the phase angle between two vectors perturbed by Gaussian noise," *IEEE Trans. on Commun.*, vol. COM-30, pp. 1828-1841 August 1982.

[49] P. Galko and S. Pasupathy, "The mean power spectral density of Markov chain driven signals," *IEEE Trans. Inform. Theory,* vol. IT-27, pp. 746-754, Nov. 1981.

[50] F. Davarian, "Channel simulation to facilitate mobile-satellite communication research," *IEEE Trans. on Commun.*, vol. COM-35, pp. 47-56, Jan 1987.

[51] W. Brawn, "A physical mobile radio channel model," *IEEE Trans. Veh. Technol.*, vol. 40, pp. 472-482, May 1991.

[52] M. Schwartz, W. Bennett and S. Stein, *"Communications Systems and Techniques,"* McGraw-Hill, 1966.

[53] W. Lee, *"Mobile Communication Engineering"*, McGraw-Hill, 1982.

[54] W. Lee, *"Mobile Communication Design Fundamentals"*, John Wiley & Sons, Inc., 1993.

[55] J. Bird and E. Felstead, "Antijam performance of fast frequency-hopped M-ary NCFSK an overview," *IEEE J. Select. Areas Commun.*, vol.SAC-4, pp. 216-233, March 1986.

[56] B. Levitt, "Use of diversity to improve FH/MFSK performance in worst case partial band noise and multitone jamming," in *Proc. IEEE Milcom,* pp 28.2.1-28.2.5, 1982.

[57] R. Robertson and K. Lee, "Performance of fast frequency-hopped MFSK receivers with linear and self-normalization combining in a Rician fading channel

with parial-band interference," *IEEE J. Select. Areas Commun.*, vol. SAC-10, pp. 731-741, May 1992.

[58] R. Robertson and T. Ha, "Error probabilities of fast frequency-hopped FSK with self-normalization combining in a fading channel with partial-band interference," *IEEE J. Select. Areas Commun.*, vol. Sac-10, pp. 714-723, May 1992.

[59] R. Robertson and T. Ha, "Error probabilities of fast frequency-hopped MFSK with noise-normalization combining in a fading channel with partial-band interference," *IEEE Trans. on Commun.*, vol. COM-40, pp. 404-412, Feb. 1992.

[60] C. Keller and M. Pursley, "Diversity combining for channels with fading and partial-band interference," *IEEE J. Select. Areas Commun.*, vol. SAC-5, pp. 248-260, Feb. 1987.

[61] C. Keller and M. Pursley, "Frequency spacing in MFSK frequency-hopped spread spectrum communications over selective fading channels," in *Proc. 17th Conf. Inform. Sci. Syst.*, Johns Hopkins Univ., Baltimore, MD, pp. 749-754, Mar. 1983.

[62] P. Hahn, "Theoretical diversity improvement in multiple frequency shift keying," *IRE Trans. on Commun. Systems*, vol. 50 , pp. 177-184, June 1962.

[63] I. Gradshteyn and I. Ryzhik, *"Table of integrals, Series, and Products,"* Academic Press, Inc., 1980.

[64] J. Proakis, "Probabilities of error for adaptive reception of M-phase signals," *IEEE Trans. on Commun.*, vol. COM-16, pp. 71-81, Feb. 1968.

[65] A. Papoulis, *"Probability, random variables, and stochastic processes,"* McGraw-Hill, New York, 1991.

[66] M. Simon and A. Polydoros "Coherent detection of frequency-hopped quadrature modulation in the presence of jamming–Part I: QPSK and QASK modulations," *IEEE Trans. on Commun*, vol. COM-29, pp. 1644-1660 , Nov. 1981.

[67] M. Simon, "Coherent detection of frequency-hopped quadrature modulation in the presence of jamming–Part II: QPR Class I modulation," *IEEE Trans. on Commun*, vol. COM-29, pp. 1661-1668 , Nov. 1981.

[68] G. Cherubini and L. Milstein "Analysis of tracking loop of phase-coherent frequency hopped spread spectrum system," in *Proc. IEEE MILCOM,* pp 31.3.1-31.3.5, 1986.

[69] G. Cherubini and L. Milstein, "Performance analysis of both hybrid and frequency hopped phase-coherent spread spectrum systems– Part I," *IEEE Trans. Commun.*, vol. COM-37, pp. 600-611, June. 1989.

[70] G. Cherubini and L. Milstein, "Performance analysis of both hybrid and frequency hopped phase-coherent spread spectrum systems– Part II," *IEEE Trans. Commun.*, vol. COM-37, pp. 612-622, June. 1989.

[71] C. Su and L. Milstein, "Comparison of joint phase/timing tracking loops for coherent frequency-hopped spread spectrum receiver," In *Proc. IEEE Globecom.*, pp. 17.3.1-17.3.5, Nov.1988.

[72] C. Su and L. Milstein, "Analysis of a coherent frequency-hopped spread spectrum receiver in the presence of jamming," *IEEE Trans. Commun.*, vol. COM-38, pp. 715-726, May 1990.

[73] C. Su and L. Milstein, "Channel equalization and performance analysis of a coherent frequency hopped spread spectrum system," *IEEE J. Select. Areas Commun.*, vol.SAC-7, pp. 548-560, May 1989.

[74] G. Cherubini and W. Stark, "Capacity of coherent frequency-hop spread spectrum communications", in *Proc. ICC-93,* pp. 458 - 462, May 1993.